# COLLAGEN LIKE PEPTIDE BIOCONJUGATES

# FOR TARGETED DRUG DELIVERY APPLICATIONS

by

Tianzhi Luo

A dissertation submitted to the Faculty of the University of Delaware in partial fulfillment of the requirements for the degree of Doctor of Philosophy in Materials Science and Engineering

Fall 2016

**COLLAGEN LIKE PEPTIDE BIOCONJUGATES**

**FOR TARGETED DRUG DELIVERY APPLICATIONS**

by

Tianzhi Luo

Approved: _____

Darrin J. Pochan, Ph.D.
Chair of the Department of Materials Science and Engineering

Approved: _____

Babatunde A. Ogunnaike, Ph.D.
Dean of the College of Engineering

Approved: _____

Ann L. Ardis, Ph.D.
Senior Vice Provost for Graduate and Professional Education

I certify that I have read this dissertation and that in my opinion it meets the academic and professional standard required by the University as a dissertation for the degree of Doctor of Philosophy.

Signed: _____

Kristi L. Kiick, Ph.D.
Professor in charge of dissertation

I certify that I have read this dissertation and that in my opinion it meets the academic and professional standard required by the University as a dissertation for the degree of Doctor of Philosophy.

Signed: _____

Darrin J. Pochan, Ph.D.
Member of dissertation committee

I certify that I have read this dissertation and that in my opinion it meets the academic and professional standard required by the University as a dissertation for the degree of Doctor of Philosophy.

Signed: _____

Xinqiao Jia, Ph.D.
Member of dissertation committee

I certify that I have read this dissertation and that in my opinion it meets the academic and professional standard required by the University as a dissertation for the degree of Doctor of Philosophy.

Signed: _____

Millicent O. Sullivan, Ph.D.
Member of dissertation committee

## ACKNOWLEDGMENTS

I am heartily thankful to all the people who supported and encouraged me and kept my spirits high during my years of the PhD. This work would not have been so exciting for me without their help. It is my honor to acknowledge them in this section.

I am very grateful to my advisor Professor Kristi L. Kiick for her excellent scientific guidance and critical discussions. I also had a great learning from her fantastic teaching skills as the instructor of several courses. Her enthusiasm and encouragement for new and exciting scientific works kept me motivated towards the commitments of my thesis work. The aptitudes acquired by me while working under her guidance has constantly shaped me in becoming a better scholar. I am deeply grateful to Professor Kiick for all her efforts to promote me as an independent scientist.

I am very grateful to my committee members, Professor Xinqiao Jia, Professor Millicent O. Sullivan, and Professor Darrin J. Pochan for their profound scientific advice and providing research facility for carrying out various works described in this thesis. I am deeply grateful to them for their flexible schedule and technical discussions with me that helped me sort out the technical details of my work.

I sincerely thank Professor Patrick Theato and Ronghe Li, at the University of Hamburg, Germany, for our excellent collaborative work on diblock collagen peptide polymer conjugate.

I sincerely thank all my past lab members (Dr. Shuang Liu, Dr. Aaron Baldwin, Dr. Sarah Grieshaber, Dr. Linqing Li, Dr. Eric Levenson, Dr. Christopher McGann, Dr. Nandita Bhagwat, Ingrid Spielman, Bo Xie, Dr. Prathamesh Kharkar, Dr. Yingkai

Liang, Dr. Samuel Lahasky, Dr. Kenneth Koehler, Dr. Shivshankar Mane) and present lab members (Dr. Rebecca Scott, Bradford Paik, Morgan Urello, Hang Kuen Lau, Michael Haider, Yu Tian, Haocheng Wu, Danielle Ferguson, Lucas Dunshee, Ming Fan) for technical and scientific discussions. Their company made my life easier on multiple occasions.

I am thankful to Rachel Letteri at University of Massachusetts for help on organic phase GPC and Dr. Chaoying Ni, Frank Kriss, Fei Deng and Jennifer Sloppy for help on TEM and cryo-TEM. I am also thankful to the efforts and support of all staffs (especially Robin Buccos, Kathy Forwood, Laura Mohr, Dionne Putney, Christine Williamson, and Charlie Garbini) of the department of Material Science and Engineering.

I would like to thank all my friends for their advice and support. They helped me make this thesis work possible and make my life easier here at UD. I especially thank Linqing Li, Bo Xie, Jun Jiang, Fan Xu, Xiaoshan Xu, Ying Hao, Hang Kuen Lau, Shuyu Xu, Eric Fowler, Nandita Bhagwat, Xiaowei Yang, Xinyi Wang, Xiaocao Hu and Bradford Paik for their great company and fun time.

I dedicate this work to my mother Xiaoping Yan who brought me to the world, my father Fei Luo who taught me the rules, and my advisor Kristi Kiick who guided me into the world of science.

## TABLE OF CONTENTS

LIST OF TABLES ..... x
LIST OF FIGURES ..... xi
ABSTRACT ..... xx

Chapter

1 BACKGROUND ..... 1

1.1 Introduction ..... 1
1.2 Triple Helix Stability ..... 3

1.2.1 Role of (4R)-hydroxyproline ..... 4
1.2.2 Electrostatic interactions ..... 6
1.2.3 Cystine knots ..... 8
1.2.4 Template stabilization ..... 9

1.3 Higher Order Assembly ..... 11

1.3.1 π-π stacking interaction ..... 12
1.3.2 Lateral electrostatic interactions ..... 13
1.3.3 Metal-triggered assembly ..... 15

1.4 Triple Helix Hybridization ..... 18
1.5 Synthetic Polymer – CLP Bioconjugates ..... 21

1.5.1 Assembly of polymer–CLP conjugates ..... 22
1.5.2 Collagen/CLP containing hydrogels ..... 24

1.6 Conclusions ..... 27
1.7 Acknowledgements ..... 28

REFERENCES ..... 29

2 THERMORESPONSIVE SELF-ASSEMBLY OF NANOSTRUCTURES FROM A COLLAGEN-LIKE PEPTIDE-CONTAINING DIBLOCK COPOLYMER ..... 41

2.1 Introduction ..... 41
2.2 Experimental Section ..... 45

2.2.1 Materials ..... 45
2.2.2 Peptide Synthesis ..... 45
2.2.3 PDEGMEMA-CLP Conjugate Synthesis ..... 46
2.2.4 Nuclear Magnetic Resonance (NMR) ..... 47
2.2.5 Gel Permeation Chromatography (GPC) ..... 47
2.2.6 Circular Dichroic Spectroscopy (CD) ..... 48
2.2.7 Dynamic Light Scattering (DLS) ..... 49
2.2.8 Transmission Electron Microscopy (TEM) ..... 49

2.3 Results and Discussion ..... 50

2.3.1 Synthesis of PDEGMEMA-CLP Diblock Polymer ..... 50
2.3.2 Triple Helix Formation ..... 54
2.3.3 Temperature Triggered Self-Assembly into Nanoparticles ..... 59

2.4 Conclusions ..... 69
2.5 Supporting Information ..... 69

2.5.1 Peptide Synthesis and Characterization ..... 69
2.5.2 PEG-CLP Conjugate Synthesis and Characterization ..... 71
2.5.3 DLS correlation function and cumulant fit curve ..... 74
2.5.4 Size Distribution of PEG-CLP and PDEGMEMA Controls ..... 75

2.6 Acknowledgements ..... 76

REFERENCES ..... 77

3 NONCOVALENT MODULATION OF THE INVERSE TEMPERATURE TRANSITION AND ASSEMBLY OF ELASTIN-B-COLLAGEN-LIKE PEPTIDE BIOCONJUGATES ..... 82

3.1 Introduction ..... 82
3.2 Experimental Section ..... 86

3.2.1 Materials ..... 86
3.2.2 Peptide synthesis ..... 87
3.2.3 ELP-CLP conjugate synthesis ..... 88
3.2.4 Gel Permeation Chromatography (GPC) ..... 89
3.2.5 Nuclear Magnetic Resonance Spectrometry (NMR) ..... 89
3.2.6 Fourier Transform Infrared Spectroscopy (FTIR) ..... 89
3.2.7 Circular Dichroic Spectroscopy (CD) ..... 90

3.2.8 Dynamic Light Scattering (DLS) ..... 90
3.2.9 Transmission Electron Microscopy (TEM) ..... 91
3.2.10 Cryo Transmission Electron Microscopy (Cryo-TEM) ..... 92

3.3 Results and Discussion ..... 92

3.3.1 Conjugate synthesis and characterization ..... 92
3.3.2 CLP domain triple helix formation ..... 101
3.3.3 Thermoresponsive self-assembly ..... 103

3.4 Conclusions ..... 109
3.5 Supporting Information ..... 111
3.6 Acknowledgements ..... 114

REFERENCES ..... 115

4 THERMORESPONSIVE ELASTIN-b-COLLAGEN-LIKE PEPTIDE BIOCONJUGATE NANOPARTICLES FOR TARGETED DRUG DELIVERY IN COLLAGEN CONTAINING MATRICES ..... 122

4.1 Introduction ..... 122
4.2 Materials and Methods ..... 125

4.2.1 ELP-CLP diblock synthesis and characterization ..... 125
4.2.2 Thermoresponsive drug release from ELP-CLP nanoparticles ..... 125

4.2.2.1 Preparation of drug loaded nanoparticles ..... 125
4.2.2.2 Particle size distribution ..... 126
4.2.2.3 Morphology ..... 126
4.2.2.4 Release profile ..... 127

4.2.3 Nanoparticle retention on collagen films ..... 127
4.2.4 Inflammatory response ..... 128
4.2.5 Fibroblast viability ..... 129
4.2.6 Chondrocyte viability and proliferation ..... 130

4.3 Results ..... 131

4.3.1 Thermoresponsive drug release from ELP-CLP nanoparticles ..... 131

4.3.1.1 Nanoparticle characterization ..... 131
4.3.1.2 Release profile ..... 133

4.3.2 Collagen retention ..... 135
4.3.3 Inflammatory response of ELP-CLP nanoparticles ..... 137

4.3.4 Fibroblast viability ..... 138
4.3.5 Chondrocyte viability and proliferation ..... 141

4.4 Conclusions ..... 143
4.5 Supporting Information ..... 144

REFERENCES ..... 149

5 CONCLUSIONS ..... 156

Appendix

A PERMISSION LETTERS ..... 158

A.1 Elsevier License Terms and Conditions ..... 158
A.2 John Wiley and Sons License Terms and Conditions ..... 166
A.3 ACS Publications License ..... 172

## LIST OF TABLES

Table 1.1 Melting temperatures of host-guest peptides (Reproduced with permission from Ref. 39 © American Chemical Society) ..... 4

Table 1.2 Comparison of melting temperature of CLP with/without the template. (Data taken in part from Ref. 62, 63 © American Chemical Society and Ref. 64 © Academic Press.) ..... 10

## LIST OF FIGURES


Figure 1.1 Structure of Ac-Flp-OMe. (Reprint with permission from Ref. 51 © American Chemical Society)..... 6

Figure 1.2 Potential interchain interaction between residue at X position of one chain and residue at Y position of another. ..... 6

Figure 1.3 Pairwise interactions between Glu and Lys in GPKGEO containing CLPs. (a) computer model proposed by Persikov et al; (b) axial (left) and lateral (right) interactions proposed by Fallas et al. (Reprinted with permission from Ref. 57 © American Chemical Society and Ref. 7 ©American Society for Biochemistry and Molecular Biology)..... 8

Figure 1.4 Two types of cystine knot connectivities. ..... 9

Figure 1.5 CLP self-assembly via π-π stacking interaction. (a) $(GPO)_{10}$ end-functionalized with pentafluorophenylalanine and phenylalanine. (b) Interface between two triple helices (one blue, one yellow) showing three aromatic stacking interactions (black double-headed arrows; A-C). (c) TEM image of self-assembled CLP. (Reproduced with permission from Ref. 68 © The National Academy of Sciences of the USA and Ref. 69 © American Chemical Society.)..... 13

Figure 1.6 Self-assembly of CLP via lateral electrostatic interaction. (a) Amino acid sequence of CLP, indicating three different domains. (b) Axial staggered interchain electrostatic interactions. (c) Well-defined D-periodicity observed via high resolution transmission electron microscopy. (d) Multi-hierarchical self-assembly of related collagen-mimetic peptides. (Figure a, b, c are reproduced with permission from Ref. 73 © American Chemical Society, Figure d is reproduced with permission from Ref. 14 © Macmillan Publishers Limited.)..... 15

Figure 1.7 (a) Scheme showing the structure of IdaCol and HisCol and subsequent tandem assembly. (b) TEM images of petal like structures with periodic bands observed from metal triggered CLP self-assembly. (c) Assembled structures depend on length of CLP domain. (d) SEM images of large aggregates of X9 (top) and PHG (bottom) after incubating with $Zn^{2+}$. (Reproduced with permission from Ref. 12, 13 and 74 © American Chemical Society)..... 17

Figure 1.8 Metal-triggered radial assembly of collagen peptide fibers. (a) amino acid sequence of the CLP. (b) Side view of the triple helix. (c) Hypothesized interaction between bipyridyl-modified lysine and $Fe^{2+}$. (d) TEM image of the assembled structure. (Reproduced with permission from Ref. 15 © American Chemical Society) ..... 18

Figure 1.9 a) Schematic of collagen triple helix hybridization; b) CLP labels collagens of human liver tissue as efficiently as collagen antibodies; c) TEM micrographs of reconstituted type I collagen fibers labelled with CLP functionalized gold nanoparticles; d) In vivo NIRF images of mice bearing PC-3 prostate tumors administered with fluorescent labelled $(GPO)_9$ CLP indicate specific tumor accumulation; e) Dual-NIRF image of the knee joint showing the uptake of fluorescent labelled CLP (red) and BoneTag™ (stains calcifying tissues in green), CLP-specific uptake can be seen within the articular cartilage and meniscus (red arrowhead) as well as focal regions within the tibia and the femur head. (reproduced with permission from Ref. 76, 78, 80, 83) 20

Figure 1.10 (a) Synthesis of hybrid triblock copolymer. Collagen like peptide sequence: $G(GPP)_3GPRGEKGERGPR(GPP)_3GPCCG$. (b) Cryo-TEM image of spherical structures at 37 °C. Scale bar = 50 μm (c) TEM image of collagen like fibrils at 75 °C. Scale bar = 0.5 μm (Reproduced with permission from Ref.38 © The Royal Society of Chemistry and Ref.66 © American Chemical Society) ..... 24

Figure 1.11 a) Self-assembly of collagen like peptide (Pro-Lys-Gly)$_4$-(Pro-Hyp-Gly)$_4$-(Asp-Hyp-Gly)4 into nanofibre and subsequent fabrication of CLP hydrogel at higher concentrations; scale bar = 1 um; b) 4-arm PEG hydrogel crosslinked via (GPO)$_9$ collagen triple helix. Left bottom panel: storage and loss modulus for the hydrogel (10 wt%) before and after the addition of free CLP solution. c) 8-arm PEG hydrogel crosslinked via collagen triple helix. Temperature sweep experiment for the hydrogel (8 wt%) suggested a high storage modulus of approximately 1500 Pa at physiological temperature. Filled symbols represent the first analysis of the hydrogels and open symbols represent analysis after recooling the samples from the first analysis. G': storage modulus (square), G'': loss modulus (triangle). (reproduced with permission from Ref[14, 117, 118]) ..... 26

Figure 2.1 Proposed two-step assembly mechanism for PDEGMEMA-CLP conjugates. ..... 44

Figure 2.2 Chemical synthesis of PDEGMEMA-CLP diblock via the reaction of the activated ester-terminated PDEGMEMA with the N-terminal amine of a collagen-like peptide. The reaction was carried out in a mixture of dimethyl sulfoxide (DMSO) and N-methyl-2-pyrrolidone (NMP) (v/v=1:1) in the presence of triethylamine at 35 °C for 3 days... 47

Figure 2.3 GPC trace of PDEGMEMA-CLP diblock and PDEGMEMA starting material. ..... 52

Figure 2.4 $^1$H NMR spectra (600 MHz) of: a) collagen-like peptide; b) PDEGMEMA; c) PDEGMEMA-CLP diblock in d$_6$-DMSO. ..... 54

Figure 2.5 a) CD spectra showing the wavelength scans for the collagen like peptide; b) Blue curve with dots (Y axis on the left side): thermal unfolding profile for CLP plotted as $[\theta]_{MRE225nm}$ versus temperature. The red curve (Y axis on the right side) is the first derivative of the unfolding curve with respect to temperature; c) Refolding profile of CLP after quenching to 5 °C; d) CD spectra showing the wavelength scans for PDEGMEMA-CLP diblock; e) Blue curve with dots (Y axis on the left side): thermal unfolding profile for PDEGMEMA-CLP diblock plotted as $[\theta]_{MRE225nm}$ versus temperature. The red curve (Y axis on the right side) is the first derivative of the unfolding curve with respect to temperature; f) Refolding profile of the PDEGMEMA-CLP diblock after quenching to 5 °C, with an inserted image from 0 – 7 minutes. ..... 57

Figure 2.6 Study of transition temperature via dynamic light scattering. a) Hydrodynamic diameter of assemblies as a function of temperature upon heating; b) Hydrodynamic diameter of assemblies as a function of temperature upon cooling. Samples were heated at each temperature for 2 minutes before measurement. Red curve with triangles: PDEGMEMA sample dissolved in water at 1 mg/mL; blue curve with circles: PDEGMEMA-CLP diblock dissolved in PBS buffer (pH = 7.4) at 1 mg/mL; orange curve with circles: PDEGMEMA-CLP diblock dissolved in water at 5 mg/mL; pink curve with circles: PDEGMEMA-CLP diblock dissolved in water at 1 mg/mL; black curve with squares: PEG-CLP diblock dissolved in water at 1 mg/mL ..... 60

Figure 2.7 Size distribution of assemblies at different temperatures. a) PDEGMEMA-CLP diblock, 1 mg/mL in water; b) PDEGMEMA-CLP diblock, 5 mg/mL in water. Correlation functions and cumulant fits are provided in the Supporting Information (Figure 2.15)..... 62

Figure 2.8 TEM images of nanoparticles formed from PDEGMEMA-CLP diblock at 50 °C, stained with phosphotungstic acid (1% PTA in water, pH adjusted to 7.0). a,b) 5 mg/mL; c,d) 1 mg/mL; e,f) 1 mg/mL, washed with deionized water after staining. Scale bars: 200 nm. ..... 63

Figure 2.9 Schematic illustration of the potential structure of vesicles formed at 50 °C in aqueous condition. ..... 66

Figure 2.10 RP-HPLC trace of collagen like peptide $(GPO)_7GG$, blue line indicates the gradient used. ..... 70

Figure 2.11 ESI-MS of purified CLP..... 70

Figure 2.12 PEG-CLP conjugation reaction ..... 71

Figure 2.13 GPC traces of PEG-CLP diblock and starting materials. a) Normalized refractive index chromatogram of PEG-CLP diblock copolymer and CLP, PEG starting material. b) 214 nm UV absorbance of PEG-CLP diblock and CLP, PEG starting material. ..... 72

Figure 2.14 $^1H$ NMR spectra (600 MHz) of: a) collagen like peptide; b) PEG5k; c) PEG-CLP diblock in $d_6$-DMSO. ..... 73

Figure 2.15 DLS data at 50 °C. a) Size distribution by intensity for 1 mg/mL diblock sample; b) Size distribution by intensity for 5 mg/mL diblock sample; c) raw correlation function for 1 mg/mL diblock sample; d) raw correlation function for 5 mg/mL diblock sample; e) Fitting curve using cumulant method for 1 mg/mL sample, empty circles indicate experimental data; f) Fitting curve using cumulant method for 5 mg/mL sample, empty circles indicate experimental data. ..... 75

Figure 2.16 Size distribution by number at different temperatures. a) PEG-CLP diblock, 1 mg/mL in water; b) PDEGMEMA, 1 mg/mL in water. ..... 75

Figure 3.1 Self-assembly of ELP conjugates. a) Self-assembly of ELP-PEG block copolymer into micelles triggered by the phase transition of the ELP domain; bottom two figures are TEM micrographs of self-assembled ELP130 functionalized with one PEG5k chain and two PEG 5k chains respectively. Scale bars = 200 nm; b) Cryo-TEM image of L4F-$(VPGAG)_{192}$ peptide vesicles, with an inserted schematic showing the structure of the vesicle; c) TEM and AFM tapping-mode height image of nanoparticles assembled from dAg-$E_{50}I_{60}$ elastin like corecombinamer. Scale bar = 200 nm; d) Schematic representation of the allosteric, calcium-triggered control of phase transition of CaM-ELP fusion proteins; e) pH responsive histidine-rich elastin like polypeptide block copolymer self-assembles at 37 °C into spherical micelles. (reproduced with permission from ref[8, 11, 13-15]) ..... 84

Figure 3.2 Solid phase peptide synthesis and molecular structure of: a) azide functionalized collagen-like peptide; b) alkyne functionalized elastin-like peptide ..... 93

Figure 3.3 RP-HPLC trace of purified peptides: a) collagen-like peptide; b) elastin-like peptide ..... 94

Figure 3.4 ESI-MS of purified CLP..... 94

Figure 3.5 ESI-MS of purified ELP..... 95

Figure 3.6 Chemical conjugation of ELP and CLP. ..... 96

Figure 3.7 GPC trace of ELP-CLP diblock and peptide starting material..... 97

Figure 3.8 CD spectra showing the wavelength scans for the ELP-CLP diblock sample dissolved in TFE at 20 °C and 40 °C. Results suggested the diblock maintained a partially folded triple helical conformation when injected into the column for GPC experiments at 40 °C. ..... 98

Figure 3.9 $^{1}$H NMR spectra (600 MHz) of: a) elastin-like peptide; b) collagen-like peptide; c) ELP-CLP diblock in $d_6$-DMSO. ..... 99

Figure 3.10 Expanded $^{1}$H NMR spectra between 2.4 ppm and 2.9 ppm of: a) elastin-like peptide; b) collagen-like peptide; c) ELP-CLP diblock. .... 100

Figure 3.11 ATR-FTIR spectra of the ELP-CLP diblock and peptide starting materials. ..... 101

Figure 3.12 a) CD spectra showing representative full-wavelength scans for the ELP-CLP conjugate; b) Thermal unfolding profile for an ELP-CLP conjugate; the first derivative of the unfolding curve with respect to temperature is shown in red; c) Refolding profile of CLP after quenching from 80 °C to 5 °C; d) Refolding profile of the ELP-CLP conjugate after quenching. ..... 103

Figure 3.13 Dynamic light scattering characterization of the assembly of ELP-CLP conjugates. a) Hydrodynamic diameter of nanostructures as a function of temperature upon heating; b) Size distributions of ELP-CLP assemblies at select temperatures. ..... 105

Figure 3.14 a)-e) TEM images of nanoparticles from ELP-CLP conjugates at various temperatures, after negative staining with phosphotungstic acid. Scale bars: 500 nm. a) 25 °C; b) 37 °C; c) 50 °C; d) 65 °C; e) 80 °C. f) Cryo-TEM image of nanoparticles of the ELP-CLP diblock at 25 °C. Scale bar: 200 nm. ..... 107

Figure 3.15 Proposed assembly/disassembly and bilayer structure of ELP-CLP vesicles. ..... 109

Figure 3.16 Thermal unfolding profile for ELP plotted as $[\theta]_{MRE225nm}$ versus temperature.It was subtracted from the diblock unfolding profile to remove the contribution from ELP domain. ..... 111

Figure 3.17 a) CD spectra showing the wavelength scans for the collagen like peptide; b) Blue curve with dots (Y axis on the left side): thermal unfolding profile for CLP; red curve (Y axis on the right side): first derivative of the unfolding curve with respect to temperature; ..... 112

Figure 3.18 Hydrodynamic diameter of assemblies as a function of temperature upon heating. a) ELP at 1 mg/mL in water; b) ELP and CLP physical mixture at 0.5 mg/mL each in water; c) ELP at 1 mg/mL in NaCl aqueous solution ..... 112

Figure 3.19 Hydrodynamic diameter of ELP-CLP diblock assemblies as a function of temperature upon cooling..... 113

Figure 3.20 Hydrodynamic diameter of VPGFG$_{3-5}$-CLP diblock assemblies as a function of temperature upon heating ..... 114

Figure 4.1 Nanoparticle characterization. a) Size distributions of ELP−CLP assemblies. b) TEM image of nanoparticles from ELP−CLP conjugates at 37 °C. c) TEM image of nanoparticles from ELP−CLP conjugates at 80 °C. d) Size distributions of fluorescein loaded ELP−CLP assemblies. e) TEM image of fluorescein loaded nanoparticles from ELP−CLP conjugates at 37 °C. c) TEM image of fluorescein loaded nanoparticles from ELP−CLP conjugates at 80 °C. Scale bars = 500 nm. ..... 133

Figure 4.2 Cumulative release of fluorescein from ELP-CLP nanoparticles as a function of time. The amount of released fluorescein was calculated by measuring the fluorescence at 535 nm using a fluorescein calibration curve. At day 21, the sample was heated at 80 °C before measurement. Each data point represents the mean ± standard deviation for a total of three separately prepared and analyzed samples. ..... 134

Figure 4.3 Cumulative release of fluorescent labelled ELP-CLP nanoparticles from type II collagen film as a function of time. Sample (red curve) was pre-heated at 65 °C to partially unfold the CLP triple helix, so that the sample would be able to bind to the collagen film via strand invasion. A non-preheated nanoparticle control (black) was also used. The amount of released nanoparticles was calculated by measuring the fluorescence at 535 nm using a FELP-CLP nanoparticle calibration curve. At day 10, the film was heated at 80 °C before measurement. Each data point for the preheated nanoparticle sample represents the mean ± standard deviation for a total of five separately prepared and analyzed samples. Data for the unpreheated nanoparticle sample represents three samples. ..... 136

Figure 4.4 Activation of murine-derived RAW264.7 macrophages treated with ELP-CLP nanoparticles. RAW264.7 macrophages were cultured on TCPS and incubated with medium only (control), 50 ng/mL LPS, or various concentrations of ELP-CLP nanoparticles for 8 hrs prior to evaluation of TNF-α secretion by macrophage. N=3. ..... 138

Figure 4.5 Cell viability results after 24 hour incubation with serum. All images are with a 10x objective. a,b) phase image and Calcien AM live stain (respectively) of 0 ug/mL NP control; c,d) phase image and Calcien AM live stain of 1000 ug/mL NPs. Scale bars = 100 µm. ..... 140

Figure 4.6 ADTC5 viability and proliferation in the presence of ELP-CLP nanoparticles in vitro. Representative images of ATDC5 cell viability via live (green fluorescence)/dead (red fluorescence) assay and proliferation (differential interference contrast microscopy) at 24 hour and 72 hours post- ELP-CLP nanoparticles application (0 and 1000 ug/mL shown at top and bottom panel, respectively). Application of ELP-CLP nanoparticles does not appear to cause ATDC5 death or change in cell proliferation. Scale bar = 200 µm and applies to all images..... 141

Figure 4.7 Quantitative analysis of ATDC5 viability and proliferation following application of ELP-CLP nanoparticles in vitro. a) ATDC5 cell viability (% live cells) and b) cell proliferation (cell area fraction) following application of 0, 50, 150, 500, and 1000 µg/mL of ELP-CLP nanoparticles. Cell viability and proliferation is unaltered by application of ELP-CLP nanoparticles at any concentration. Results are presented as mean ± SD (n = 3-5 /timepoint/concentration)..... 143

Figure 4.8 Schematic illustration of fluorescein loading and releasing from the ELP-CLP nanoparticles..... 144

Figure 4.9 Dynamic light scattering characterization of the assembly of fluorescein labelled ELP−CLP conjugates. Hydrodynamic diameter of nanostructures (solid spheres) and derived count rate of the scattering light (hollow spheres) were plotted as a function of temperature upon heating. ..... 145

Figure 4.10 Schematic illustration of ELP-CLP nanoparticle retention experiment on type II collagen films..... 146

Figure 4.11 Normalized metabolic activity of RAW264.7 macrophages cultured with ELP-CLP nanoparticles at various concentrations, calculated via fluorescence measurement of the overall reductive capability of the cells. The data was normalized with the results from cells in culture medium without the nanoparticles. Each set of data represents the mean ± standard deviation for a total of at least three separately prepared samples. ..... 146

Figure 4.12 NIH-3T3 fibroblast viability after 24-hour incubation with the ELP-CLP nanoparticles. All images are with a 10x objective. Scale bars = 100 µm. ..... 147

Figure 4.13 ADTC5 viability and proliferation in the presence of ELP-CLP nanoparticles in vitro. Representative images of ATDC5 cell viability via live (green fluorescence)/dead (red fluorescence) assay and proliferation (differential interference contrast microscopy) at 24 hour and 72 hours post- ELP-CLP nanoparticles. Application of ELP-CLP nanoparticles does not appear to cause ATDC5 death or change in cell proliferation. Scale bar = 200 µm and applies to all images. ..... 148

## ABSTRACT

Collagen is the most abundant protein in mammals, and there has been long-standing interest in understanding and controlling collagen assembly in the design of new materials. Collagen-like peptides (CLP), also known as collagen-mimetic peptides (CMP), are short synthetic peptides which mimic the triple helical conformation of native collagens. In the past few decades, collagen like peptides and their conjugated hybrids have become a new class of biomaterials that possesses unique structures and properties. In addition to traditional applications of using CLPs to decipher the role of different amino acid residues and tripeptide motifs in stabilizing the collagen triple helix and mimicking collagen fibril formation, with the introduction of specific interactions including electrostatic interactions, π-π stacking interaction and metal-ligand coordination, a variety of artificial collagen-like peptides with well-defined sequences have been designed to create higher order assemblies with specific biological functions. The CLPs have also been widely used as bioactive domains or physical cross-linkers to fabricate hydrogels, which have shown potential to improve cell adhesion, proliferation and ECM macromolecule production. Despite this widespread use, the utilization of CLPs as domains in stimuli responsive bioconjugates represents a relatively new area for the development of functional polymeric materials.

In this work, a new class of thermoresponsive diblock conjugates, containing collagen-like peptides and a thermoresponsive polymer, namely poly(diethylene glycol methyl ether methacrylate) (PDEGMEMA), is introduced. The CLP domain

maintains its triple helix conformation after conjugation with the polymer. The engineered LCST of these conjugates has enabled temperature-induced assembly under aqueous conditions, at physiologically relevant temperatures, into well-defined vesicles with diameters of approximately 50-200 nm. The formation of nanostructures was driven by the coil/globule conformational transition of the PDEGMEMA building block above its LCST with stabilization of the nanostructures by the hydrophilic CLP. To the best of our knowledge, this is the first report on such assembled nanostructures from collagen-like peptide containing copolymers. Due to the strong propensity for CLPs to bind to natural collagen via strand invasion processes, these nanosized vesicles may be used as drug carriers for targeted delivery.

In addition to synthetic polymers, the collagen like peptide is then conjugated with a thermoresponsive elastin-like peptide (ELP). The resulting ELP-CLP diblock conjugates show a remarkable reduction in the inverse transition temperature of the ELP domain, attributed to the anchoring effect of the CLP triple helix. The lower transition temperature of the conjugate enables facile formation of well-defined vesicles at physiological temperature and the unexpected resolubilization of the vesicles at *elevated* temperatures upon unfolding of the CLP domain. Given the ability of CLPs to modify collagens, this work provides not only a simple and versatile avenue for controlling the inverse transition behavior of elastin-like peptides, but also suggest future opportunities for these thermoresponsive nanostructures in biologically relevant environments.

In the last section, the potential of using the ELP-CLP nanoparticles as drug delivery vehicles for targeting collagen containing matrices is evaluated. A sustained release of clinically relevant amount of encapsulated modelled drug is achieved within

three weeks, followed by a thermally controlled burst release. As expected, the ELP-CLP nanoparticles show strong retention on collagen substrate, via specific binding through collagen triple helix hybridization. Additionally, cell viability and proliferation studies using fibroblasts and chondrocytes suggest the nanoparticles are non-cytotoxic. Additionally, almost no TNF-α expression from macrophages is observed, suggesting that the nanoparticles do not initiate inflammatory response. Endowed with specific collagen binding, controlled thermoresposiveness, excellent cytocompatibility, and non-immune responsiveness, we believe the ELP-CLP nanoparticles are promising candidates as drug delivery vehicles for targeting collagen containing matrices.

Considering the critical role of collagens in extracellular matrix and the unique ability of the CLP to target native collagens, our work offers significant opportunities for the design of collagen-like peptides and their bioconjugates for targeted application in the biomedical arena.

# Chapter 1

# BACKGROUND

## 1.1 Introduction

Collagen is the main component of the extracellular matrix (ECM) and comprises 25% to 35% of whole body protein content in humans. The collagens are a large family of proteins, comprising 29 different types, which have widespread functions such as mediating cell adhesion, cell migration, tissue scaffolding and repairing. The most prevalent class of collagen – fibrous collagen – includes type I, II, and III collagens and is the main component of tendon, ligament, skin, cartilage and bone. Other types of collagens, such as type IV and type VIII collagen, play a vital role in the formation of network structures such as basement membranes. Fundamentals about the classification and biological functions of collagen will not be discussed here, but interested readers are directed to previous reviews for more detailed information on this topic.[1, 2]

Although the architectures and roles of these collagens vary widely, they all comprise triple helix bundles.[3] The collagen triple helix comprises three polyproline-II type helices held together by periodic interchain hydrogen bonding between the glycine amide in one chain and the carbonyl of the amino acid of an adjacent chain. Each strand of the helix consists of regularly repeated Gly-X-Y tripeptide repeats, with every third residue comprising glycine. Proline (Pro) and (4R)-hydroxyproline (Hyp) occupy the X and Y positions of the triplet repeats at the highest statistical frequency within native collagens.

Due to the excellent gel-forming abilities and biodegradability of the natural collagens, they have been widely used as biomedical materials for tissue support and regeneration.[4, 5] However, some of the limitations of using animal-derived collagens, such as their thermal instability, possible contamination with pathogenic substances,[6] and relative difficulty in the introduction of specific sequence modifications, have motivated the use of synthetic model collagens, also known as collagen-like peptides (CLPs) or collagen-mimetic peptides (CMPs), in these types of applications. These collagen-mimetic sequences have been employed to elucidate the triple helix structure and the stabilization effect of different amino acid residues,[7-11] and more recently, a variety of CLPs with novel sequences and interactions have been developed to mimic collagen fibril formation and to produce other higher-order supramolecular structures.[12-16]

In addition to peptide-based assembly, the self-assembly of amphiphilic block copolymers has long been a very useful tool to fabricate nanostructured materials. Combining advantages of synthetic polymers, such as flexibility in architecture and functionality,[17-19] biocompatibility, and mechanical strength, as well as stimuli responsiveness,[20] with advantages of (poly)peptides including monodispersity, precise primary to tertiary structure, and specified bioactivity,[21] polymer-peptide bioconjugates are of particular recent interest, especially in biomedical applications such as drug and gene delivery.[22-24] Polymer conjugates with α-helical coiled-coil peptide domains,[25-28] β-sheet peptide motifs,[29-31] and elastin mimetic peptides[32-34] have been widely employed. However, compared to these biohybrid materials, polymer-collagen like peptide bioconjugates represent a relatively new area for the development of functional polymeric materials.[35-38]

## 1.2 Triple Helix Stability

The increasing demand for collagen-related peptides, as drug delivery vehicles, labeling agents, and tissue engineering scaffolds with select bioactivity, requires understanding of the thermal stability and specific binding properties with of CLPs with certain biomaterials. Understanding triple helix stability and factors affecting it is thus of particular significance in the design of such sequences. In early work in this area, Brodsky and coworkers[39] described the propensities for all natural amino acids to form stable triple helical structures. Triplets with the form Gly-X-Hyp and Gly-Pro-Y were used as guest sequences in the context of the $(Gly\text{-}Pro\text{-}Hyp)_8$ host peptide, to form model CLPs with the sequence Ac-$(Gly\text{-}Pro\text{-}Hyp)_3$-Gly-X-Hyp-$(Gly\text{-}Pro\text{-}Hyp)_4$-Gly-Gly-$CONH_2$ or Ac-$(Gly\text{-}Pro\text{-}Hyp)_3$-Gly-Pro-Y-$(Gly\text{-}Pro\text{-}Hyp)_4$-Gly-Gly-$CONH_2$. The melting temperatures of these model peptides with substitutions of all natural amino acids in the X and Y positions were studied via circular dichroic spectroscopy (CD); the results of these detailed studies are provided in Table 1. These results confirmed that placement of the imino acids Pro at the X position and Hyp at Y position have the best stabilizing effect, while Gly and aromatic residues tend to destabilize the triple helix. Since then, there have been a wide variety of studies aimed at determining the molecular details of stable triple helix assembly.

Table 1.1 Melting temperatures of host-guest peptides (Reproduced with permission from Ref. 39 © American Chemical Society)

| Gly-X-Hyp | Tm (˚C) | Gly-Pro-Y | Tm (˚C) |
|---|---|---|---|
| **Pro** | 47.3 | Hyp | 47.3 |
| **Glu** | 42.9 | Arg | 47.2 |
| **Ala** | 41.7 | Met | 42.6 |
| **Lys** | 41.5 | Ile | 41.5 |
| **Arg** | 40.6 | Gln | 41.3 |
| **Gln** | 40.4 | Ala | 40.9 |
| **Asp** | 40.1 | Val | 40.0 |
| **Leu** | 39.0 | Glu | 39.7 |
| **Val** | 38.9 | Thr | 39.7 |
| **Met** | 38.6 | Cys | 37.7 |
| **Ile** | 38.4 | Lys | 36.8 |
| **Asn** | 38.3 | His | 35.7 |
| **Ser** | 38.0 | Ser | 35.0 |
| **His** | 36.5 | Asp | 34.0 |
| **Thr** | 36.2 | Gly | 32.7 |
| **Cys** | 36.1 | Leu | 31.7 |
| **Thr** | 34.3 | Asn | 30.3 |
| **Phe** | 33.5 | Thy | 30.2 |
| **Gly** | 33.2 | Phe | 28.3 |
| **Trp** | 31.9 | Trp | 26.1 |

### 1.2.1 Role of (4R)-hydroxyproline

From Table 1, it is clear that, when only considering the natural amino acids, any replacement of Pro in the X position and Hyp in the Y position destabilizes the collagen triple helix. The importance of Pro and Hyp in the X and Y residues in the collagen triple helix is further suggested by the fact that 10.5% of Gly-X-Y triplets within human collagens are Gly-Pro-Hyp and 38% of the amino acids in the Y position are (4R)-hydroxyproline.[40] While the glycine residues are buried in the middle, the side chains of amino acids in the X and Y positions are generally exposed to water,[41] and the particular importance of Hyp residue at the Y position in

collagen structures was originally attributed to the formation of water-mediated hydrogen bonds between the strands.[42-45]

This long-held hypothesis was challenged by work reported by Raines and coworkers in 1998, [46, 47] in which the hydroxyprolines in $(Gly\text{-}Pro\text{-}Hyp)_{10}$ were replaced with (2S, 4R)-4-fluoroproline (Flp) to yield the new sequence $(Gly\text{-}Pro\text{-}Flp)_{10}$. The new peptide was able to form a hyperstable triple helix with a melting temperature of 91°C, dramatically higher than that of $(Gly\text{-}Pro\text{-}Pro)_{10}$ or $(Gly\text{-}Pro\text{-}Hyp)_{10}$. Since fluorine groups do not form strong hydrogen bonds,[48] the stabilization imparted by the inclusion of Flp was indicated to arise from the high electronegativity of the Cγ substitute.[49] Additionally, CLPs with peptide sequences $(Gly\text{-}Pro\text{-}hyp)_{10}$ and $(Gly\text{-}Pro\text{-}flp)_{10}$ (where hyp stands for (4S)-hydroxyproline and flp stands for (4S)-4-fluoroproline) do not form triple helix,[50, 51] indicating that the stereoelectronic effect of the Cγ substitute is another factor which affects triple helix stability.[51, 52] Through studying the molecular structure of Ac-Flp-OMe, Bretscher et al.[51] demonstrated that the trans prolyl peptide bond isomer and an optimal main-chain dihedral angle (ψ), required for triple helix formation, were stabilized by the strong $O_0 \cdots C_1$ interaction afforded by Flp (Figure 1.1, black arrow). The stereoelectronic effect was also observed to stabilize 4-chloroproline containing CLP $(Pro\text{-}Clp\text{-}Gly)_{10}$[53]. Furthermore, introduction of an azobenzene-derived chromophore [54] permits control the folding and unfolding of collagen triple helix by photo-isomerization of the “light switch”, thus narrowing the gap between theoretical and experimental investigations on collagen like triple helix.

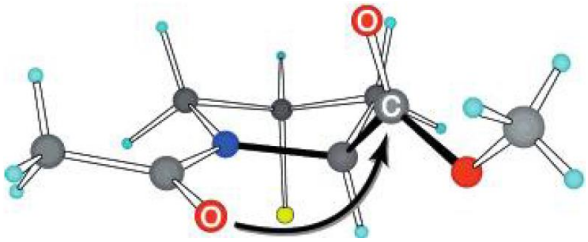

Figure 1.1 Structure of Ac-Flp-OMe. (Reprint with permission from Ref. 51 © American Chemical Society)

### 1.2.2 Electrostatic interactions

In addition to the imino acids Pro and Hyp, non-imino residues, especially charged amino acids such as Lys, Arg, Glu and Asp, comprise up to 15-20% of all residues in collagen and more than 40% of Gly-X-Y triplets contain at least one of these ionizable residues.[40] These charged amino acids are crucial for self-association of collagen fibers and ligand binding to certain biomolecules, as well as contributions to collagen triple helix stability. The importance of these interactions arises from the one-residue staggering between chains of the triple helix structure and the right-handed rotation of the helix bundle, which brings the residues into very close proximity and gives rise to possible interchain electrostatic interaction and hydrogen bonding between charged residues located at these positions (Figure 1.2).[55, 56]

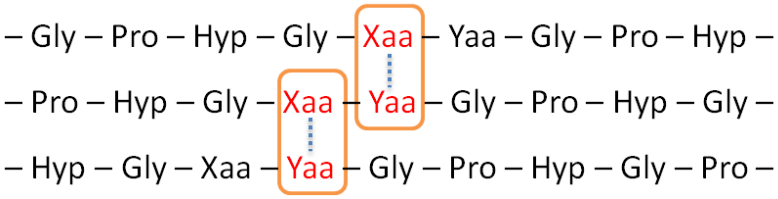


Figure 1.2 Potential interchain interaction between residue at X position of one chain and residue at Y position of another.

Such pairwise interactions have been widely studied using model peptides. Investigations of the melting temperatures of host-guest CLPs ($(GPO)_3GXY(GPO)_4GG$) [55] illustrated that triplets with opposite charged residues at X and Y position (such as Gly-Lys-Asp and Gly-Arg-Asp) showed a major stabilizing electrostatic interaction; while triplets with like-charged residues (e.g., Gly-Lys-Arg and Gly-Arg-Lys) showed electrostatic repulsion and destabilization of the collagen helix. In addition to interactions within the same triplets, similar stabilizing electrostatic interactions were also observed between adjacent triplets. A study of the thermal stability of peptides in the form $(GPO)_3$-G-X-Y-G-X'-Y'-$(GPO)_3$[57] suggested a strong stabilization effect in the presence of GPKGEO or GPKGDO sequences, leading to $T_m$ values of the two peptides equal to that in unsubstituted $(GPO)_8$. Molecular modeling studies suggested that the stabilization may be attributed to interstrand pairwise interaction between positively charged Lys and negatively charged Glu/Asp in the adjacent triplet (Figure 1.3a). Hartgerink and coworkers further divided this interaction into two categories: one called axial contact, involving interactions from the leading chain to the middle chain as well as from the middle chain to the lagging chain; another called lateral contacts involving interactions from the lagging chain to the leading chain. They further proposed that the stabilization mainly originates from the two axial interactions (Figure 1.3b).[7, 58] Deciphering such interchain electrostatic interactions are crucial to understand the stability and the registration process of natural collagens as well as to more effectively design collagen related peptides.

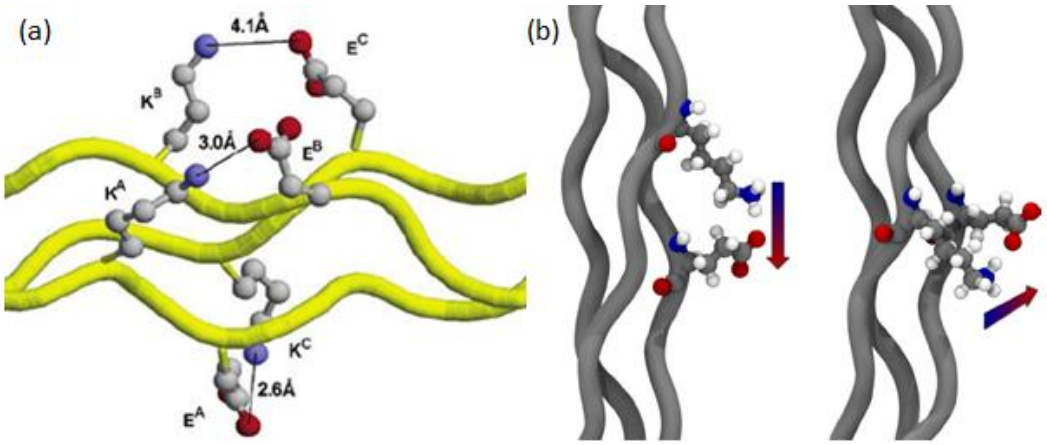


Figure 1.3 Pairwise interactions between Glu and Lys in GPKGEO containing CLPs. (a) computer model proposed by Persikov et al; (b) axial (left) and lateral (right) interactions proposed by Fallas et al. (Reprinted with permission from Ref. 57 © American Chemical Society and Ref. 7 ©American Society for Biochemistry and Molecular Biology)

### 1.2.3 Cystine knots

The homotrimeric collagen type III contains two adjacent cysteine residues at the C-terminus, which form three disulfide bonds between the chains at the non-collagenous domains (Figure 1.4).[59] This cystine knot was found to provide an efficient nucleus for triple helix growth from C-terminus in a zipper-like mechanism[60]. Moroder and coworkers[10] studied the role of the cystine knot on collagen folding and stability and found that the thermostability of cystine knot-linked $(POG)_5$ was dramatically improved (compared with $(POG)_5$ without a cystine knot), with an increase of melting temperature from 20.3 °C to 68.0 °C. Similar stabilization was also observed in hydroxyproline-lacking collagen-like peptides.[16, 61]

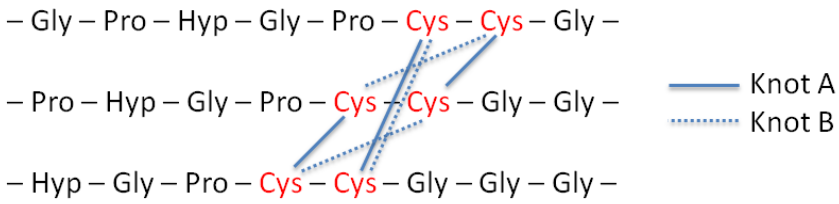


Figure 1.4 Two types of cystine knot connectivities.

### 1.2.4 Template stabilization

In addition to natural templates such as the cystine knot, another well-known method to stabilize the collagen helix is to link three α-chains covalently at the C-terminus. When conjugated to templates such as cis,cis-1,3,5-trimethylcyclohexane-1,3,5-tricarboxylic acid (Kemp triacid),[62, 63] tris(2-aminoethyl)amine-(suc-OH)$_3$ (TREN-(suc-OH)$_3$)[63] and the N-terminus of the bacteriophage T4 fibritin foldon domain,[64] the thermostablility of various collagen-like peptides has been dramatically improved (Table 2), and the triple helix folding process also significantly accelerated.[62] The stabilization from these templates arises from the reduction of the entropy difference between the unfolded and folded states of the CLP domain, as well as the presence of a higher concentration of collagen strand at the C-terminus.

Table 1.2 Comparison of melting temperature of CLP with/without the template. (Data taken in part from Ref. 62, 63 © American Chemical Society and Ref. 64 © Academic Press.)

| Collagen like peptides | Melting temperature (°C) | | | |
|---|---|---|---|---|
| | n=3 | n=5 | n=6 | n=10 |
| Ac-(Gly-Pro-Hyp)$_n$-NH$_2$ | NT[a] | 18 | 36 | - |
| KTA-[Gly-(Gly-Pro-Hyp)$_n$-NH$_2$]$_3$ | 30 | 70 | 81 | - |
| Ac-(Gly-Nleu-Pro)$_n$-NH$_2$ | NT | - | 26 | - |
| KTA-[Gly-(Gly-Nleu-Pro)$_n$-NH$_2$]$_3$ | NT | - | 36 | - |
| TREN-[suc-(Gly-Nleu-Pro)$_n$-NH$_2$]$_3$ | NT | 38 | 46 | - |
| (Gly-Pro-Hyp)$_n$ | - | - | - | 23 |
| T4 fibritin foldon (Gly-Pro-Hyp)$_n$ | - | - | - | 65 |

[a]NT denotes no transition observed.

Similar stabilization has been observed for CLPs in which the C-terminus is conjugated to hydrophobic groups or synthetic polymers. Instead of a template that covalently links the three strands, the hydrophobic interactions of the attached moieties bring the strands into close proximity in aqueous solution, thus accelerating triple helix formation. For example, the thermostability of collagen triple helices from peptide-amphiphiles with collagen-peptide head groups and alkyl chain tails is substantially higher than that of peptides without lipidation and the stability increases with the length of the lipid tail.[35, 36, 65] Most recently, our group, in collaboration with the Theato group,[38, 66] designed a polymer-CLP-polymer triblock system, in which both C- and N-termini of the collagen-like peptide were conjugated to a thermoresponsive polymer, to investigate the influence of conjugated macromolecules on the conformational behavior of the collagen domain. The denaturing profile of the

triblock, assessed via circular dichroic spectroscopy, suggested that the polymer-conjugated peptide domain was still capable of assembly into a stable collagen triple helix. More interestingly, in contrast to the standard sigmoidal unfolding curve for the CLP alone, the triblock showed a more gradual unfolding with two potential transitions, indicating that above its LCST, the collapsed thermoresponsive polymer constricted the unfolding of the peptide and stabilized the collagen-like triple helical domain.

### 1.3 Higher Order Assembly

In vivo, natural collagens self-assemble into higher order hierarchical structures with precise chemical compositions and molecular structures, which are of essential importance in ECM pathology and development.[2] The wealth of knowledge in understanding collagen structure accumulated in the past few decades has given rise to a surge in research activities focused on supramolecular assembly of collagen-like peptides. Although much of the research is still in early stages, the results are of significant importance in developing collagen-like materials in biomedical applications. Collagen-like peptides as simple as $(Pro\text{-}Hyp\text{-}Gly)_{10}$ are indicated to form higher order structures[67] via a nucleation and growth mechanism, similar to natural collagen, although form branched filamentous structures rather than the long fibrous structures of native collagen. Recently, synthetic collagen fibers which bear more similarity to natural collagen fibers have been produced successfully by various well-designed CLP systems and assembly strategies.

### 1.3.1 π-π stacking interaction

Maryanoff and coworkers reported a novel collagen like peptide that is able to self-assemble into triple helical, micrometer-scale fibrillar structure through noncovalent end-to-end interactions.[68, 69] In this work, phenylalanine, which has an electron-rich benzyl ring, and pentafluorophenylalanine, which has an electron-poor benzyl ring, were introduced at the C- and N-terminus of the collagen-like peptide $(Gly\text{-}Pro\text{-}Hyp)_{10}$ (Figure 1.5a). When the phenyl/pentafluorophenyl pairs from two adjacent triple helices approached face to face, the overall interface energy decreased about 55.2kcal/mol, leading to the formation of micrometer-long fibrils with an average diameter of 0.26 μm (Figure 1.5b, c). In addition to end-to-end (linear) interactions, the dimensions of these fibrils also require side-to-side (lateral) interaction. Most importantly, this CLP stimulated aggregation of human blood platelets, demonstrating the potential use of the peptide as a hemostatic material.

In addition to π-π stacking, similar interactions, such as CH···π interaction between imino acids (Pro and Hyp) and aromatic residues (Phe and Tyr);[70] as well as cation···π interaction between positive charged N-terminal Arg and C-terminal Phe[71] were also introduced for the fabrication of collagen like fibrillar structures.

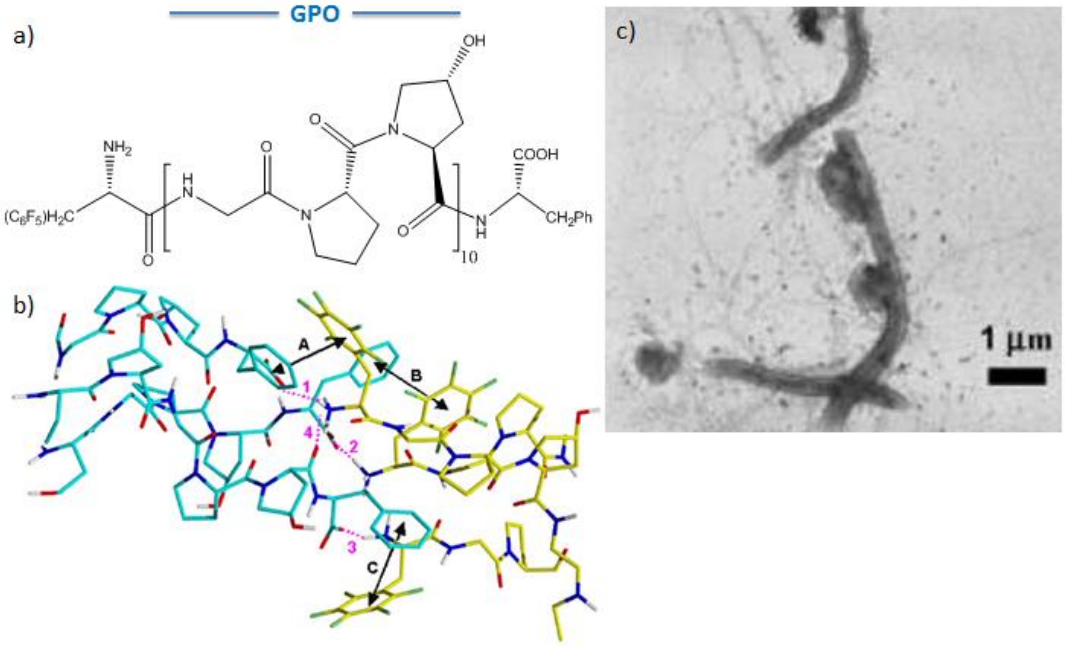


Figure 1.5 CLP self-assembly via π-π stacking interaction. (a) $(GPO)_{10}$ end-functionalized with pentafluorophenylalanine and phenylalanine. (b) Interface between two triple helices (one blue, one yellow) showing three aromatic stacking interactions (black double-headed arrows; A-C). (c) TEM image of self-assembled CLP. (Reproduced with permission from Ref. 68 © The National Academy of Sciences of the USA and Ref. 69 © American Chemical Society.)

### 1.3.2 Lateral electrostatic interactions

Natural collagen type I, II, III, V and XI self-assemble into 67nm-periodic cross-striated fibrils.[2] This D-periodicity arises from the differential inter-procollagen interactions, including hydrophobic interaction and electrostatic interactions between oppositely charged side chains. These interactions are optimized when the protomers are placed parallel to the nearest neighbor, with a pre-defined stagger distance.[72] Partially due to the difficulty in precise control of these interactions between the protomers at staggered positions, artificial collagen-like fibrils with periodic bands have not been produced until recently.

Work by Rele et al. [73] first reported a fibrous structure with well-defined D-periodicity from collagen-like peptide self-assembly. The peptide $(PRG)_4(POG)_4(EOG)_4$ contains three different domains, with a central POG repeat sequence flanked by a positively charged domain at N-terminus and a negatively charged domain at the C-terminus (Figure 1.6a). After 9-day incubation at room temperature, micron-length fibers with well-defined transverse bands were observed via transmission electron microscopy (TEM) (Figure 1.6c). These fibers were self-associated following a nucleation-growth mechanism, driven by hydrophobic interaction between the central domain and lateral electrostatic interaction between oppositely charged residues from two neighboring triple helices (Figure 1.6b).

More recently, O'Leary et al.[14] demonstrated that due to the very tight hydrogen bonding between the arginine side chain and the backbone carbonyl of an adjacent strand, the arginine residue in the CLP mentioned above was unable to interact with the glutamic acid efficiently. By replacing all the Arg residues with Lys residues, and Glu residues with Asp, a new peptide with sequence $(PKG)_4(POG)_4(DOG)_4$ was produced, which had stronger interaction between intermolecular, oppositely charged Lys and Asp residues. As predicted, the new peptide formed homogeneous collagen mimetic nanofibers. More interestingly, these nanofibers were also able to form high quality hydrogels, which degrades at a similar rate to rat-tail collagen (Figure 1.6d).

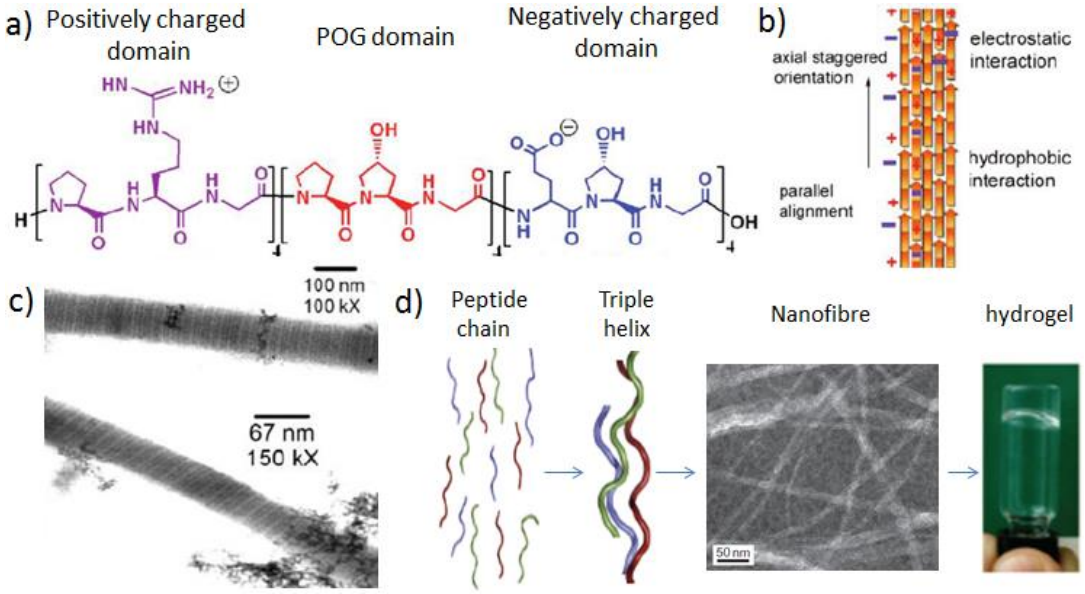


Figure 1.6 Self-assembly of CLP via lateral electrostatic interaction. (a) Amino acid sequence of CLP, indicating three different domains. (b) Axial staggered interchain electrostatic interactions. (c) Well-defined D-periodicity observed via high resolution transmission electron microscopy. (d) Multi-hierarchical self-assembly of related collagen-mimetic peptides. (Figure a, b, c are reproduced with permission from Ref. 73 © American Chemical Society, Figure d is reproduced with permission from Ref. 14 © Macmillan Publishers Limited.)

### 1.3.3 Metal-triggered assembly

In addition to lateral electrostatic interactions, coordination bonds between metal ions and specific ligands can also be introduced for controlled self-assembly of collagen-like peptides. Chmielewski and coworkers designed a stimuli-responsive coassembly system, which involves two collagen-like peptides, each individually containing a $(Pro\text{-}Hyp\text{-}Gly)_9$ core and identical metal binding units at both termini (Figure 1.7a).[13] One peptide, HisCol, contains two histidines at both termini; the other peptide, IdaCol, contains an iminodiacetic acid (Ida) moiety incorporated onto the side chain of lysine at both termini. By adding divalent metal ions such as $Ni^{2+}$,

$Zn^{2+}$ and $Cu^{2+}$, the CLPs co-assemble into petal-like microstructures with a periodic banding at the nanometer scale. The distance between the banding gaps was found to be in the range of 9-12 nm, which approximately corresponds to the length of $(POG)_9$ collagen triple helix with termini modifications (Figure 1.7b). Subsequent results from the same group demonstrated that by varying the length of the $(POG)_n$ core of the peptides, a range of distinct structures including microflorettes, stacked sheet microsaddles, and fiberlike meshes, can be generated (Figure 1.7c).[12] Similar metal-triggered assembly of supramolecular structures was also obtained from hydroxyproline-lacking CLPs designed by Hsu and coworkers.[74] In this work, histidine residues were not only incorporated at the termini of the peptide domain, but also incorporated in the center of the peptide domain. Two distinct CLPs, with sequences HG(PPG)9GH (X9) and HG(PPG)4(PHG)(PPG)4GH (PHG) were synthesized respectively. A variety of higher-order structures were obtained from incubation with metal ions, ranging from nanofibrils to microscale spherical, laminated and granulated assemblies (Figure 1.7d).

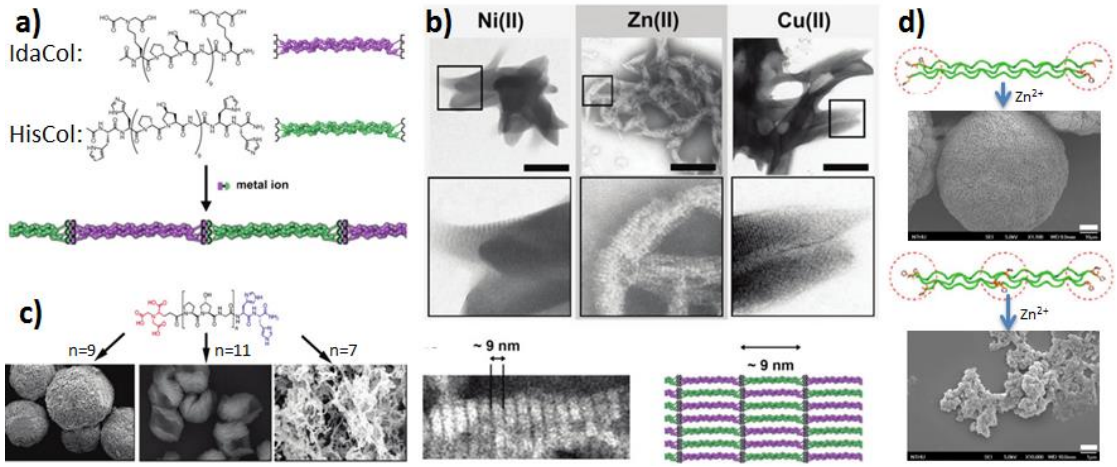


Figure 1.7 (a) Scheme showing the structure of IdaCol and HisCol and subsequent tandem assembly. (b) TEM images of petal like structures with periodic bands observed from metal triggered CLP self-assembly. (c) Assembled structures depend on length of CLP domain. (d) SEM images of large aggregates of X9 (top) and PHG (bottom) after incubating with $Zn^{2+}$. (Reproduced with permission from Ref. 12, 13 and 74 © American Chemical Society)

In addition to end-to-end metal-ligand coordination, metal-triggered radial growth of collagen-like peptide triple helices into fibrous structures can also be achieved via these methods.[15] By replacing the hydroxyproline residue in the central tripeptide of $(Pro\text{-}Hyp\text{-}Gly)_9$ with a bipyridyl-modified lysine, the new peptide can be triggered to form branched collagen fibers by addition of metal ions ($Fe^{2+}$) (Figure 1.8). Although the assembled fibers lack the periodic bands of natural collagen, these data provide proof that collagen-like fibers can be generated via nonlinear assembly.

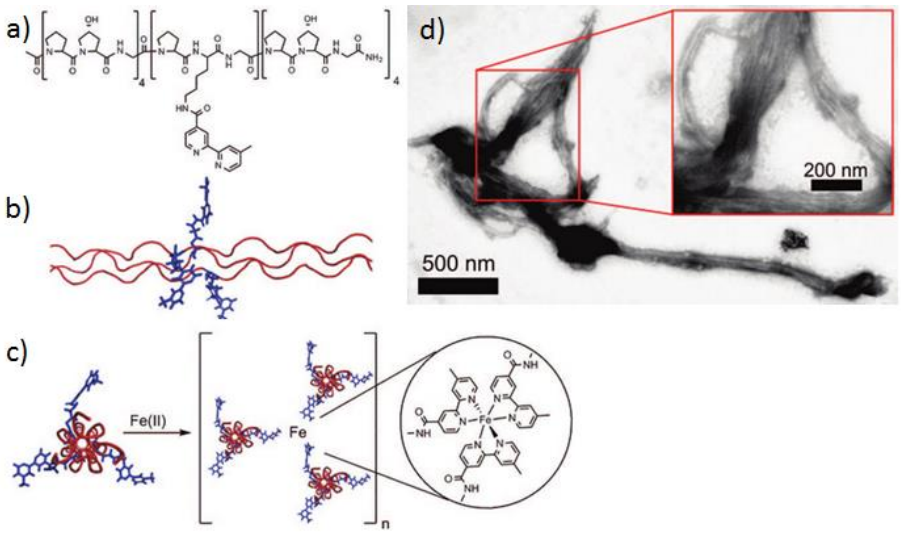


Figure 1.8 Metal-triggered radial assembly of collagen peptide fibers. (a) amino acid sequence of the CLP. (b) Side view of the triple helix. (c) Hypothesized interaction between bipyridyl-modified lysine and $Fe^{2+}$. (d) TEM image of the assembled structure. (Reproduced with permission from Ref. 15 © American Chemical Society)

## 1.4 Triple Helix Hybridization

In addition to the majority of CLP research that studies triple helix stability and higher order assembly, Yu and coworkers have made important contributions to utilizing the binding interactions between CLP and native collagens for a range of applications. They reported that unfolded single stranded collagen-like peptides have a strong propensity to bind to natural collagen via a strand invasion process (Figure 1.9a).[75] CLPs attached to natural collagens were visualized via transmission electron microscopy conducted on CLP functionalized with electron-dense gold nanoparticles (Figure 1.9c).[76]

Based on this physical hybridization binding effect, they further introduced fluorescently labeled CLPs as collagen-specific stains in sodium dodecyl sulfate polyacrylamide gel electrophoresis (SDS-PAGE) for direct detection of various types

of collagens including intact type I, II, IV collagen, and MMP-cleaved type I collagen.[77] Collagen bands containing as little as 5 ng were successfully detected, suggesting a high staining efficiency. These fluorescently labeled CLPs were also utilized as staining reagents for native collagens in human tissues including skin, cornea, bone[77] and liver.[78] Images of CLP-stained human liver tissue were almost identical to images stained by collagen antibodies (Figure 1.9b).[78]

The binding interaction between CLP and natural collagen was also used for encoding cellular cues in collagen scaffolds. For example, studies from the same group[79] reported a new collagen-like peptide consisting of eight negatively charged glutamic acid residues at the N-terminus of $(Pro\text{-}Hyp\text{-}Gly)_9$. The anionic CLP was not only able to bind to type I collagen via strand-strand hybridization, but also able to attract vascular endothelial growth factors (VEGFs) through electrostatic interactions, which then induced tubulogenesis of endothelial cells (ECs) pre-encapsulated within the collagen substrate.

In order to test the ability of the CLP to target pathological tissues of high MMP activity, *in vivo* tumor targeting experiments were conducted on mice bearing subcutaneous PC-3 prostate tumor xenografts.[80] The results suggested that the fluorescently labeled CLP was able to permeate the tumor vasculature and accumulate at the tumor sites (Figure 1.9d). In addition to tumors, *in vivo* studies also suggested a high level of accumulation of the CLP within the skeleton and joints, especially in regions with high MMP and collagen remodeling activity such as articular cartilage of the knee joints (Figure 1.9e).

As the peptide can be integrated, with high stability, into native collagen both *in vitro* and *in vivo*, these research activities suggest that approaches which employ

CLPs should thus offer particular promise for biomedical applications such as tumor, bone and cartilage imaging, as well as targeted drug delivery into these regions. Despite this widespread use, the utilization of CLPs as domains in responsive nanoparticles has been described in only a very limited number of reports.[37, 38, 81, 82]

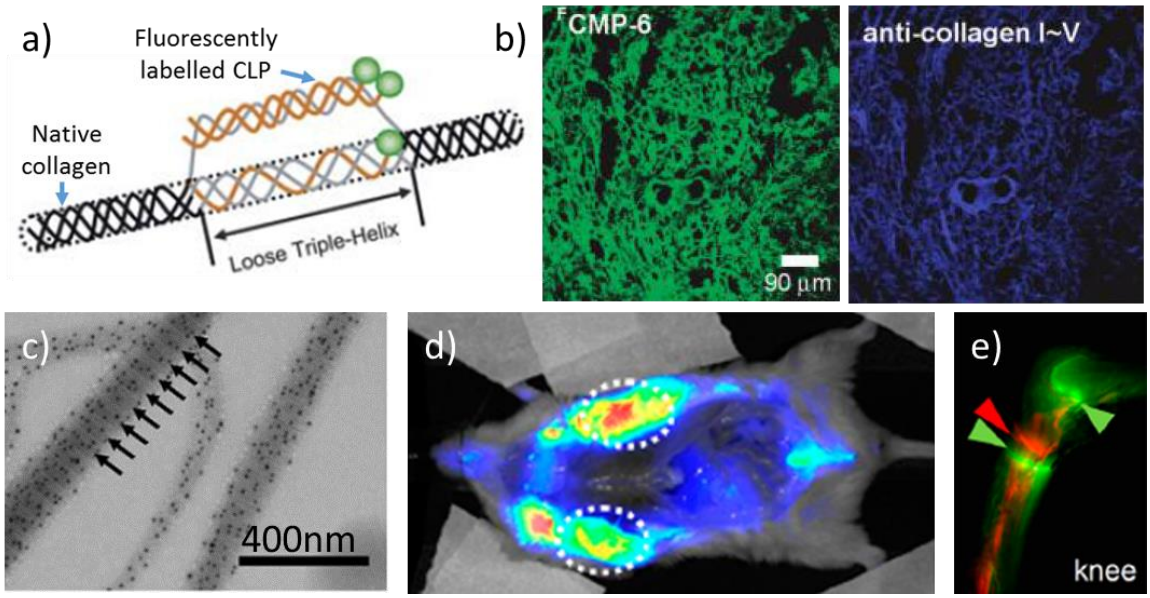


Figure 1.9 a) Schematic of collagen triple helix hybridization; b) CLP labels collagens of human liver tissue as efficiently as collagen antibodies; c) TEM micrographs of reconstituted type I collagen fibers labelled with CLP functionalized gold nanoparticles; d) *In vivo* NIRF images of mice bearing PC-3 prostate tumors administered with fluorescent labelled $(GPO)_9$ CLP indicate specific tumor accumulation; e) Dual-NIRF image of the knee joint showing the uptake of fluorescent labelled CLP (red) and BoneTag™ (stains calcifying tissues in green), CLP-specific uptake can be seen within the articular cartilage and meniscus (red arrowhead) as well as focal regions within the tibia and the femur head. (reproduced with permission from Ref. 76, 78, 80, 83)

## 1.5 Synthetic Polymer – CLP Bioconjugates

Polymer–peptide bioconjugates are hybrid materials, in which one or more traditional synthetic polymeric domains are covalently bound to peptide domains with specific sequences and functionalities.[83] The combination of peptides with synthetic polymers in a single hybrid molecule offers unique opportunities to combine the advantages of the two. Although peptide-based materials exhibit a variety of well-defined hierarchical structures and important biological functions such as cell recognition and adhesion,[84-86] their use in therapeutic applications is limited since they can cause immune response and are easily degraded by enzymes and thus have short circulation times *in vivo*.[87, 88] On the other hand, while biocompatibility and high resistance to enzymatic degradation have been observed for well controlled synthetic polymers, they are biologically inactive due to the lack of precisely controlled molecular structures. The bioconjugation of peptide and synthetic polymers has thus become a useful tool to overcome these limitations of the two components. For example, conjugation of poly(ethylene glycol) (PEG) to various protein-based drugs, enzymes and antibodies endows the conjugates with certain beneficial properties such as improved solubility, reduced immunogenicity, as well as increased blood circulation time.[87] Compared to the recent surge of research activities on polymer-peptide conjugates involving peptides with α-helix and β-sheet secondary structure,[29] such conjugates with collagen like-peptides have not been as intensively studied.[37, 38]

The most convenient way to synthesize polymer-peptide conjugates is to couple a functionalized peptide, either at the termini or side chain, with a complementary functionalized synthetic polymer. Although there are some difficulties in this approach, such as low accessibility of functional groups on macromolecules

and separation of the desired conjugate from the starting materials, a variety of chemical reactions have been employed for efficient conjugation, including traditional solid phase peptide coupling chemistry,[89-91] Staudinger ligation,[92] Schiff base formation,[93-96] click reaction[97-100] and Michael-type addition.[101-104]

### 1.5.1 Assembly of polymer–CLP conjugates

The utilization of the efficient conjugation reactions discovered in the past few decades has given rise to an expansion in the design of novel self-assembled structures based on polymer-peptide biohybrid materials with promising chemical and biological functions.[105, 106] Nonetheless, self-assembly of polymer conjugates with collagen-like peptides remains a fresh research area, and in 2011, Tong and coworkers[37] reported the self-assembly of a collagen-like peptide amphiphile. With a C16 lipophilic tail attached to the C-terminus of a CLP with the sequence $(GPO)_3GFOGER(GPO)_3$, the amphiphile self-assembled into micrometer-long nanofibers with a diameter of approximately 16nm under aqueous conditions. More importantly, given the inclusion of the integrin-specific binding sequence GFOGER, the amphiphile was shown to promote the adhesion and spreading of HepG2 cells.

More recently, we have reported the conformational and assembly behavior of a thermoresponsive polymer-CLP-polymer triblock.[38, 66] The triblock comprises a thermoresponsive polymer, namely poly(diethylene glycol methyl ether methacrylate) (PDEGMEMA), conjugated to both termini of a triple-helix forming hydroxyproline-lacking collagen-like peptide (Figure 1.10a). Morphology study at 37 °C suggested that the collapse of polymeric domain above its LCST caused the formation of large hollow spherical structures (Figure 1.10b). More interestingly, a morphological transformation into fibrils (Figure 1.10c) was observed at 75 °C, likely due to the

unfolding of the collagen triple helix domain. As a negative control, PEG-CLP conjugates were also synthesized, but did not assemble into such structures. This work provides further evidence that higher-order structures, including fibrils, can be obtained from appropriately designed polymer-conjugated collagen-like peptides.

In addition to copolymers containing CLP and traditional synthetic polymers, CLP-related peptide-peptide conjugates have also been studied very recently. Yu and coworkers [75, 76, 80] reported that unfolded collagen-like peptides had a strong propensity to bind to denatured collagen strands via stereo-selective triple-helical hybridization. Based on this physical hybridization binding effect, they further designed a conjugate peptide including eight negative charged glutamic acid at the N-terminal of $(Pro\text{-}Hyp\text{-}Gly)_9$.[79] The new peptide is not only able to bind collagen scaffolds via strand-strand hybridization, but also able to immobilize vascular endothelial growth factor (VEGF) through electrostatic interactions. These results show that polymer-CLP bioconjugates may have potential in targeted drug delivery, especially for cartilage- and bone-related diseases.

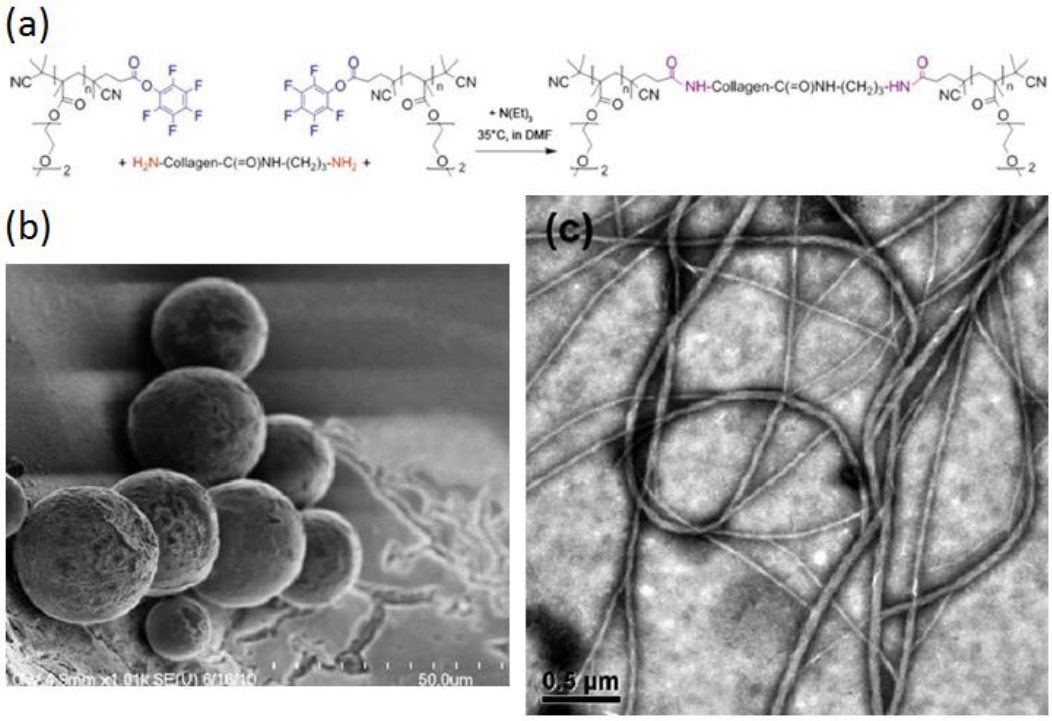


Figure 1.10 (a) Synthesis of hybrid triblock copolymer. Collagen like peptide sequence: $G(GPP)_3GPRGEKGERGPR(GPP)_3GPCCG$. (b) Cryo-TEM image of spherical structures at 37 °C. Scale bar = 50 µm (c) TEM image of collagen like fibrils at 75 °C. Scale bar = 0.5 µm (Reproduced with permission from Ref.38 © The Royal Society of Chemistry and Ref.66 © American Chemical Society)

### 1.5.2 Collagen/CLP containing hydrogels

Due to the excellent mechanical and unique biological properties of collagen, collagen containing 3-dimentional porous hybrid hydrogels has become a very useful tool to mimic the structure and functions of microenvironment in extracellular matrix (ECM) and has been widely used in articular cartilage tissue engineering and regeneration. In order to obtain desired mechanical and physiological properties of the scaffolds, a variety of other components rather than collagen have been incorporated to form the hydrogels. These components includes not only synthetic polymers such as

poly(ethylene glycol) (PEG),[107-109] poly(ethylene oxide) diacrylate (PEODA),[110] poly(lactic-co-glycolic acid) (PLGA),[111, 112] and poly(ethylene terephthalate) (PET),[113] but also naturally occurring biomacromolecules such as hyaluronic acid,[108, 114-116] and chitosan.[109, 115]

In addition to produce higher-order supramolecular structures from well-designed sequences, collagen like peptides have also been used to fabricate scaffolds for tissue engineering applications. For example, Hartgerink and coworkers reported CLP with sequence $(Pro\text{-}Lys\text{-}Gly)_4(Pro\text{-}Hyp\text{-}Gly)_4(Asp\text{-}Hyp\text{-}Gly)_4$ was able to form stable hydrogel at concentrations as low as 0.5 wt%, triggered and stabilized by lateral electrostatic interaction between triple helices (Figure 2a).[14] The hydrogel exhibited a storage modulus of approximately 700 Pa and it could be degraded by collagenase at a similar rate to that of natural collagen. Because CLPs have the capacity to form stable triple helix at physiological temperature, they have also been utilized as physical hydrogel cross-linkers. By conjugating the N-terminal amine of CLP single strand to NHS ester functionalized 4-armed, Yu and coworkers[117] reported a novel type of PEG-hydrogel, which was cross linked by intermolecular collagen triple helix formation (Figure 2b). Due to the reversible thermoresponsive folding and unfolding of the triple helix domain, the mechanical properties of the hydrogel was temperature dependent. More interestingly, by adding free CLPs for competing triple helix formation, the stiffness of the hydrogel could be easily manipulated (Figure 2b), which endowed the hydrogel with potential to detect physicochemical signals. Similar hydrogels were also reported from Chmielewski and coworkers (Figure 2c).[118] By conjugating the CLP with the 8-arm PEG using Michael type addition, the mechanical properties of the hydrogel was drastically enhanced.

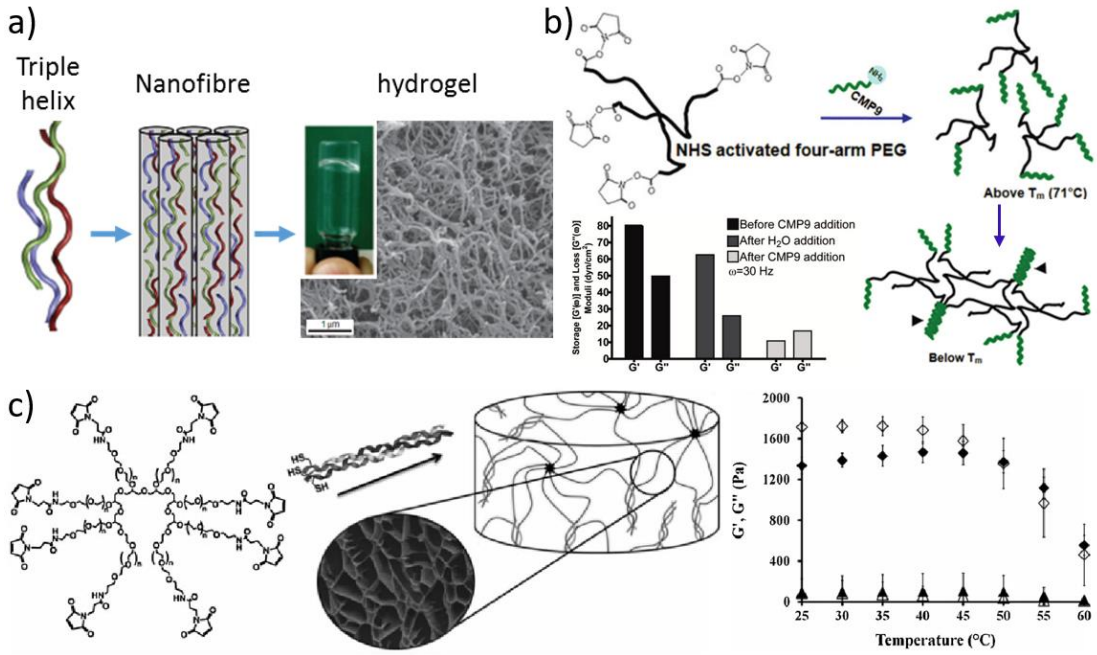


Figure 1.11 a) Self-assembly of collagen like peptide $(Pro\text{-}Lys\text{-}Gly)_4$-$(Pro\text{-}Hyp\text{-}Gly)_4$-(Asp-Hyp-Gly)4 into nanofibre and subsequent fabrication of CLP hydrogel at higher concentrations; scale bar = 1 um; b) 4-arm PEG hydrogel crosslinked via $(GPO)_9$ collagen triple helix. Left bottom panel: storage and loss modulus for the hydrogel (10 wt%) before and after the addition of free CLP solution. c) 8-arm PEG hydrogel crosslinked via collagen triple helix. Temperature sweep experiment for the hydrogel (8 wt%) suggested a high storage modulus of approximately 1500 Pa at physiological temperature. Filled symbols represent the first analysis of the hydrogels and open symbols represent analysis after recooling the samples from the first analysis. G': storage modulus (square), G'': loss modulus (triangle). (reproduced with permission from Ref[14, 117, 118])

In addition to physical cross-linkers, CLPs integrated with certain bioactive domains have also been widely used to fabricate hydrogels to improve cell adhesion and ECM production. For example, Yu and coworkers reported a CLP-conjugated poly (ethylene glycol) diacrylate (PEODA) hydrogel which was not only able to retain cell secreted glycosaminoglycan (GAG) and collagen from encapsulated

chondrocytes,[119] but also help direct the differentiation of stem cells into the chondrogenic pathway.[110] More recently, they further encoded the PEODA-CLP hydrogel with CLP-RGD conjugates.[107] Adhesion and proliferation of encapsulated fibroblasts were studied on the hydrogels with different RGD peptide concentration. Tong and coworkers[37] synthesized a CLP amphiphile with a C16 lipophilic tail attached to the C-terminus of a CLP with sequence $(GPO)_3GFOGER(GPO)_3$. Given the inclusion of integrin specific binding sequence GFOGER, hydrogels formed from the amphiphile was shown to promote the adhesion and spreading of HepG2 cells. By introducing a hydroxyproline free CLP containing integrin binding motif Glycine-Glutamic acid-Arginine (GER) triplet, our group successfully promoted integrin-mediated adhesion, spreading and proliferation of human mesenchymal stem cells (hMSCs) in a hyaluronic acid (HA) particle-based hydrogel surface.[84]

## 1.6 Conclusions

Collagen-like peptide-based biomaterials have emerged as a new class of biomaterials that possesses unique structure and properties. Abundant research has been conducted in the past few decades in deciphering the role of different amino acid residues and tripeptide motifs in stabilizing the collagen triple helix, as well as elucidating intermolecular interactions and other factors affecting collagen fibrogenesis. A variety of artificial collagen-like peptides with well-defined sequences have been designed to create higher order assemblies with specific biological functions. However, compared with polymer conjugates with α-helix and β-sheet peptides that have already been used in clinical trials, synthetic conjugates of polymers with collagen-like peptides are relatively unexplored. Considering the critical role of

collagen in extracellular matrix (ECM) biology, collagen-like peptides and their bioconjugates may eventually become an indispensable component in artificial tissue scaffolds and targeted drug delivery systems.

## 1.7 Acknowledgements

Related work in the authors' laboratories has been funded in part by the National Science Foundation (DMR 0907478 to KLK) and the National Center for Research Resources (NCRR), a component of the National Institutes of Health (P30-RR031160 for instrument resources). This work was also supported in part by the Center for Neutron Science at UD under award (U.S. Department of Commerce) #70NANB7H6178. Its contents are solely the responsibility of the authors and do not necessarily represent the official views of the NCRR, NIH, or Department of Commerce.

## REFERENCES


1. M.D. Shoulders, R.T. Raines, Collagen Structure and Stability. In *Annu. Rev. Biochem.*, Annual Reviews: Palo Alto, 2009; Vol. 78, pp 929-958.

2. K.E. Kadler, C. Baldock, J. Bella, R.P. Boot-Handford, Collagens at a glance. *J. Cell Sci.* **2007,** *120* (12), 1955-1958.

3. G.N. Ramachandran, G. Kartha, STRUCTURE OF COLLAGEN. *Nature* **1955,** *176* (4482), 593-595.

4. T. von Arx, D. Buser, Horizontal ridge augmentation using autogenous block grafts and the guided bone regeneration technique with collagen membranes: a clinical study with 42 patients. *Clin. Oral Implant. Res.* **2006,** *17* (4), 359-366.

5. W. Haslik, L.P. Kamolz, G. Nathschlager, H. Andel, G. Meissl, M. Frey, First experiences with the collagen-elastin matrix Matriderm((R)) as a dermal substitute in severe burn injuries of the hand. *Burns* **2007,** *33* (3), 364-368.

6. T. Nemoto, M. Horiuchi, N. Ishiguro, M. Shinagawa, Detection methods of possible prion contaminants in collagen and gelatin. *Arch. Virol.* **1999,** *144* (1), 177-184.

7. J.A. Fallas, J.H. Dong, Y.Z.J. Tao, J.D. Hartgerink, Structural Insights into Charge Pair Interactions in Triple Helical Collagen-like Proteins. *J. Biol. Chem.* **2012,** *287* (11), 8039-8047.

8. A.V. Persikov, J.A.M. Ramshaw, B. Brodsky, Prediction of collagen stability from amino acid sequence. *J. Biol. Chem.* **2005,** *280* (19), 19343-19349.

9. S.P. Boudko, J. Engel, Structure formation in the C terminus of type III collagen guides disulfide cross-linking. *J. Mol. Biol.* **2004,** *335* (5), 1289-1297.

10. D. Barth, O. Kyrieleis, S. Frank, C. Renner, L. Moroder, The role of cystine knots in collagen folding and stability, part II. Conformational properties of (Pro-Hyp-Gly)(n) model trimers with N- and C-terminal collagen type III cystine knots. *Chem-Eur J* **2003,** *9* (15), 3703-3714.

11. W. Yang, V.C. Chan, A. Kirkpatrick, J.A.M. Ramshaw, B. Brodsky, Gly-Pro-Arg confers stability similar to Gly-Pro-Hyp in the collagen triple-helix of host-guest peptides. *J. Biol. Chem.* **1997,** *272* (46), 28837-28840.

12. M.M. Pires, J. Lee, D. Ernenwein, J. Chmielewski, Controlling the Morphology of Metal-Promoted Higher Ordered Assemblies of Collagen Peptides with Varied Core Lengths. *Langmuir* **2012,** *28* (4), 1993-1997.

13. M.M. Pires, D.E. Przybyla, C.M.R. Perez, J. Chmielewski, Metal-Mediated Tandem Coassembly of Collagen Peptides into Banded Microstructures. *J Am Chem Soc* **2011,** *133* (37), 14469-14471.

14. L.E.R. O'Leary, J.A. Fallas, E.L. Bakota, M.K. Kang, J.D. Hartgerink, Multi-hierarchical self-assembly of a collagen mimetic peptide from triple helix to nanofibre and hydrogel. *Nat. Chem.* **2011,** *3* (10), 821-828.

15. D.E. Przybyla, J. Chmielewski, Metal-triggered radial self-assembly of collagen peptide fibers. *J Am Chem Soc* **2008,** *130* (38), 12610-+.

16. O.D. Krishna, K.L. Kiick, Supramolecular Assembly of Electrostatically Stabilized, Hydroxyproline-Lacking Collagen-Mimetic Peptides. *Biomacromolecules* **2009,** *10* (9), 2626-2631.

17. J.M. Rathfon, G.N. Tew, Synthesis of thermoresponsive poly (N-isopropylmethacrylamide) and poly(acrylic acid) block copolymers via post-functionalization of poly(N-methacryloxysuccinimide). *Polymer* **2008,** *49* (7), 1761-1769.

18. C.L. McCormick, B.S. Sumerlin, B.S. Lokitz, J.E. Stempka, RAFT-synthesized diblock and triblock copolymers: thermally-induced supramolecular assembly in aqueous media. *Soft Matter* **2008,** *4* (9), 1760-1773.

19. R. Shunmugam, G.N. Tew, Efficient route to well-characterized homo, block, and statistical polymers containing terpyridine in the side chain. *J. Polym. Sci. Pol. Chem.* **2005,** *43* (23), 5831-5843.

20. J.F. Lutz, H.G. Borner, Modern trends in polymer bioconjugates design. *Prog Polym Sci* **2008,** *33* (1), 1-39.

21. O.D. Krishna, K.L. Kiick, Protein- and Peptide-Modified Synthetic Polymeric Biomaterials. *Biopolymers* **2010,** *94* (1), 32-48.

22. D.A. Rothenfluh, H. Bermudez, C.P. O'Neil, J.A. Hubbell, Biofunctional polymer nanoparticles for intra-articular targeting and retention in cartilage. *Nat. Mater.* **2008,** *7* (3), 248-254.

23. K. Osada, K. Kataoka, Drug and gene delivery based on supramolecular assembly of PEG-polypeptide hybrid block copolymers. In *Peptide Hybrid Polymers*, H.A. Klok, H. Schlaad, Eds. Springer-Verlag Berlin: Berlin, 2006; Vol. 202, pp 113-153.

24. A. Mitra, A. Nan, J.C. Papadimitriou, H. Ghandehari, B.R. Line, Polymer-peptide conjugates for angiogenesis targeted tumor radiotherapy. *Nucl. Med. Biol.* **2006,** *33* (1), 43-52.

25. J.X. Ding, C.S. Xiao, Z.H. Tang, X.L. Zhuang, X.S. Chen, Highly Efficient "Grafting From" an alpha-Helical Polypeptide Backbone by Atom Transfer Radical Polymerization. *Macromol. Biosci.* **2011,** *11* (2), 192-198.

26. J. Wigenius, P. Bjork, M. Hamedi, D. Aili, Supramolecular Assembly of Designed alpha-Helical Polypeptide-Based Nanostructures and Luminescent Conjugated Polyelectrolytes. *Macromol. Biosci.* **2010,** *10* (8), 836-841.

27. J.Y. Shu, C. Tan, W.F. DeGrado, T. Xu, New design of helix bundle peptide-polymer conjugates. *Biomacromolecules* **2008,** *9* (8), 2111-2117.

28. E. Sahin, K.L. Kiick, Macromolecule-Induced Assembly of Coiled-Coils in Alternating Multiblock Polymers. *Biomacromolecules* **2009,** *10* (10), 2740-2749.

29. J. Kopecek, J.Y. Yang, Self-assembly of hybrid copolymers grafted with beta-sheet and alpha-helix peptides. *Abstr. Pap. Am. Chem. Soc.* **2011,** *241*.

30. A.N. Elder, N.M. Dangelo, S.C. Kim, N.R. Washburn, Conjugation of beta-Sheet Peptides to Modify the Rheological Properties of Hyaluronic Acid. *Biomacromolecules* **2011,** *12* (7), 2610-2616.

31. O.S. Lee, Y.M. Liu, G.C. Schatz, Molecular dynamics simulation of beta-sheet formation in self-assembled peptide amphiphile fibers. *J. Nanopart. Res.* **2012,** *14* (8).

32. S. Aluri, M.K. Pastuszka, A.S. Moses, J.A. MacKay, Elastin-Like Peptide Amphiphiles Form Nanofibers with Tunable Length. *Biomacromolecules* **2012,** *13* (9), 2645-2654.

33. S.E. Grieshaber, A.J.E. Farran, S. Lin-Gibson, K.L. Kiick, X.Q. Jia, Synthesis and Characterization of Elastin-Mimetic Hybrid Polymers with Multiblock, Alternating Molecular Architecture and Elastomeric Properties. *Macromolecules* **2009,** *42* (7), 2532-2541.

34. S.E. Grieshaber, A.J.E. Farran, S. Bai, K.L. Kiick, X.Q. Jia, Tuning the Properties of Elastin Mimetic Hybrid Copolymers via a Modular Polymerization Method. *Biomacromolecules* **2012,** *13* (6), 1774-1786.

35. Y.C. Yu, P. Berndt, M. Tirrell, G.B. Fields, Self-assembling amphiphiles for construction of protein molecular architecture. *J Am Chem Soc* **1996,** *118* (50), 12515-12520.

36. T. Gore, Y. Dori, Y. Talmon, M. Tirrell, H. Bianco-Peled, Self-assembly of model collagen peptide amphiphiles. *Langmuir* **2001,** *17* (17), 5352-5360.

37. J.N. Luo, Y.W. Tong, Self-Assembly of Collagen-Mimetic Peptide Amphiphiles into Biofunctional Nanofiber. *Acs Nano* **2011,** *5* (10), 7739-7747.

38. O.D. Krishna, K.T. Wiss, T.Z. Luo, D.J. Pochan, P. Theato, K.L. Kiick, Morphological transformations in a dually thermoresponsive coil-rod-coil bioconjugate. *Soft Matter* **2012,** *8* (14), 3832-3840.

39. A.V. Persikov, J.A.M. Ramshaw, A. Kirkpatrick, B. Brodsky, Amino acid propensities for the collagen triple-helix. *Biochemistry-Us* **2000,** *39* (48), 14960-14967.

40. J.A.M. Ramshaw, N.K. Shah, B. Brodsky, Gly-X-Y tripeptide frequencies in collagen: A context for host-guest triple-helical peptides. *J. Struct. Biol.* **1998,** *122* (1-2), 86-91.

41. E.Y. Jones, A. Miller, ANALYSIS OF STRUCTURAL DESIGN-FEATURES IN COLLAGEN. *J. Mol. Biol.* **1991,** *218* (1), 209-219.

42. E. Suzuki, R.D.B. Fraser, T.P. Macrae, ROLE OF HYDROXYPROLINE IN THE STABILIZATION OF THE COLLAGEN MOLECULE VIA WATER-MOLECULES. *Int. J. Biol. Macromol.* **1980,** *2* (1), 54-56.

43. W. Traub, SOME STEREOCHEMICAL IMPLICATIONS OF MOLECULAR-CONFORMATION OF COLLAGEN. *Isr. J. Chem.* **1974,** *12* (1-2), 435-439.

44. Ramachan.Gn, M. Bansal, Bhatnaga.Rs, HYPOTHESIS ON ROLE OF HYDROXYPROLINE IN STABILIZING COLLAGEN STRUCTURE. *Biochimica Et Biophysica Acta* **1973,** *322* (1), 166-171.

45. M. Bansal, C. Ramakrishnan, G.N. Ramachandran, STABILIZATION OF COLLAGEN STRUCTURE BY HYDROXYPROLINE RESIDUES. *Proceedings of the Indian Academy of Sciences Section A* **1975,** *82* (4), 152-164.

46. S.K. Holmgren, K.M. Taylor, L.E. Bretscher, R.T. Raines, Code for collagen's stability deciphered. *Nature* **1998,** *392* (6677), 666-667.

47. S.K. Holmgren, L.E. Bretscher, K.M. Taylor, R.T. Raines, A hyperstable collagen mimic. *Chem. Biol.* **1999,** *6* (2), 63-70.

48. J.D. Dunitz, R. Taylor, Organic fluorine hardly ever accepts hydrogen bonds. *Chem-Eur J* **1997,** *3* (1), 89-98.

49. E.S. Eberhardt, N. Panasik, R.T. Raines, Inductive effects on the energetics of prolyl peptide bond isomerization: Implications for collagen folding and stability. *J Am Chem Soc* **1996,** *118* (49), 12261-12266.

50. K. Inouye, S. Sakakibara, D.J. Prockop, EFFECTS OF STEREO-CONFIGURATION OF HYDROXYL GROUP IN 4-HYDROXYPROLINE ON TRIPLE-HELICAL STRUCTURES FORMED BY HOMOGENEOUS PEPTIDES RESEMBLING COLLAGEN. *Biochimica Et Biophysica Acta* **1976,** *420* (1), 133-141.

51. L.E. Bretscher, C.L. Jenkins, K.M. Taylor, M.L. DeRider, R.T. Raines, Conformational stability of collagen relies on a stereoelectronic effect. *J Am Chem Soc* **2001,** *123* (4), 777-778.

52. M.L. DeRider, S.J. Wilkens, M.J. Waddell, L.E. Bretscher, F. Weinhold, R.T. Raines, J.L. Markley, Collagen stability: Insights from NMR spectroscopic and hybrid density functional computational investigations of the effect of electronegative substituents on prolyl ring conformations. *J Am Chem Soc* **2002,** *124* (11), 2497-2505.

53. M.D. Shoulders, I.A. Guzei, R.T. Raines, 4-chloroprolines: Synthesis, conformational analysis, and effect on the collagen triple helix. *Biopolymers* **2008,** *89* (5), 443-454.

54. U. Kusebauch, S.A. Cadamuro, H.J. Musiol, M.O. Lenz, J. Wachtveitl, L. Moroder, C. Renner, Photocontrolled folding and unfolding of a collagen triple helix. *Angew. Chem.-Int. Edit.* **2006,** *45* (42), 7015-7018.

55. A.V. Persikov, J.A.M. Ramshaw, A. Kirkpatrick, B. Brodsky, Peptide investigations of pairwise interactions in the collagen triple-helix. *J. Mol. Biol.* **2002,** *316* (2), 385-394.

56. R.Z. Kramer, M.G. Venugopal, J. Bella, P. Mayville, B. Brodsky, H.M. Berman, Staggered molecular packing in crystals of a collagen-like peptide with a single charged pair. *J. Mol. Biol.* **2000,** *301* (5), 1191-1205.

57. A.V. Persikov, J.A.M. Ramshaw, A. Kirkpatrick, B. Brodsky, Electrostatic interactions involving lysine make major contributions to collagen triple-helix stability. *Biochemistry-Us* **2005,** *44* (5), 1414-1422.

58. J.A. Fallas, L.E.R. O'Leary, J.D. Hartgerink, Synthetic collagen mimics: self-assembly of homotrimers, heterotrimers and higher order structures. *Chem Soc Rev* **2010,** *39* (9), 3510-3527.

59. E. Chung, E.M. Keele, E.J. Miller, ISOLATION AND CHARACTERIZATION OF CYANOGEN-BROMIDE PEPTIDES FROM ALPHA 1 (III) CHAIN OF HUMAN COLLAGEN. *Biochemistry-Us* **1974,** *13* (17), 3459-3464.

60. H.P. Bachinger, P. Bruckner, R. Timpl, D.J. Prockop, J. Engel, FOLDING MECHANISM OF THE TRIPLE HELIX IN TYPE-III COLAGEN AND TYPE-III PN-COLLAGEN - ROLE OF DISULFIDE BRIDGES AND PEPTIDE-BOND ISOMERIZATION. *Eur. J. Biochem.* **1980,** *106* (2), 619-632.

61. D.E. Mechling, H.P. Bachinger, The collagen-like peptide (GER)(15)GPCCG forms pH-dependent covalently linked triple helical trimers. *J. Biol. Chem.* **2000,** *275* (19), 14532-14536.

62. Y.B. Feng, G. Melacini, J.P. Taulane, M. Goodman, Acetyl-terminated and template-assembled collagen-based polypeptides composed of Gly-Pro-Hyp sequences .2. Synthesis and conformational analysis by circular dichroism, ultraviolet absorbance, and optical rotation. *J Am Chem Soc* **1996,** *118* (43), 10351-10358.

63. J. Kwak, A. De Capua, E. Locardi, M. Goodman, TREN (tris(2-aminoethyl)amine): An effective scaffold for the assembly of triple helical collagen mimetic structures. *J Am Chem Soc* **2002,** *124* (47), 14085-14091.

64. S. Frank, R.A. Kammerer, D. Mechling, T. Schulthess, R. Landwehr, J. Bann, Y. Guo, A. Lustig, H.P. Bachinger, J. Engel, Stabilization of short collagen-like triple helices by protein engineering. *J. Mol. Biol.* **2001,** *308* (5), 1081-1089.

65. G.B. Fields, J.L. Lauer, Y. Dori, P. Forns, Y.C. Yu, M. Tirrell, Proteinlike molecular architecture: Biomaterial applications for inducing cellular receptor binding and signal transduction. *Biopolymers* **1998,** *47* (2), 143-151.

66. K.T. Wiss, O.D. Krishna, P.J. Roth, K.L. Kiick, P. Theato, A Versatile Grafting-to Approach for the Bioconjugation of Polymers to Collagen-like Peptides Using an Activated Ester Chain Transfer Agent. *Macromolecules* **2009,** *42* (12), 3860-3863.

67. K. Kar, P. Amin, M.A. Bryan, A.V. Persikov, A. Mohs, Y.H. Wang, B. Brodsky, Self-association of collagen triple helix peptides into higher order structures. *J. Biol. Chem.* **2006,** *281* (44), 33283-33290.

68. M.A. Cejas, W.A. Kinnney, C. Chen, J.G. Vinter, H.R. Almond, K.M. Balss, C.A. Maryanoff, U. Schmidt, M. Breslav, A. Mahan, E. Lacy, B.E. Maryanoff, Thrombogenic collagen-mimetic peptides: Self-assembly of triple helix-based fibrils driven by hydrophobic interactions. *P Natl Acad Sci USA* **2008,** *105* (25), 8513-8518.

69. M.A. Cejas, W.A. Kinney, C. Chen, G.C. Leo, B.A. Tounge, J.G. Vinter, P.P. Joshi, B.E. Maryanoff, Collagen-related peptides: Self-assembly of short, single strands into a functional biomaterial of micrometer scale. *J Am Chem Soc* **2007,** *129* (8), 2202-+.

70. K. Kar, S. Ibrar, V. Nanda, T.M. Getz, S.P. Kunapuli, B. Brodsky, Aromatic Interactions Promote Self-Association of Collagen Triple-Helical Peptides to Higher-Order Structures. *Biochemistry-Us* **2009,** *48* (33), 7959-7968.

71. C.C. Chen, W. Hsu, T.C. Kao, J.C. Horng, Self-Assembly of Short Collagen-Related Peptides into Fibrils via Cation-pi Interactions. *Biochemistry-Us* **2011,** *50* (13), 2381-2383.

72. K.E. Kadler, D.F. Holmes, J.A. Trotter, J.A. Chapman, Collagen fibril formation. *Biochem. J.* **1996,** *316*, 1-11.

73. S. Rele, Y.H. Song, R.P. Apkarian, Z. Qu, V.P. Conticello, E.L. Chaikof, D-periodic collagen-mimetic microfibers. *J Am Chem Soc* **2007,** *129* (47), 14780-14787.

74. W. Hsu, Y.L. Chen, J.C. Horng, Promoting Self-Assembly of Collagen-Related Peptides into Various Higher-Order Structures by Metal-Histidine Coordination. *Langmuir* **2012,** *28* (6), 3194-3199.

75. A.Y. Wang, X. Mo, C.S. Chen, S.M. Yu, Facile modification of collagen directed by collagen mimetic peptides. *J Am Chem Soc* **2005,** *127* (12), 4130-4131.

76. X. Mo, Y.J. An, C.S. Yun, S.M. Yu, Nanoparticle-assisted visualization of binding interactions between collagen mimetic peptide and collagen fibers. *Angew. Chem.-Int. Edit.* **2006,** *45* (14), 2267-2270.

77. Y. Li, D. Ho, H. Meng, T.R. Chan, B. An, H. Yu, B. Brodsky, A.S. Jun, S.M. Yu, Direct Detection of Collagenous Proteins by Fluorescently Labeled Collagen Mimetic Peptides. *Bioconjugate Chem.* **2013,** *24* (1), 9-16.

78. A.Y. Wang, C.A. Foss, S. Leong, X. Mo, M.G. Pomper, S.M. Yu, Spatio-temporal modification of collagen scaffolds mediated by triple helical propensity. *Biomacromolecules* **2008,** *9* (7), 1755-1763.

79. A.Y. Wang, S. Leong, Y.C. Liang, R.C.C. Huang, C.S. Chen, S.M. Yu, Immobilization of Growth Factors on Collagen Scaffolds Mediated by Polyanionic Collagen Mimetic Peptides and Its Effect on Endothelial Cell Morphogenesis. *Biomacromolecules* **2008,** *9* (10), 2929-2936.

80. Y. Li, C.A. Foss, D.D. Summerfield, J.J. Doyle, C.M. Torok, H.C. Dietz, M.G. Pomper, S.M. Yu, Targeting collagen strands by photo-triggered triple-helix hybridization. *P Natl Acad Sci USA* **2012,** *109* (37), 14767-14772.

81. T.Z. Luo, K.L. Kiick, Noncovalent Modulation of the Inverse Temperature Transition and Self-Assembly of Elastin-b-Collagen-like Peptide Bioconjugates. *J Am Chem Soc* **2015,** *137* (49), 15362-15365.

82. T.Z. Luo, L.R. He, P. Theato, K.L. Kiick, Thermoresponsive Self-Assembly of Nanostructures from a Collagen-Like Peptide-Containing Diblock Copolymer. *Macromol. Biosci.* **2015,** *15* (1), 111-123.

83. O.S. Rabotyagova, P. Cebe, D.L. Kaplan, Protein-Based Block Copolymers. *Biomacromolecules* **2011,** *12* (2), 269-289.

84. O.D. Krishna, A.K. Jha, X.Q. Jia, K.L. Kiick, Integrin-mediated adhesion and proliferation of human MSCs elicited by a hydroxyproline-lacking, collagen-like peptide. *Biomaterials* **2011,** *32* (27), 6412-6424.

85. Z. Zhang, Y.X. Lai, L. Yu, J.D. Ding, Effects of immobilizing sites of RGD peptides in amphiphilic block copolymers on efficacy of cell adhesion. *Biomaterials* **2010,** *31* (31), 7873-7882.

86. J.O. Humtsoe, J.K. Kim, Y. Xu, D.R. Keene, M. Hook, S. Lukomski, K.K. Wary, A streptococcal collagen-like protein interacts with the alpha(2)beta(1) integrin and induces intracellular signaling. *J. Biol. Chem.* **2005,** *280* (14), 13848-13857.

87. J.M. Harris, R.B. Chess, Effect of pegylation on pharmaceuticals. *Nat. Rev. Drug Discov.* **2003,** *2* (3), 214-221.

88. H.A. Klok, Biological-synthetic hybrid block copolymers: Combining the best from two worlds. *J. Polym. Sci. Pol. Chem.* **2005,** *43* (1), 1-17.

89. M. Pechar, J. Brus, L. Kostka, C. Konak, M. Urbanova, M. Slouf, Thermoresponsive self-assembly of short elastin-like polypentapeptides and their poly(ethylene glycol) derivatives. *Macromol. Biosci.* **2007,** *7* (1), 56-69.

90. G.W.M. Vandermeulen, C. Tziatzios, H.A. Klok, Reversible self-organization of poly(ethylene glycol)-based hybrid block copolymers mediated by a De Novo four-stranded alpha-helical coiled coil motif. *Macromolecules* **2003,** *36* (11), 4107-4114.

91. A. Rosler, H.A. Klok, I.W. Hamley, V. Castelletto, O.O. Mykhaylyk, Nanoscale structure of poly(ethylene glycol) hybrid block copolymers containing amphiphilic beta-strand peptide sequences. *Biomacromolecules* **2003,** *4* (4), 859-863.

92. B.L. Nilsson, L.L. Kiessling, R.T. Raines, High-yielding Staudinger ligation of a phosphinothioester and azide to form a peptide. *Org Lett* **2001,** *3* (1), 9-12.

93. A. Top, C.J. Roberts, K.L. Kiick, Conformational and Aggregation Properties of a PEGylated Alanine-Rich Polypeptide. *Biomacromolecules* **2011,** *12* (6), 2184-2192.

94. A. Top, Controlling assembly of helical peptides via PEGylation strategies. *Soft Matter* **2011**.

95. M.J. Roberts, M.D. Bentley, J.M. Harris, Chemistry for peptide and protein PEGylation. *Adv Drug Deliver Rev* **2002,** *54* (4), 459-476.

96. O. Kinstler, G. Molineux, M. Treuheit, D. Ladd, C. Gegg, Mono-N-terminal poly(ethylene glycol)-protein conjugates. *Adv Drug Deliver Rev* **2002,** *54* (4), 477-485.

97. R. Huisgen, 1.3-DIPOLARE CYCLOADDITIONEN - RUCKSCHAU UND AUSBLICK. *Angew. Chem.-Int. Edit.* **1963,** *75* (13), 604-+.

98. C.W. Tornoe, C. Christensen, M. Meldal, Peptidotriazoles on solid phase: 1,2,3 -triazoles by regiospecific copper(I)-catalyzed 1,3-dipolar cycloadditions of terminal alkynes to azides. *J Org Chem* **2002,** *67* (9), 3057-3064.

99. V.V. Rostovtsev, L.G. Green, V.V. Fokin, K.B. Sharpless, A stepwise Huisgen cycloaddition process: Copper(I)-catalyzed regioselective "ligation" of azides and terminal alkynes. *Angew. Chem.-Int. Edit.* **2002,** *41* (14), 2596-+.

100. A.J.T. Dirks, S.S. van Berkel, N.S. Hatzakis, J.A. Opsteen, F.L. van Delft, J. Cornelissen, A.E. Rowan, J.C.M. van Hest, F. Rutjes, R.J.M. Nolte, Preparation of biohybrid amphiphiles via the copper catalysed Huisgen 3+2 dipolar cycloaddition reaction. *Chem. Commun.* **2005,** (33), 4172-4174.

101. A.B. Lowe, Thiol-ene "click" reactions and recent applications in polymer and materials synthesis. *Polym. Chem.* **2010,** *1* (1), 17-36.

102. B.D. Mather, K. Viswanathan, K.M. Miller, T.E. Long, Michael addition reactions in macromolecular design for emerging technologies. *Prog Polym Sci* **2006,** *31* (5), 487-531.

103. M. Friedman, J.F. Cavins, J.S. Wall, RELATIVE NUCLEOPHILIC REACTIVITIES OF AMINO GROUPS AND MERCAPTIDE IONS IN ADDITION REACTIONS WITH ALPHA BETA-UNSATURATED COMPOUNDS. *J Am Chem Soc* **1965,** *87* (16), 3672-&.

104. A.D. Baldwin, K.L. Kiick, Tunable Degradation of Maleimide-Thiol Adducts in Reducing Environments. *Bioconjugate Chem.* **2011,** *22* (10), 1946-1953.

105. A. Carlsen, S. Lecommandoux, Self-assembly of polypeptide-based block copolymer amphiphiles. *Curr. Opin. Colloid Interface Sci.* **2009,** *14* (5), 329-339.

106. D. Chow, Peptide-based biopolymers in biomedicine and biotechnology. **2008**.

107. P.J. Stahl, S.M. Yu, Encoding cell-instructive cues to PEG-based hydrogels via triple helical peptide assembly. *Soft Matter* **2012,** *8* (40), 10409-10418.

108. L.A.S. Callahan, A.M. Ganios, D.L. McBurney, M.F. Dilisio, S.D. Weiner, W.E. Horton, M.L. Becker, ECM Production of Primary Human and Bovine Chondrocytes in Hybrid PEG Hydrogels Containing Type I Collagen and Hyaluronic Acid. *Biomacromolecules* **2012,** *13* (5), 1625-1631.

109. M. Rafat, F.F. Li, P. Fagerholm, N.S. Lagali, M.A. Watsky, R. Munger, T. Matsuura, M. Griffith, PEG-stabilized carbodiimide crosslinked collagen-chitosan hydrogels for corneal tissue engineering. *Biomaterials* **2008,** *29* (29), 3960-3972.

110. H.J. Lee, C. Yu, T. Chansakul, N.S. Hwang, S. Varghese, S.M. Yu, J.H. Elisseeff, Enhanced Chondrogenesis of Mesenchymal Stem Cells in Collagen Mimetic Peptide-Mediated Microenvironment. *Tissue Eng. Part A* **2008,** *14* (11), 1843-1851.

111. H.X. Lu, N. Kawazoe, T. Kitajima, Y. Myoken, M. Tomita, A. Umezawa, G.P. Chen, Y. Ito, Spatial immobilization of bone morphogenetic protein-4 in a collagen-PLGA hybrid scaffold for enhanced osteoinductivity. *Biomaterials* **2012,** *33* (26), 6140-6146.

112. W.D. Dai, N. Kawazoe, X.T. Lin, J. Dong, G.P. Chen, The influence of structural design of PLGA/collagen hybrid scaffolds in cartilage tissue engineering. *Biomaterials* **2010,** *31* (8), 2141-2152.

113. M.C. Burrows, V.M. Zamarion, F.B. Filippin-Monteiro, D.C. Schuck, H.E. Toma, A. Campa, C.R.S. Garcia, L.H. Catalani, Hybrid Scaffolds Built From PET and Collagen as a Model For Vascular Graft Architecture. *Macromol. Biosci.* **2012,** *12* (12), 1660-1670.

114. H.J. Kim, K.K. Kim, I.K. Park, B.S. Choi, J.H. Kim, M.S. Kim, Hybrid Scaffolds Composed of Hyaluronic Acid and Collagen for Cartilage Regeneration. *Tissue Eng. Regen. Med.* **2012,** *9* (2), 57-62.

115. Y.C. Lin, F.J. Tan, K.G. Marra, S.S. Jan, D.C. Liu, Synthesis and characterization of collagen/hyaluronan/chitosan composite sponges for potential biomedical applications. *Acta Biomater* **2009,** *5* (7), 2591-2600.

116. S.Z. Fu, P.Y. Ni, B.Y. Wang, B.Y. Chu, L. Zheng, F. Luo, J.C. Luo, Z.Y. Qian, Injectable and thermo-sensitive PEG-PCL-PEG copolymer/collagen/n-HA hydrogel composite for guided bone regeneration. *Biomaterials* **2012,** *33* (19), 4801-4809.

117. P.J. Stahl, N.H. Romano, D. Wirtz, S.M. Yu, PEG-Based Hydrogels with Collagen Mimetic Peptide-Mediated and Tunable Physical Cross-Links. *Biomacromolecules* **2010,** *11* (9), 2336-2344.

118. C.M.R. Perez, A. Panitch, J. Chmielewski, A Collagen Peptide-Based Physical Hydrogel for Cell Encapsulation. *Macromol. Biosci.* **2011,** *11* (10), 1426-1431.

119. H.J. Lee, J.S. Lee, T. Chansakul, C. Yu, J.H. Elisseeff, S.M. Yu, Collagen mimetic peptide-conjugated photopolymerizable PEG hydrogel. *Biomaterials* **2006,** *27* (30), 5268-5276.

# Chapter 2

# THERMORESPONSIVE SELF-ASSEMBLY OF NANOSTRUCTURES FROM A COLLAGEN-LIKE PEPTIDE-CONTAINING DIBLOCK COPOLYMER

## 2.1 Introduction

Collagen is the main component of the extracellular matrix (ECM) in mammals. It comprises 28 different types of proteins, which have widespread functions such as mediating cell adhesion, cell m igration, and tissue scaffolding and repair.[1] Although the roles of these proteins vary widely, they all contain (at least in part) the same secondary structure, a collagen triple helix,[2] which comprises three polypropline-II helices. Each strand of the helix consists of a repetitive amino acid sequence, glycine-X-Y, where X and Y are frequently proline (Pro) and hydroxyproline (Hyp).[3] Due to their excellent gel-forming ability and biodegradability, collagens have been widely used as biomedical materials for the delivery of chemotherapeutic drugs such as paclitaxel,[4] doxorubicin,[5] and antibacterial drugs such as gentamicin,[6] as well as for tissue support and regeneration applications including skin replacement, bone substitutes, and artificial blood vessels.[7] However, some of the limitations of animal-derived collagens, such as their thermal instability, possible contamination with pathogenic substances, and relative difficulty in the introduction of specific sequence modifications, have limited their versatility. Accordingly, sequences modeled after the collagens, also known as collagen-like peptides (CLPs), collagen-mimetic peptides (CMPs), or collagen-related peptides (CRPs) have been explored.[8-10]

CLPs form a triple helical structure almost identical to that of natural collagen,[10] but because of their low molecular mass (<5 kDa), they exhibit reversible folding and unfolding behavior. Traditionally, CLPs were employed to elucidate the triple helix structure and the stabilization effect of different amino acid residues in collagens.[8,11-16] CLPs with novel sequences and interactions have also been developed to mimic collagen fibril formation[17-22] and to produce other higher-order supramolecular structures.[23-25] These include but are not limited to: (i) micrometer-scale fibrillar structure through noncovalent π-π end-to-end interactions;[20,21] (ii) fibrous structures with well-defined D-periodicity assembled from multi-domain CLPs such as $(PRG)_4(POG)_4(EOG)_4$[22] and $(PKG)_4(POG)_4(DOG)_4$;[17] (iii) metal cation-triggered assembled structures such as microflorettes, fiberlike meshes,[23,24] nanofibrils,[25] and microscale spheres;[25] (iv) hydrogel networks and scaffolds crosslinked by CLP triple helix association[26,27] or metal cation – CLP coordination[28].

More recently, Wang et al. have reported that unfolded single strand collagen-like peptides have a strong propensity to bind to natural collagen via a strand invasion process.[29] Short synthetic CLPs were successfully utilized as a staining reagent for natural collagens in human tissues including skin, cornea, bone[30] and liver.[31] *In vivo* studies[32] suggest that CLPs are able to permeate tumor vasculature and accumulate at tumor sites. A high level of accumulation of the CLP within the skeleton and joints has also been observed, especially in regions with high MMP and collagen remodeling activity, such as the articular cartilage of knee joints. These results suggest the great potential of CLPs as novel tool and material for tracking pathogenic collagens for diagnostic and drug delivery purposes.

While these CLPs and other (poly)peptide-based biomaterials exhibit well defined hierarchical structures and variety of biological functions such as cell recognition, adhesion and proliferation,[33-35] their use in therapeutics can be limited due to elevated immune responses, rapid degradation by enzymes, and short circulation times *in vivo*.[36,37] Chemical conjugation of (poly)peptides with synthetic polymers thus has become a widely used method to overcome these limitations while maintaining desirable bioactivities. For instance, the attachment of polyethylene glycol (PEG) – or PEGylation – to protein-based drugs, enzymes, and antibodies greatly improves the solubility of the biomolecules, reducing their immunogenicity and increasing their blood circulation time.[36] In addition, a variety of (poly)peptides including α-helical coiled-coil peptide domains,[38-41] β-sheet peptide motifs,[42-44] and elastin-mimetic peptides[45-48] have been successfully employed to produce polymer-peptide hybrid materials, which show potential in biomedical applications such as drug and gene delivery. However, compared with the recent surge in research on these peptide-polymer conjugates, collagen-like peptide hybrid materials remain relatively less explored. Yu et al.[49] attached one or two C12 head groups to a collagen-like peptide and found that it improved the thermal stability of the collagen triple helix, and self-assembly of the amphiphiles into various structures, dependent on the length of the amphiphile, was also observed.[50] Luo et al.[51] reported that after a C16 lipophilic tail was attached to a CLP with the sequence $(GPO)_3GFOGER(GPO)_3$ (F: phenylalanine; O: hydroxyproline), the amphiphile self-assembled into micrometer-long nanofibers with a diameter of approximately 16 nm.  More recently, our groups have reported a polymer-CLP-

polymer triblock,[52] which self-assembled into micron-scale hollow spheres at 37 °C and transformed into nanofibers at higher temperature.

In this study, we have conjugated a thermoresponsive polymer, poly (diethylene glycol methyl ether methacrylate) (PDEGMEMA), to the *N*-terminus of a triple-helix forming collagen-like peptide ($(GPO)_7GG$), to synthesize a polymer-CLP diblock (Figure 2.1). Due to the thermoresponsiveness of the polymer domain, we anticipated temperature-triggered assembly of the diblock into nanoparticles in aqueous conditions above the lower critical solution temperature (LCST) of the polymer, in a two-step process (Figure 2.1). The first level of assembly involved the formation of collagen triple helix from diblock monomers, with a second level of assembly triggered by increasing the temperature of the solution, leading to the collapse of the polymer domain and assembly into higher-order nanoparticles. A poly (ethylene glycol) - CLP diblock copolymer was studied as a non-thermoresponsive control. The thermally responsive diblock polymers provide a novel approach to the formation of nanoparticles that may be uniquely responsive to biological environments.

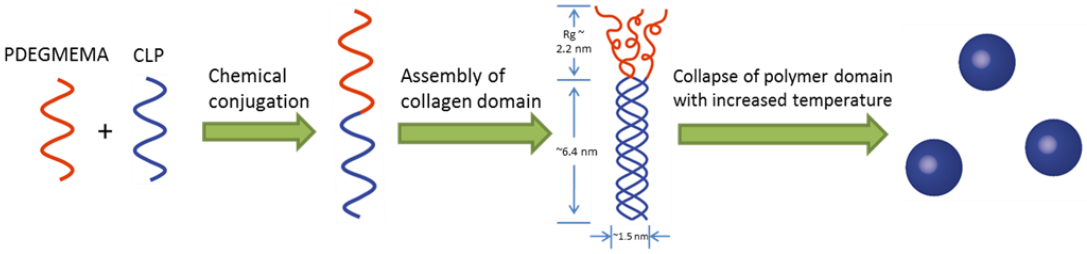


Figure 2.1 Proposed two-step assembly mechanism for PDEGMEMA-CLP conjugates.

## 2.2 Experimental Section

### 2.2.1 Materials

Fmoc-protected amino acids, Rink amide MBHA resin, *N,N,N′,N′*-tetramethyl-*O*-(1*H*-benzotriazol-1-yl) uronium hexafluorophosphate (HBTU), and piperidine for solid-phase peptide synthesis were purchased from AAPPTEC Inc. (Louisville, KY). HPLC-grade acetonitrile and dimethylformamide (DMF) were purchased from Fisher Scientific (Fairlawn, NJ). N-Methyl-2-pyrrolidone (NMP), trifluoroacetic acid (TFA), triisopropylsilane (TIS), triethylamine (TEA), and diisopropylethylamine (DIEA) were purchased from Sigma-Aldrich (St. Louis, MO).

### 2.2.2 Peptide Synthesis

A collagen-like peptide with the sequence $(GPO)_7GG$ was synthesized via traditional solid-phase peptide synthesis methods (SPPS) using a Focus XC automatic peptide synthesizer (AAPPTec Inc., Louisville, KY). Rink amide MBHA resin with a loading capacity of 0.52 mmol/g was used for the synthesis. The amino acids were activated for coupling with HBTU in the presence of 2 M diisopropylethylamine (DIEA) in NMP. Deprotection of the Fmoc group was conducted using 20% piperidine in DMF. One-hour coupling cycles were used for all the residues. Cleavage of the peptide from the resin was conducted in 95:2.5:2.5 (v:v:v) trifluoroacetic acid (TFA) /triisopropylsilane (TIS) /water for 3 hours. The TFA was mostly evaporated and the cleaved peptide was precipitated in cold ether. The peptide was then redissolved in water and lyophilized.

Crude peptide was purified via reverse-phase HPLC (Waters Inc., Milford, MA) on a Waters Symmetry 300, C-18 column. The mobile-phase comprised gradients of degassed deionized water with 0.1% TFA and acetonitrile with 0.1% TFA, at a flow

rate of 5 ml/min. Peptide was detected by UV absorbance at 214 nm; fractions with product were collected and lyophilized. The molecular weight of the peptide was confirmed via electrospray ionization mass spectrometry (ESI-MS, AutospecQ, VG Analytical, Manchester, UK) and the purity of the peptide was confirmed via analytical scale, reverse-phase HPLC (Waters 2996; Symmetry C18, 3.5 μm, 4.6 x 75 mm).

### 2.2.3 PDEGMEMA-CLP Conjugate Synthesis

The synthesis of the conjugate was performed via the reaction of *N*-terminal amine of the collagen-like peptide with activated-ester end-functionalized PDEGMEMA, following a recently developed protocol.[53] The activated ester end-functionalized PDEGMEMA was synthesized via RAFT polymerization described earlier.[54] The PDEGMEMA-CLP diblock copolymer was synthesized by mixing 3 equiv of PDEGMEMA per primary amine group of the peptide. The reaction was conducted in 2 mL 50:50 (v:v) NMP/DMSO, with the addition of 6 μL triethylamine (TEA), for 3 days at 35 °C (Figure 2.2). The resulting hybrid polymer was precipitated into a 5-fold volume of cold diethyl ether and redissolved in 50:50 (v:v) NMP/DMSO (repeated 5 times) to removed excessive PDEGMEMA starting material, followed by dissolution in water and lyophilization.

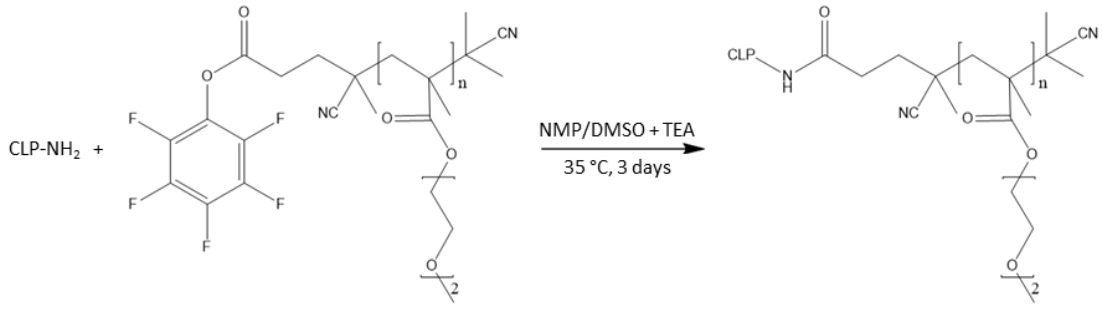


Figure 2.2 Chemical synthesis of PDEGMEMA-CLP diblock via the reaction of the activated ester-terminated PDEGMEMA with the *N*-terminal amine of a collagen-like peptide. The reaction was carried out in a mixture of dimethyl sulfoxide (DMSO) and N-methyl-2-pyrrolidone (NMP) (v/v=1:1) in the presence of triethylamine at 35 °C for 3 days.

### 2.2.4 Nuclear Magnetic Resonance (NMR)

$^{1}$H NMR spectra were recorded under standard quantitative conditions on a Bruker AVIII spectrometer operating at 600 MHz, using at least 64 scans. All samples were dissolved in deuterated dimethyl sulfoxide (δ ($d_6$-DMSO) = 2.50 ppm) at a concentration of 2 mg/mL. The resulting spectra were analyzed using Mnova software (Mestrelab Research, Santiago de Compostela, Spain).

### 2.2.5 Gel Permeation Chromatography (GPC)

GPC measurement of the PDEGMEMA-CLP conjugate was performed in DMF with 0.01 M lithium chloride at 30 °C. The system was operated at 1 mL/min with a Sonntek HPLC pump (K-501), one 50 mm x 7.5 mm PL gel mixed guard column, one 300 mm x 7.5 mm PL gel 5 μm mixed C column, one 300 mm x 7.5 mm PL gel 5 μm mixed D column, a Knauer refractive index detector (K-2301), and an Alltech solvent recycler 3000. Poly (methyl methacrylate) (PMMA) standards with Mw 875 Da, 3070 Da, 10570 Da and 30620 Da were used for molecular weight

calibration. All samples were dissolved in DMF at 1 mg/mL and 100 μL of solution was injected.

GPC measurement of the PEG-CLP conjugate was performed in 10 mM PBS buffer (pH 7.4, 137 mM NaCl and 2.7 mM KCl) using a combination of two Waters ultrahydro linear column (WAT011545 and WAT011525) with a nominal flow rate of 1 mL/min. A refractive index detector (Waters 2414), a UV absorbance detector (Waters 2996) were used. PEG standards with Mw 400 Da, 1970 Da, 6430 Da and 21030 Da were used to calculate molecular weights of the products. CLP and PEG starting material samples were dissolved in PBS at a concentration of 2 mg/mL, PEG-CLP diblock conjugate sample was dissolved in PBS at a concentration of 1 mg/mL. 100 μL solution was injected for all samples.

### 2.2.6 Circular Dichroic Spectroscopy (CD)

Characterization of the secondary structure of the CLP domain was conducted via circular dichroic spectroscopy (Jasco 810 circular dichroism spectropolarimeter, Jasco Inc., Easton, MD, USA). Either CLP or PDEGMEMA-CLP conjugate were dissolved at a concentration of 100 μM in PBS (10 mM, pH 7.4, 137 mM NaCl and 2.7 mM KCl) and incubated overnight to allow triple helix formation. The CD spectra were recorded using quartz cells with a 0.2 cm optical path length.

Full wavelength scans were collected to study the conformation of the peptide domain at selected temperatures. The sample was incubated at each temperature for 10 min before measurement. The scanning rate was 50 nm/min, with a response time of 4 s. The wavelength scans were obtained from 200 nm to 250 nm and were recorded every 1 nm. In order to precisely measure the melting temperature of the CLP domain, variable temperature experiments were conducted at a constant wavelength of 225 nm

with a 0.25 °C/min heating rate. Refolding kinetics were studied via temperature-jump experiments. The sample solution was incubated at 80 °C for 30 min followed by quenching to 5 °C in less than 2 minutes. The ellipticity at 225 nm as a function of time was monitored at 5 °C beginning right after the temperature jump.

### 2.2.7 Dynamic Light Scattering (DLS)

Analysis of particles sizes in solution was conducted via dynamic light scattering (DLS) on a ZetaSizer Nano Series (Nano ZS, Malvern Instruments, U.K.) at a scattering angle of 173°, and data fitting using the cumulant method. PEG-CLP and PDEGMEMA-CLP samples were prepared at 1 mg/mL in PBS (10 mM, pH 7.4, 137 mM NaCl and 2.7 mM KCl). PDEGMEMA-CLP samples were also prepared in water at a concentration of 1 mg/mL and 5 mg/mL. A PDEGMEMA sample was prepared in water as the polymer alone was not soluble in PBS. All samples were incubated at 4 °C overnight before measurement. The lower critical solution temperature (LCST) of the polymer and conjugate was assessed by measurement of the average size of particles at temperatures from 5 °C to 80 °C. Samples were incubated at each temperature for 2 minutes before measurements. The LCST was assigned as the temperature at which the intensity of scattered light began to increase. For particle size distribution studies at 5 °C, 25 °C, 37 °C, 50 °C, and 70 °C, each sample was incubated for 10 min at the desired temperature before measurements. The reported data represent an average of at least three measurements.

### 2.2.8 Transmission Electron Microscopy (TEM)

Samples for TEM were prepared on carbon-coated copper grids (CF300-Cu, Electron Microscopy Sciences Inc.). The grids, pipette tips, and samples were

incubated in an isothermal oven (VWR Signature™ Forced Air Safety Ovens, VWR Inc.) at desired temperature (25 °C and 50 °C) for at least 30 min before sample preparation, which was also conducted in the oven. PDEGMEMA-CLP and PEG-CLP diblock samples were dissolved in water at concentrations of 1 mg/mL and 5 mg/mL. 5 μL of the sample solution was drop cast on the grid and blotted after 60 seconds. For staining, 1% phosphotungstic acid (PTA) (pH adjusted to 7.0 using 1 M NaOH) as a negative stain was used. 5 μL of the PTA solution was drop cast on the grid and blotted after 10 seconds. The sample was allowed to dry in the oven at the desired temperature for 30 minutes and then was air-dried for 2 hours. TEM images were taken on a Tecnai G2 12 TEM (FEI Company, Hillsboro, OR) at an acceleration voltage of 120 keV.

## 2.3 Results and Discussion

### 2.3.1 Synthesis of PDEGMEMA-CLP Diblock Polymer

The collagen-like peptide with the sequence $(GPO)_7GG$ was synthesized via traditional Fmoc-based, solid-phase peptide synthesis methods (SPPS). Two glycines at the *C*-terminus were introduced to avoid the formation of diketopiperazine.[55] After purification with reverse-phase HPLC, peptide with purity greater than 99% was obtained (Figure 2.10). The molecular weight of the peptide was verified via ESI-MS (Figure 2.11).

The thermoresponsive polymer, PDEGMEMA, was synthesized via reversible addition−fragmentation chain-transfer polymerization (RAFT) using a standard procedure described earlier.[54] The polymer was conjugated to the CLP via the reaction of the activated ester end group of PDEGMEMA with the *N*-terminal amine

of the peptide. The molecular weight distribution of purified products was studied via gel permeation chromatography (GPC) using DMF as the mobile phase (Figure 2.3). DMF was used instead of water because both the polymer and the diblock showed aggregation behavior in aqueous solution (see below). The traces shown were obtained using refractive index detection and were normalized to give a better comparison between the diblock and starting material. The chromatogram for the collagen-like peptide was not collected because the CLP was insoluble in DMF. As shown in Figure 2.3, the elution time of the diblock was clearly shifted to the higher molecular weight region compared with the PDEGMEMA starting material. The results suggest successful conjugation of the two building blocks and the single product peak without any shoulders indicates complete removal of excess PDEGMEMA starting material. A rough estimation of molecular weight from a calibration employing linear poly (methyl methacrylate) (PMMA) standards yielded a Mw of 7.1 kDa of the PDEGMEMA, with a polydispersity index (PDI) of 1.16. Interestingly, the results also suggested a PDI of 1.13 for the diblock and a Mw of 22.1 kDa, which was larger than anticipated, likely due to the potential physicochemical differences between the CLP domain of the diblock and PMMA standards, which would affect their mobility and/or hydrodynamic volume in the mobile phase.

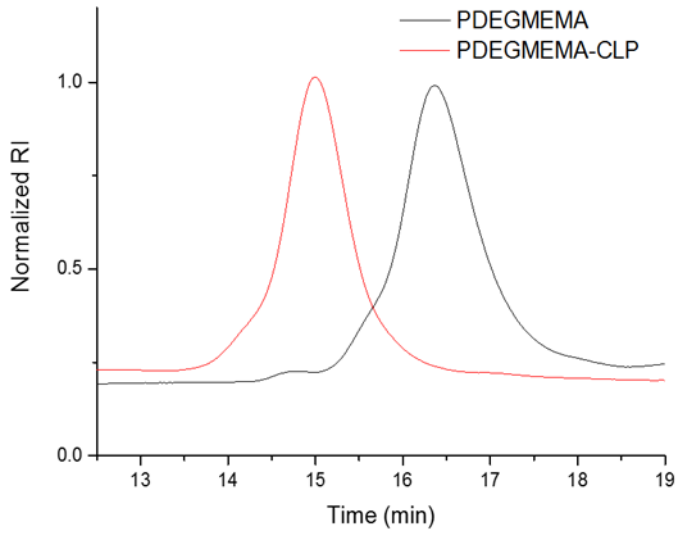


Figure 2.3 GPC trace of PDEGMEMA-CLP diblock and PDEGMEMA starting material.

$^{1}$H NMR spectroscopy was utilized to confirm the presence of both the peptide and polymer domain in the diblock product. Figure 2.4a provides the $^{1}$H NMR spectrum of the collagen-like peptide with typical regions of interest: protons from peptide backbone amide bonds from 7.0 ppm to 8.2 ppm (10H, CO-N*H*-CHR and CO-N$H_2$, labeled $H^{e,e',e''}$ in the figure); α-protons from amino acid residues located from 4.2 ppm to 5.3 ppm (30H, NH-C*H*R-CO and NH-C$H_2$-CO, $H^{c,c',c'',c'''}$); and methylene protons from the pyrrolidine ring from 1.5 ppm to 2.3 ppm (42H, CONR-C$H_2$C$H_2$C$H_2$-CH and CH(OH)-C$H_2$-CH, $H^{d,d',d''}$). The spectrum of PDEGMEMA given in Figure 2.4b shows strong peaks for side-chain ethylene protons at 4.02 ppm (2H, COO-C$H_2$-C$H_2$, $H^{c}$) as well as 3.62 ppm, 3.54 ppm and 3.47 ppm (6H, COO-C$H_2$C$H_2$O-C$H_2$C$H_2$O-CH3, $H^{d,d',d''}$), side-chain methyl group protons at 3.28 pm (3H, OC$H_3$, $H^{e}$), backbone methylene protons from 1.7 ppm to 1.9 ppm (2H, -CRC$H_3$-C$H_2$-,

$H^b$), and methyl group protons at 0.81 ppm and 0.97 ppm (3H, -CRC$H_3$-$CH_2$-, $H^a$). A solvent peak located at 5.76 ppm arises from dichloromethane (DCM), which was introduced to the sample when concentrating the polymer. The spectrum of the PDEGMEMA-CLP diblock, given in Figure 2.4c, showed all corresponding characteristic signals from the polymer as well as the peptide building block. The peaks from DCM observed in the polymer (Figure 2.4b) were completely removed, indicating complete separation by precipitating into cold ether. These results, together with the higher MW suggested by GPC, indicate successful synthesis and purification of the diblock. Comparison between the integrals from peptide α-protons ($H^{c,c',c'',c'''}$ in Figure 2.4a, 30 protons per molecule) with protons from the polymer side-chain methylene group ($H^c$ in Figure 2.4b, 79 protons per molecule) suggested the molecular weight of the polymer domain in the diblock to be 7.4 kDa, which was consistent with the molecular weight determined via GPC.

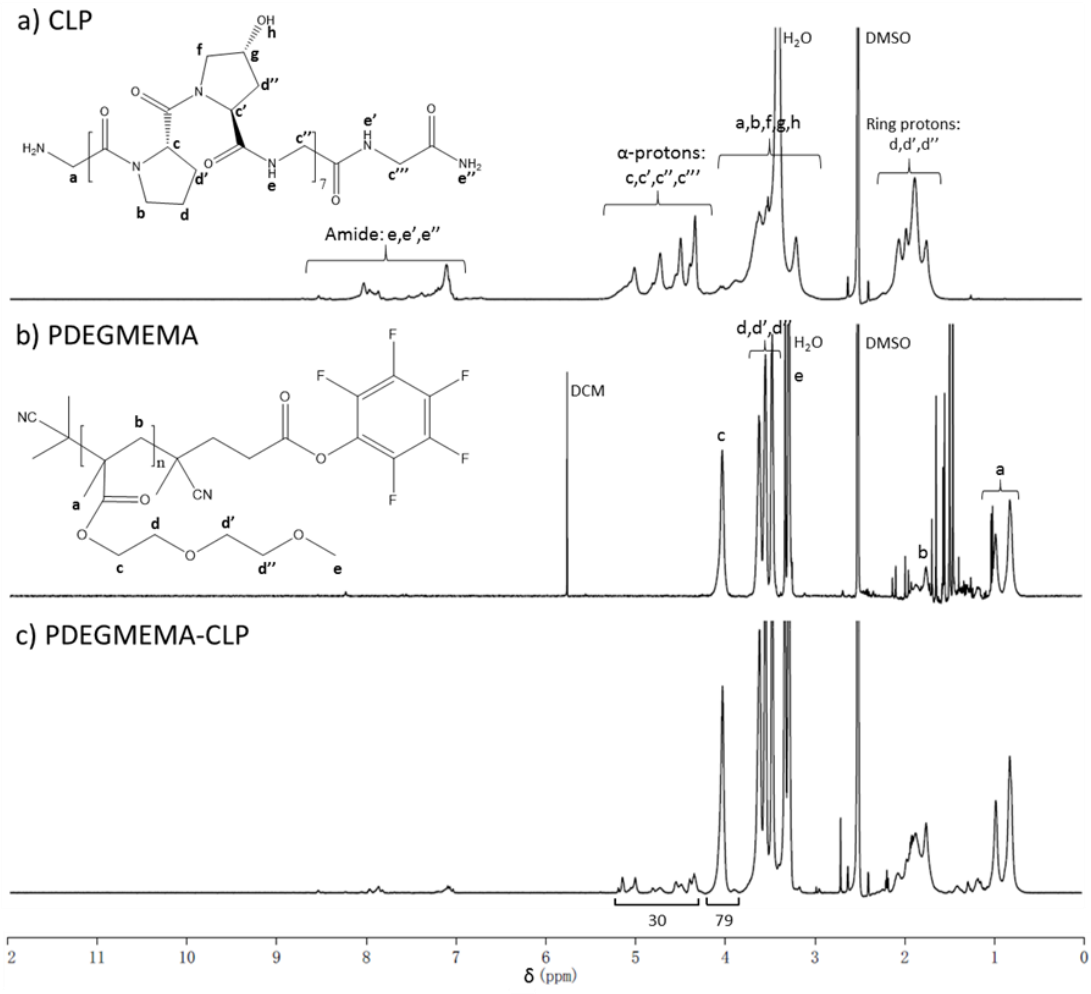


Figure 2.4 $^{1}$H NMR spectra (600 MHz) of: a) collagen-like peptide; b) PDEGMEMA; c) PDEGMEMA-CLP diblock in $d_6$-DMSO.

### 2.3.2 Triple Helix Formation

Although native collagens have a variety of biological functions, at the molecular level, they all share the characteristic triple helical secondary structure. The ability of the collagen-like peptide, as well as the CLP domain in the diblock, to form triple helix is fundamental for specific binding with native collagen via triple helix hybridization. Circular dichroic spectroscopy (CD) was utilized to characterize the

conformation of the peptide products; representative data are shown in Figure 2.5. The CD spectra of the collagen-like peptide and PDEGMEMA-CLP diblock at variable temperatures ranging from 5 °C to 80 °C are plotted in Figure 2.5a and 2.5d, respectively. Both the peptide and diblock exhibited a triple helix characteristic peak at 225 nm and a crossover at 213 nm,[17,19,56] confirming triple helix formation of the CLP, as well as the ability of the CLP domain to maintain the structure after conjugation to the polymer. The intensity of the 225 nm peak was reduced with an increase in temperature (black arrows in Figure 2.5a and 2.5d), consistent with the triple helix domain gradually unfolding upon heating.

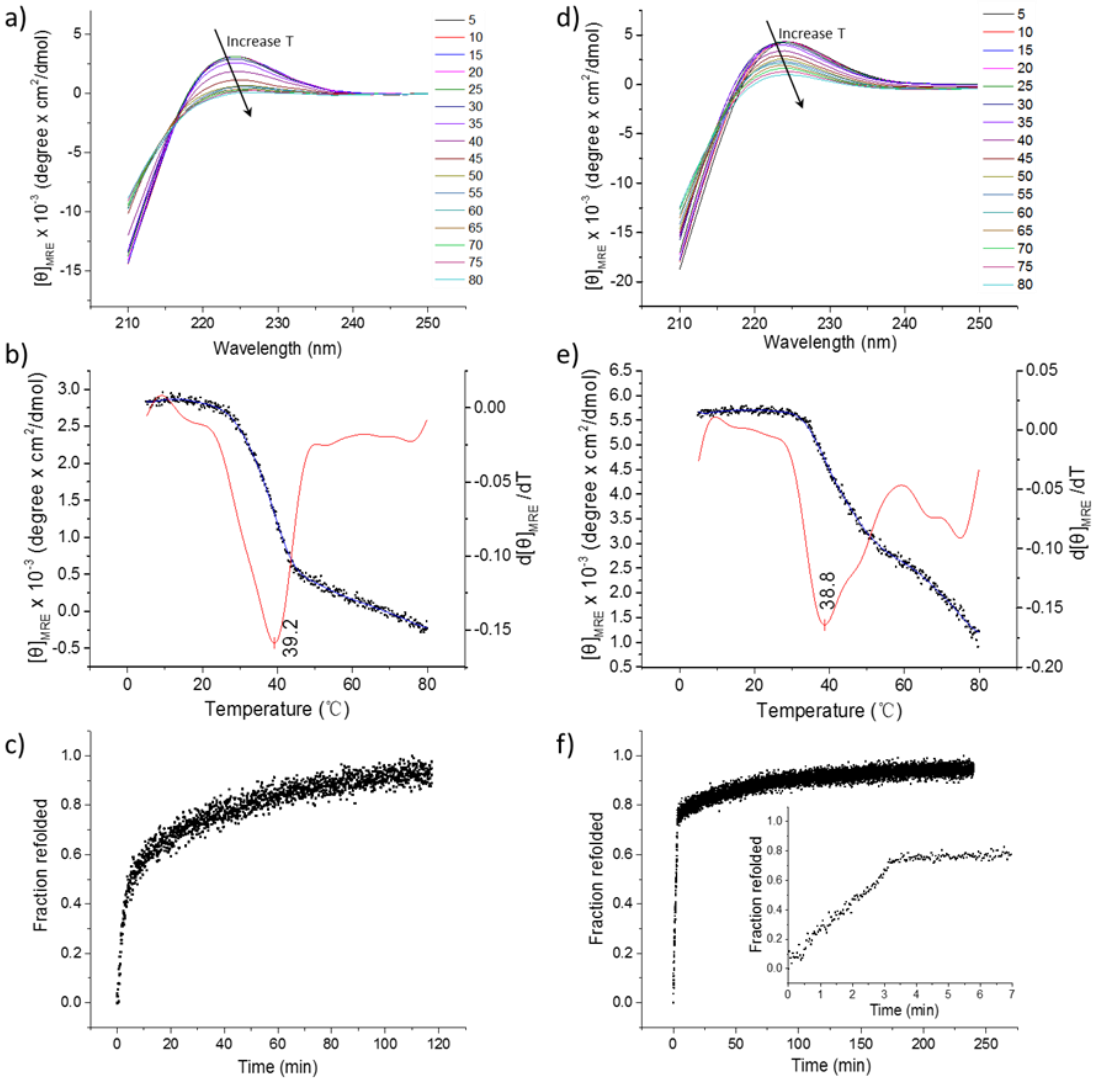
a)
Increase T
5
10
15
20
25
30
35
40
45
50
55
60
65
70
75
80
[θ]MRE x 10-3 (degree x cm2/dmol)
Wavelength (nm)
d)
Increase T
Wavelength (nm)
b)
39.2
d[θ]MRE /dT
Temperature (℃)
e)
38.8
Temperature (℃)
c)
Fraction refolded
Time (min)
f)
Fraction refolded
Time (min)

Figure 2.5 a) CD spectra showing the wavelength scans for the collagen like peptide; b) Blue curve with dots (Y axis on the left side): thermal unfolding profile for CLP plotted as $[\theta]_{MRE225nm}$ versus temperature. The red curve (Y axis on the right side) is the first derivative of the unfolding curve with respect to temperature; c) Refolding profile of CLP after quenching to 5 °C; d) CD spectra showing the wavelength scans for PDEGMEMA-CLP diblock; e) Blue curve with dots (Y axis on the left side): thermal unfolding profile for PDEGMEMA-CLP diblock plotted as $[\theta]_{MRE225nm}$ versus temperature. The red curve (Y axis on the right side) is the first derivative of the unfolding curve with respect to temperature; f) Refolding profile of the PDEGMEMA-CLP diblock after quenching to 5 °C, with an inserted image from 0 – 7 minutes.

The thermal stability of the triple helices was investigated via monitoring the mean residue ellipticity at $\lambda = 225$ nm as a function of temperature while the sample was heated at a slow rate (0.25 °C/min). The thermal unfolding profile (red) and the first derivative of the melting curve (blue) for the CLP and diblock are plotted in Figure 2.5b and 2.5e respectively. The data in Figure 2.5b yield a melting temperature (*Tm*) of 39.2 °C for the peptide and those in Figure 2.5e yield a melting temperature of 38.8 °C for the diblock. The melting temperature of the CLP is consistent with previously reported results for $(Gly\text{-}Pro\text{-}Hyp)_n$ collagen-like peptides.[31,57,58] By comparing the thermal unfolding curves of the CLP and the diblock (blue curves in Figure 2.5b and 2.5e), it is apparent that the triple helix domain in the diblock sample started to melt at a much higher temperature (32 °C) than the peptide alone (20 °C), indicating the greater energy required for the unfolding of the triple helix in the conjugate. Additionally, while the peak at 225 nm for the peptide vanished upon heating (Figure 2.5a), the unfolding process for the triple helix domain in the conjugate was not complete even at 80 °C (Figure 2.5d and 2.5e). These results indicate that the conjugation of PDEGMEMA to the peptide constricts the unfolding

of the triple helix. The constriction is likely attributed to the anchoring effect of the polymer domain when it collapsed above its LCST (32 °C in PBS, Figure 2.6a, described below). Such triple helix stability enhancements via hydrophobic conjugation were also reported in our previous studies,[52,53] as well as by the Fields and the Tong research groups.[49,51]

Temperature jump experiments were conducted to analyze the refolding kinetics of the peptide domain. In these experiments, the samples were incubated at 80 °C for 30 min, followed by quenching to 5 °C to allow triple helix refolding. The ratio of mean residue ellipticity recovered compared to the original value at 5 °C was plotted as a function of time. Figure 2.5c shows the refolding profile for the CLP. After quenching to 5 °C, the CLP gradually refolded to nearly 90% of its original value, following third order reaction kinetics, consistent with previous reports.[59] A rate constant of $k = 3.43 \times 10^{7}$ $M^{-2} \cdot s^{-1}$ was derived from the curve using a third-order reaction model. Interestingly, the PDEGMEMA-CLP diblock reached 80% of its original CD intensity within only 3 minutes (Figure 2.5f), indicating the refolding of the peptide domain within the diblock was much faster than that for the peptide alone. The refolding profile also exhibited a constant refolding rate in the first three minutes, suggesting a zero-order process with a rate constant derived as $1.5 \times 10^{-7}$ $M \cdot s^{-1}$. This difference in the order of the folding process in the free peptide versus the diblock likely originates from the collapsed polymer domain acting as an anchoring point, which significantly increased the local concentration of the peptide strands and refolding rate of the triple helix. Additionally, once the CLPs were anchored at close proximity, long range molecular collision of three CLP single strands driven by Brownian motion was not the main prerequisite for the refolding process, which

changed the order of the reaction. Similar stabilization of secondary structures from such anchoring effects has also been observed in poly(N-isopropylacrylamide)-containing copolymers. For example, the stability of an α-helical peptide domain was increased in a diblock copolymer comprising poly(N-isopropylacrylamide)-*block*-poly($N^5$-(4-hydroxybutyl)-L-glutamine) (PNIPAAm-*b*-PHBG) when compared with that of the PHBG homopolymer.[60]

### 2.3.3 Temperature Triggered Self-Assembly into Nanoparticles

Diblock copolymers consisting of one thermoresponsive block and one hydrophilic block were expected to exhibit reversible self-assembly behaviors as temperature changes. One typical example is poly(ethylene glycol)-*b*-poly(*N*-isopropylacrylamide) (PEG-PNIPAAM), which self assembles into micelles in water above the lower critical solution temperature (LCST) of PNIPAAM.[61-63] The diblock in this work consists of a hydrophilic collagen-like peptide block and a thermoresponsive PDEGMEMA block, thus is anticipated to undergo self-assembly in aqueous conditions when the polymer domain collapses above its LCST. Dynamic light scattering studies were conducted to determine the LCST of the PDEGMEMA-CLP diblock as well as that of the polymer itself by observing the temperature-induced increase in hydrodynamic size. All samples were prepared at concentrations similar to those in the CD experiments, pre-incubated at 4 °C to allow triple helix formation, and filtered to remove dust before the measurements.

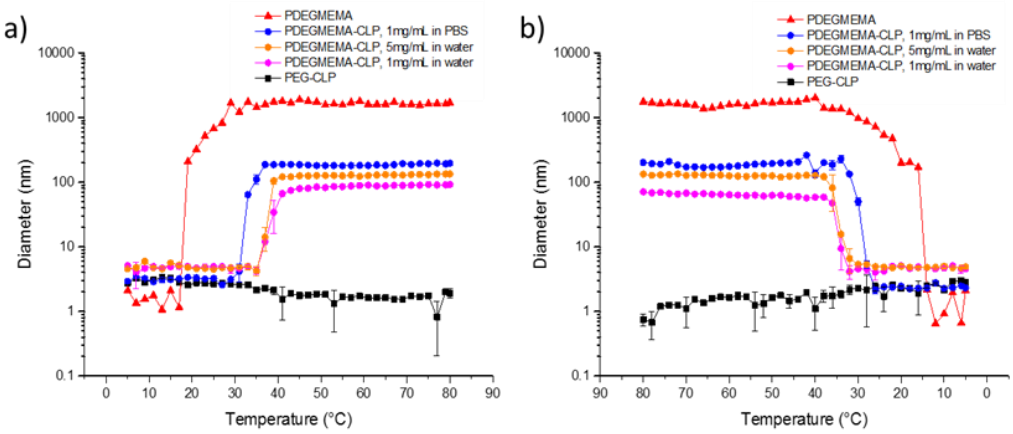


Figure 2.6 Study of transition temperature via dynamic light scattering. a) Hydrodynamic diameter of assemblies as a function of temperature upon heating; b) Hydrodynamic diameter of assemblies as a function of temperature upon cooling. Samples were heated at each temperature for 2 minutes before measurement. Red curve with triangles: PDEGMEMA sample dissolved in water at 1 mg/mL; blue curve with circles: PDEGMEMA-CLP diblock dissolved in PBS buffer (pH = 7.4) at 1 mg/mL; orange curve with circles: PDEGMEMA-CLP diblock dissolved in water at 5 mg/mL; pink curve with circles: PDEGMEMA-CLP diblock dissolved in water at 1 mg/mL; black curve with squares: PEG-CLP diblock dissolved in water at 1 mg/mL

The transition temperature of the conjugate and PDEGMEMA were tested via monitoring of the hydrodynamic diameter as a function of increasing temperature (Figure 2.6a). Diblock sample dissolved in PBS (10 mM, pH 7.4, 137 mM NaCl and 2.7 mM KCl) at a concentration of 1 mg/mL, as well as samples dissolved in water at concentrations of 1 mg/mL and 5 mg/mL were measured. The results show an increase in intensity upon heating and suggested a transition temperature of 18 °C for the polymer and 32 °C for the diblock. As expected, the PEG-CLP control does not exhibit any phase transition behavior in the entire temperature range. The increase in the transition temperature for the PDEGMEMA-CLP diblock compared with the

polymer is consistent with the conjugation of the hydrophilic peptide block to the polymer. Changes in LCST due to hydrophobicity differences have also been reported in PNIPAAM containing copolymers modified with short hydrophilic DNA segments[64] or poly(lysine) segments,[65] as well as elastin-like peptides (ELP) with amino acid valine (V) substituted by more hydrophobic residues such as leucine, isoleucine and phenylalanine.[66,67]

Due to practical difficulties in studies of assembly morphology with transmission electron microscopy using samples in PBS buffer, samples dissolved in water (at either 1 mg/mL or 5 mg/mL) were also prepared. Both samples exhibited a transition temperature of 37 °C, which was higher than that for samples dissolved in PBS. The lower LCST observed for diblock sample in PBS buffer is likely attributed to the salting out effect of kosmotropic ions added to the solution.[68,69] Cooling experiments were conducted to test the reversibility of this transition; the data are shown in Figure 2.6b. As illustrated in the figure, each sample shows only a small hysteresis in the transition, with LCSTs determined as 15 °C for PDEGMEMA, 29 °C for the diblock in PBS, and 34 °C for the diblock in $H_2O$. The consistency of these values with those of the heating experiments confirms the reversibility of these transitions under the experimental conditions tested.

DLS was also utilized to study the size distribution of the nanostructures formed by the conjugate. Figure 2.7a and 2.7b show the size distributions for PDEGMEMA-CLP diblock samples dissolved in water, at 1 mg/mL and 5 mg/mL respectively. In both cases, no higher order assembly was observed at 25 °C. The small objects with diameters of approximately 5 nm were attributed to the soluble trimers of the diblock, consistent with previous reports.[18,21] For the 1 mg/mL

sample, nanostructures with average diameter of approximately 45 nm were formed at higher temperatures, while nanostructures with diameters around 110 nm were observed in the 5 mg/mL sample. Larger structures formed at 5 mg/mL may be attributed to a fusion process of smaller structures at higher concentrations (see below). Although CLP peptides alone have been reported to aggregate at high concentrations,[19,58] a PEG-CLP diblock control at the lower concentrations here did not show any aggregation at any temperatures measured (Figure 2.16a), while on the other hand, heating a PDEGMEMA solution above its LCST (18 °C) yielded large aggregates with diameters of approximately 1.7 μm (Figure 2.16b). These observations confirm both the role of the PDEGMEMA in the thermally induced aggregation and the role of the CLP in stabilization of the observed nanostructures.

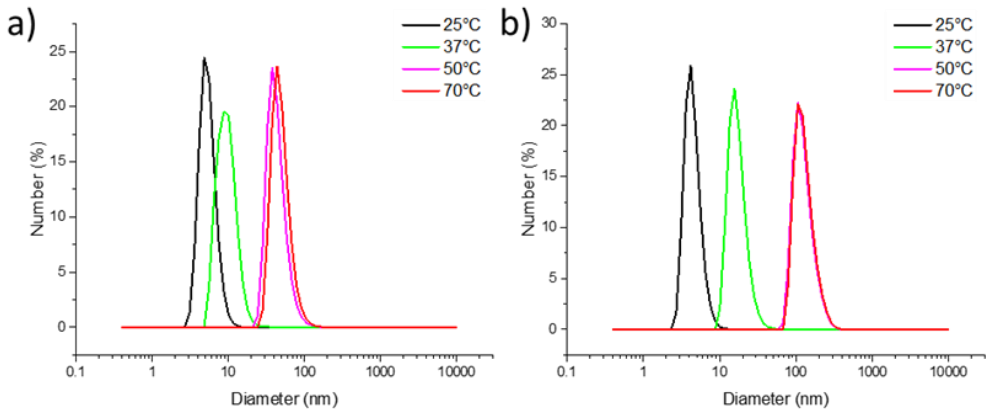


Figure 2.7 Size distribution of assemblies at different temperatures. a) PDEGMEMA-CLP diblock, 1 mg/mL in water; b) PDEGMEMA-CLP diblock, 5 mg/mL in water. Correlation functions and cumulant fits are provided in the Supporting Information (Figure 2.15)

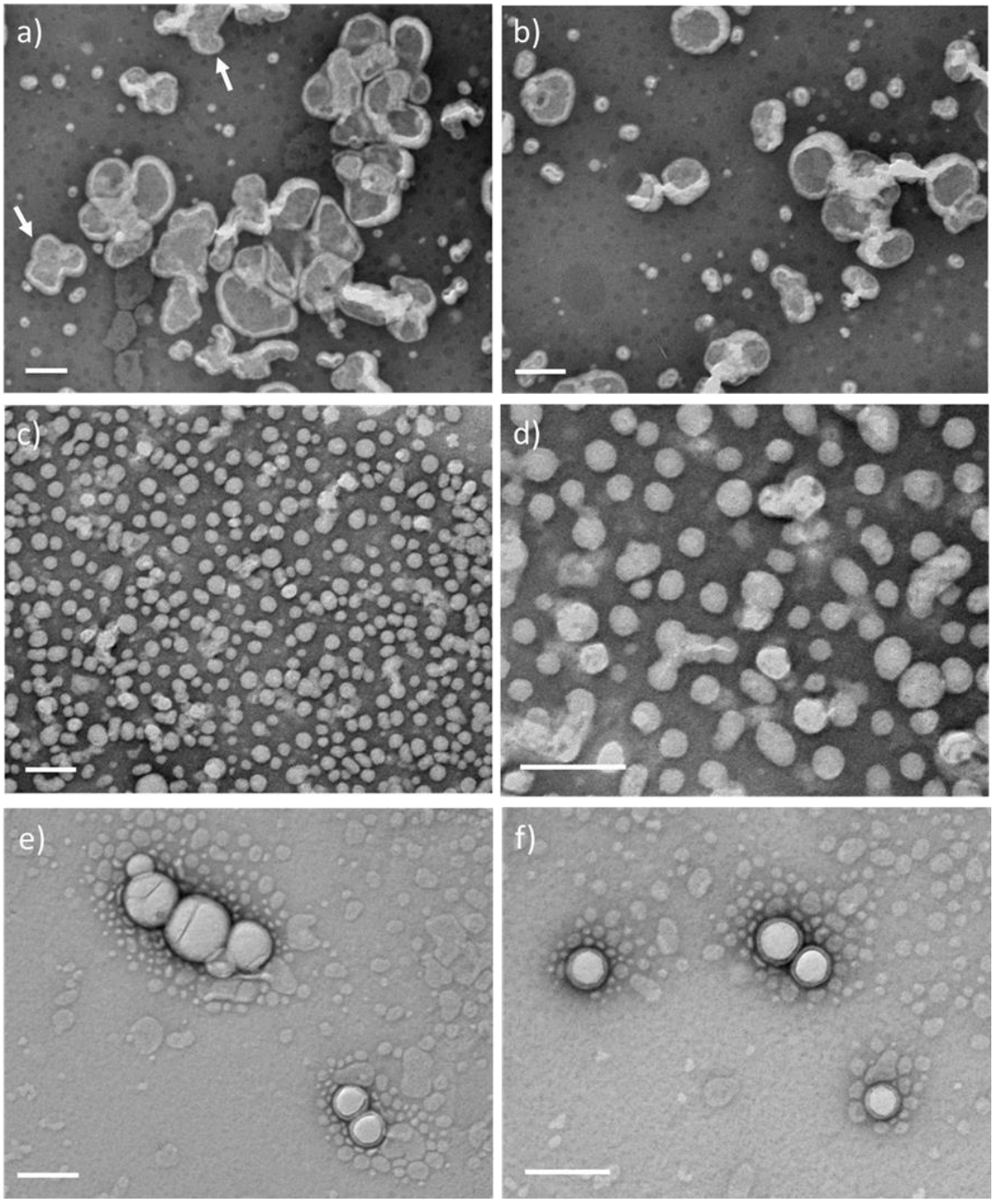


Figure 2.8 TEM images of nanoparticles formed from PDEGMEMA-CLP diblock at 50 °C, stained with phosphotungstic acid (1% PTA in water, pH adjusted to 7.0). a,b) 5 mg/mL; c,d) 1 mg/mL; e,f) 1 mg/mL, washed with deionized water after staining. Scale bars: 200 nm.

To obtain insight into the morphologies of the nanostructures observed via DLS, transmission electron microscopy (TEM) measurements were also conducted. To better visualize the nanostructures, a 1% phosphotungstic acid (PTA, pH adjusted to 7.0 using NaOH) aqueous solution was used as negative stain. At 25 °C, which was below the LCST of PDEGMEMA domain in the diblock, no nanostructures were detected under any solution conditions (data not shown). When the diblock solutions were heated above the transition temperature, the polymer domain became hydrophobic and collapsed in aqueous solution, causing the solution to immediately become cloudy. Representative TEM images of the nanostructures formed at 50 °C by the 5 mg/mL sample are shown in Figure 2.8a and 2.8b. Nanostructures with an average diameter of approximately 70 – 200 nm were observed, which is consistent with the DLS measurements discussed above (Figure 2.7b). As observed in the images, both the exterior and interior surface of the nanoparticles are clearly observed, suggesting that the particles may have a hollow vesicular structure. It is possible that the solvent evaporation process employed during sample preparation destabilized the vesicles, and exposed the interior of the vesicles to the staining agent. Similar observations were also reported for bilayer vesicles formed from synthetic lipids 1,2-di-n-hexadecyloxypropyl-4-(beta-nitrostyryl) phosphate (DHPBNS) under aqueous conditions.[70] Some large particles with d ≈ 300 – 400 nm were also observed, which were likely generated via fusion of smaller particles during solvent evaporation (indicated by arrows in Figure 2.8a). For samples prepared at 1 mg/mL, smaller nanoparticles with an average diameter of approximately 50 nm are observed (Figure 2.8c and 2.8d), which is also consistent with DLS results (Figure 2.7a). The vesicular morphology of these particles was resolved more clearly when the sample grid was

washed with deionized water after staining (Figure 2.8e and 2.8f). TEM analysis of PDEGMEMA solutions was found to be difficult practically because PDEGMEMA with Mw = 7 kDa is a liquid. As in the DLS experiments, no vesicular structures were observed for the hydrophilic-hydrophilic PEG-CLP diblock conjugate investigated under the same conditions, indicating that the thermally responsive collapse of the PDEGMEMA is crucial for the assembly of the vesicles.

The nanoscale vesicular structures observed in this work are similar to those previously reported from other thermoresponsive polymer-based systems. For example, due to its high biocompatibility and its LCST of approximately 32 °C,[71] poly(*N*-isopropylacrylamide) (PNIPAAM) has become one of the most widely used building blocks for producing copolymers with thermoresponsive behavior. Otsuka et al.[72] observed vesicular morphologies with a diameter of 300 nm from the assembly of maltoheptose-*block*-poly(*N*-isopropylacrylamide) (Mal7-*b*-PNIPAAMn) hybrid diblock copolymers at 90 °C. More recently, Zhao et al.[73] synthesized polyethylene-*graft*-poly(*N*-isopropylacrylamide) copolymers (PE-*g*-PNIPAM) using coordination copolymerization and RAFT copolymerization. The amphiphilic graft copolymer formed vesicles with average diameters of 170-190 nm in aqueous solution when incubated at temperatures between 20-32 °C.

Nanoscale vesicles have also been observed from the assembly of other polymer-peptide conjugates, although to our knowledge not from samples in which the polymer block shows thermally responsive behavior. For example, Marsden et al.[74] reported vesicles with a diameter of 100 – 400 nm from the self-assembly, in aqueous conditions, of a conjugate diblock comprising poly(γ-benzyl L-glutamate) (PBLG) and a coiled-coil forming peptide with the sequence G(EIAALEK)$_3$. Similar vesicular

structures with diameter of 30 – 100 nm were also reported by Koga et al.,[75] using a β-sheet peptide-inserted amphiphilic block copolymer, polystyrene-*block*-tetra(leucine)-*block*-poly(ethylene glycol) (PS-*b*-L4-*b*-PEG). More recently, Bacinello et al.[76] reported the self-assembly of amphiphilic peptide-polymer hybrids comprising poly(trimethylene carbonate) (PTMC) and a matrix metalloproteinase-2 (MMP-2)-degradable peptide PVGLIG. Various morphologies including core-shell micelles and nanoscale vesicles with diameters of approximately 40 – 70 nm were reported. In one study involving CLP-based conjugates, Luo et al.[51] reported the self-assembly of a CLP-containing amphiphile with a C16 lipophilic tail attached to the *C*-terminus. Micrometer-long nanofibers with a diameter of approximately 16 nm were observed under aqueous conditions.

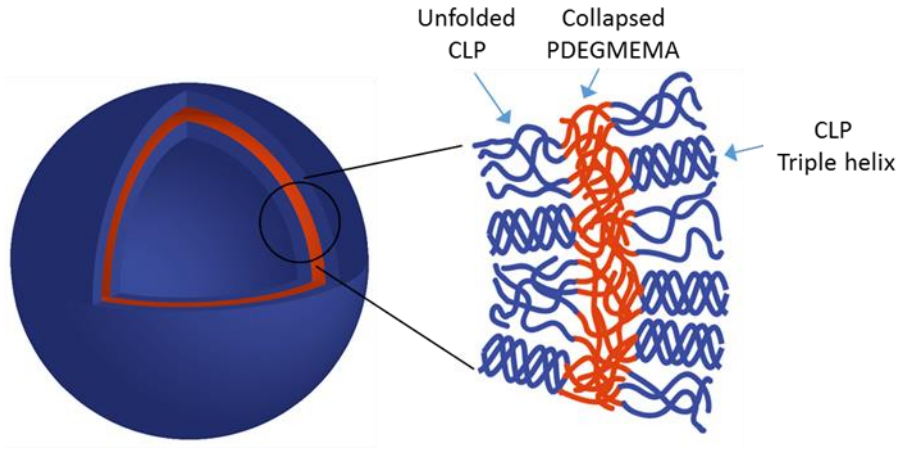


Figure 2.9 Schematic illustration of the potential structure of vesicles formed at 50 °C in aqueous condition.

Compared with the surge in research on thermoresponsive polymers and other peptide-polymer conjugates, there are few reports focused on the assembly of

collagen-like peptide containing copolymers, and none to our knowledge in which nanovesicles are produced. Figure 2.9 illustrates the potential molecular organization of the vesicles observed at 50 °C in deionized water. Although other assembly mechanisms are possible, the proposed bilayer vesicular assembly pathway is likely for the nanostructures that we observed; the parallel orientation of the CLP domains are expected on the basis of previous reports.[24,27,30,77,78] At 25 °C, both building blocks of the diblock are hydrophilic, thus the diblock is fully soluble in deionized water, in the form of the triple helix-containing trimer. As the solution is heated to above the LCST of PDEGMEMA (37 °C), the polymer domain collapses and triggers coacervation. The radius of gyration (Rg) of 7 kDa PDEGMEMA in aqueous solution is calculated to be 2.2 nm below its LCST (good solvent) and 0.83 nm above LCST (bad solvent).[79] The collagen triple helix of $(GPO)_7GG$ is a semi-flexible rod with the length of 6.4 nm and diameter of 1.5 nm.[80] When the solution is heated above 37 °C, the diblock trimer thus can be treated as a rod-coil structure with dimensions of roughly 6.4 nm (rod)-1.2 nm (coil) (Rg of three anchored polymer chains). For a conventional coil-coil amphiphilic diblock, assemblies adopt rounded interfaces in order to minimize the interfacial contact between the solvent and the less soluble block. However, for rod-coil copolymers, the packing of the rods at a highly curved surface creates liquid crystalline defects, which increases the free energy of the assemblies.[81] It is likely that the tradeoffs between the liquid crystalline defect energy and surface energy give rise to the formation of vesicles, which have a lower interface curvature compared with micelles. Further heating of the solution to a higher temperature unfolds the collagen triple helix, but due to the stabilization of the collapsed PDEGMEMA as an anchoring point, this unfolding process is not completed until

above 80 °C (Figure 2.5b and 2.5e). Thus at 50 °C, the CLP domain remains partially unfolded (Figure 2.9). It is noteworthy that once the particles have been formed, their size does not change upon heating (Figure 2.6a), suggesting that unfolding of the CLP domain on the vesicle exterior and interior surfaces does not change the morphology of the vesicle. Although the size of the CLP may change during unfolding, the changes must be small compared to the size of the nanostructures. According to the TEM results (Figure 2.8f), the thickness of the vesicle surfaces is of approximately 10.5 – 19 nm, which is consistent with the calculated thickness of the bilayer proposed in Figure 2.9 (approximately 15nm based on the length of the $GPO_7$ triple helix (6.4 nm) and the Rg of three collapsed PDEGMEMA chains (~1.2 nm)).

Instead of using a conventional thermoresponsive polymer like PNIPAAM, the use of PDEGMEMA offers the improvement of a much lower LCST (18 °C in this case), so that after conjugation with the hydrophilic peptide, the polymer remains soluble at room temperature, with higher order assemblies being triggered at physiological temperature. Although understanding of the detailed role of the peptide trimerization and unfolding on the formation of observed nanostructures will require further investigation, the introduction of CLP domains at the exterior surface of the vesicles may serve as a specific means to target native collagens via triple helix hybridization. These peptide-based, dually thermally responsive conjugates thus offer intriguing opportunities for potential applications in targeted delivery of therapeutics for a range of pathologic conditions associated with collagen denaturation and reconstitution, such as tumor and rheumatoid arthritis.[82]

## 2.4 Conclusions

The conformational properties and assembly of a new class of thermoresponsive diblock conjugates, containing collagen-like peptides and PDEGMEMA, were introduced in this work. Circular dichroism (CD) experiments confirmed the ability for the peptide domain to adopt a triple helix conformation after conjugation with the polymer. The engineered LCST of these conjugates has enabled temperature-induced assembly under aqueous conditions, at physiologically relevant temperatures, into well-defined vesicles with diameters of approximately 50-200 nm. The formation of nanostructures was driven by the coil/globule conformational transition of the PDEGMEMA building block above its LCST with stabilization of the nanostructures by the hydrophilic CLP. To the best of our knowledge, this is the first report on such assembled nanostructures from collagen-like peptide containing copolymers. Due to the strong propensity for CLPs to bind to natural collagen via strand invasion processes,[29] these nanosized vesicles may be used as drug carriers for targeted delivery.

## 2.5 Supporting Information

### 2.5.1 Peptide Synthesis and Characterization

Figure 2.10 shows the RP-HPLC trace of purified peptide. The single highly symmetric peak indicates a pure product was obtained. The molecular weight of the peptide was verified via ESI-MS (Figure 2.11). Mw of $(GPO)_7GG$ =2002.1 Da; m/z = 1001.7 [$(M+2H)^{2+}$, calcd 1002.1], m/z = 1012.9 [$(M+H+Na)^{2+}$, calcd 1013.1], m/z = 1024.6 [$(M+2Na)^{2+}$, calcd 1024.1], m/z = 683.2 [$(M+H+2Na)^{3+}$, calcd = 683.0]

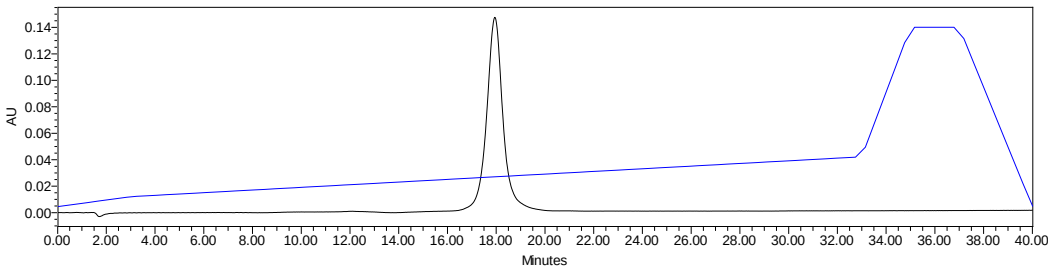


Figure 2.10 RP-HPLC trace of collagen like peptide $(GPO)_7GG$, blue line indicates the gradient used.

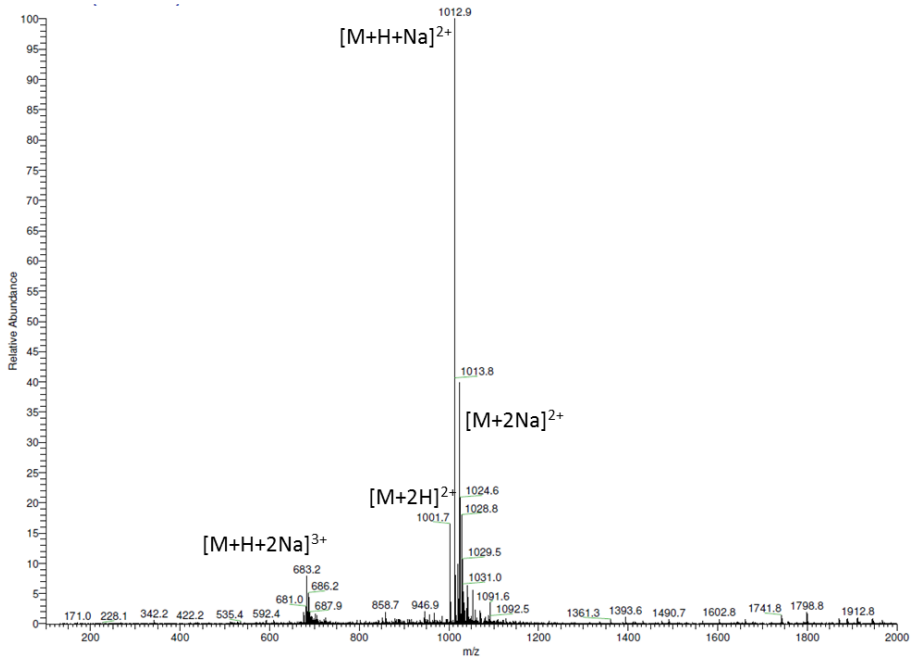


Figure 2.11 ESI-MS of purified CLP.

### 2.5.2 PEG-CLP Conjugate Synthesis and Characterization

PEG was attached to the collagen-like peptide using an "on resin" method (Figure 2.12). 100 mg resin with CMP loaded (0.0115 mmol) was swelled in DCM for 30 min. 230 mg PEG-NHS ester (0.046 mmol, 4 x equivalence of CLP) was dissolved in 1 mL DMSO and the solution was reacted with the resin, with the addition of 3 μL triethylamine, for 3 days at 35 °C in an oil bath. After conjugation, the resin was filtered out and washed with 3 x DMSO and 3 x DCM to remove excess PEG starting material. A negative Kaiser test result for the PEG conjugated resin suggested that the CLP *N*-terminal amine was fully reacted. The conjugate was then cleaved off the resin, dialyzed against water and lyophilized.

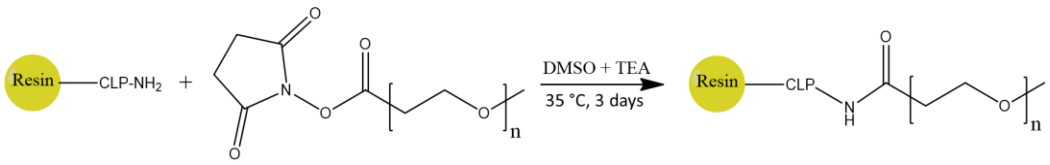


Figure 2.12 PEG-CLP conjugation reaction

GPC measurement of the PEG-CLP conjugate was performed in 10 mM PBS buffer (pH 7.4, 137 mM NaCl and 2.7 mM KCl) using a combination of two Waters ultrahydro linear column (WAT011545 and WAT011525) with a nominal flow rate of 1 mL/min. A refractive index detector (Waters 2414), a UV absorbance detector (Waters 2996) were used. PEG standards with Mw 400 Da, 1970 Da, 6430 Da and 21030 Da were used to calculate molecular weights of the products. CLP and PEG

starting material samples were dissolved in PBS at a concentration of 2 mg/mL, PEG-CLP diblock conjugate sample was dissolved in PBS at a concentration of 1 mg/mL. 100 µL solution was injected for all samples.

Figure 2.13a and 2.13b showed the refractive index and 214 nm UV absorbance (typical amide bond absorbance wavelength) chromatogram of PEG-CLP diblock and related starting materials respectively. The diblock product signal was clearly shifted to the higher molecular weight compared to either of the building blocks. A small shoulder on the right side of the main peak was observed for the diblock and the collagen-like peptide. This is attributed to the existence of both triple-helical trimer and single-stranded monomer in aqueous conditions at room temperature.

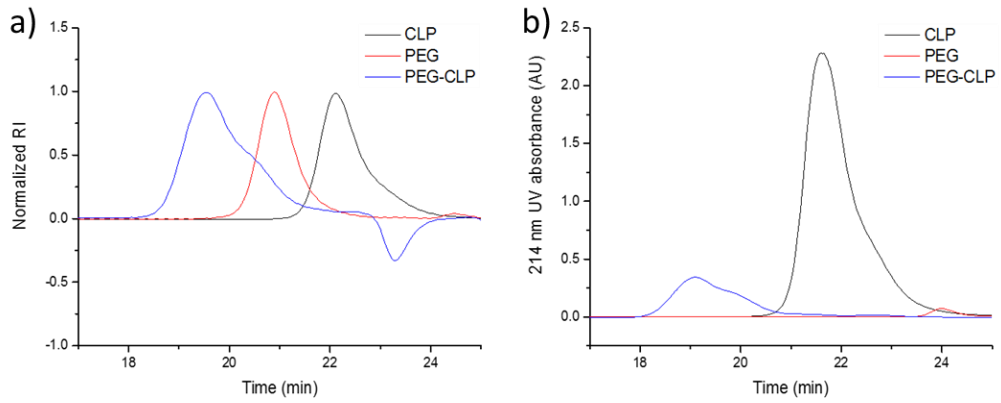


Figure 2.13 GPC traces of PEG-CLP diblock and starting materials. a) Normalized refractive index chromatogram of PEG-CLP diblock copolymer and CLP, PEG starting material. b) 214 nm UV absorbance of PEG-CLP diblock and CLP, PEG starting material.

Figure 2.14 showed the $^{1}$H NMR spectra of PEG-CLP diblock and related starting materials dissolved in $d_6$-DMSO. The spectrum of the diblock showed strong signals of the PEG building block as well as the peptide building block. For example, signals from the amide bond protons located at 6.5 – 8.5 ppm, signals from the α-carbon protons between 4-5.5 ppm and signals from PEG backbone protons at 3.54 ppm.

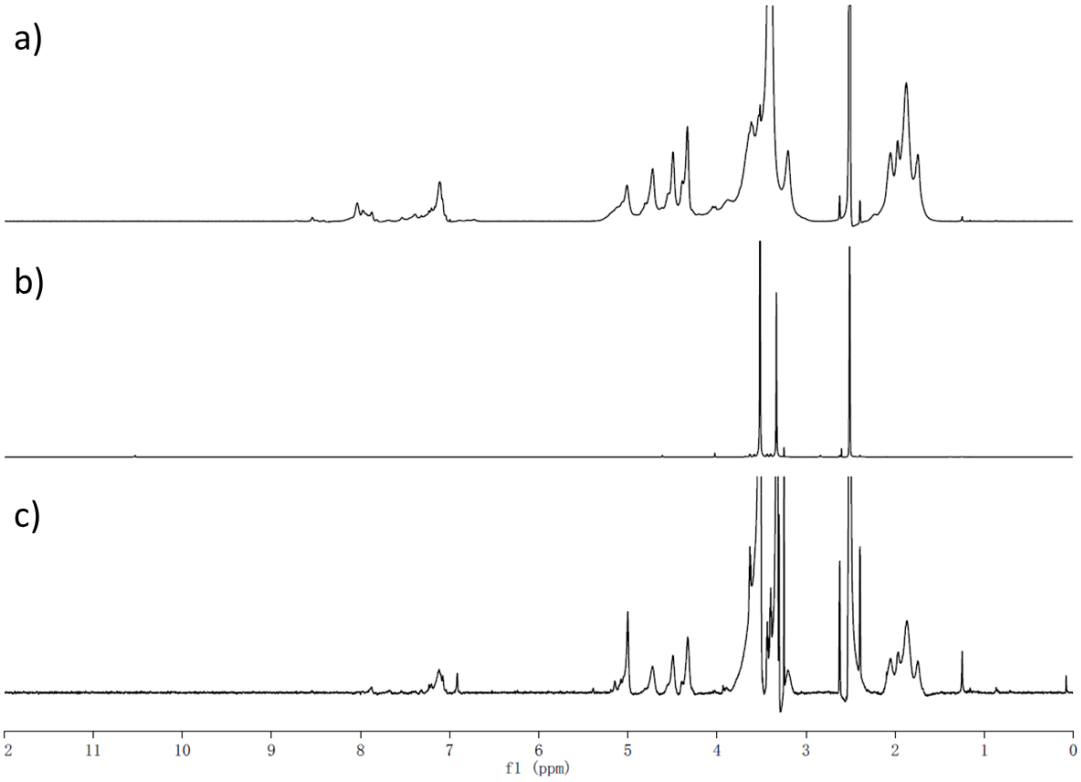


Figure 2.14 $^{1}$H NMR spectra (600 MHz) of: a) collagen like peptide; b) PEG5k; c) PEG-CLP diblock in $d_6$-DMSO.

### 2.5.3 DLS correlation function and cumulant fit curve

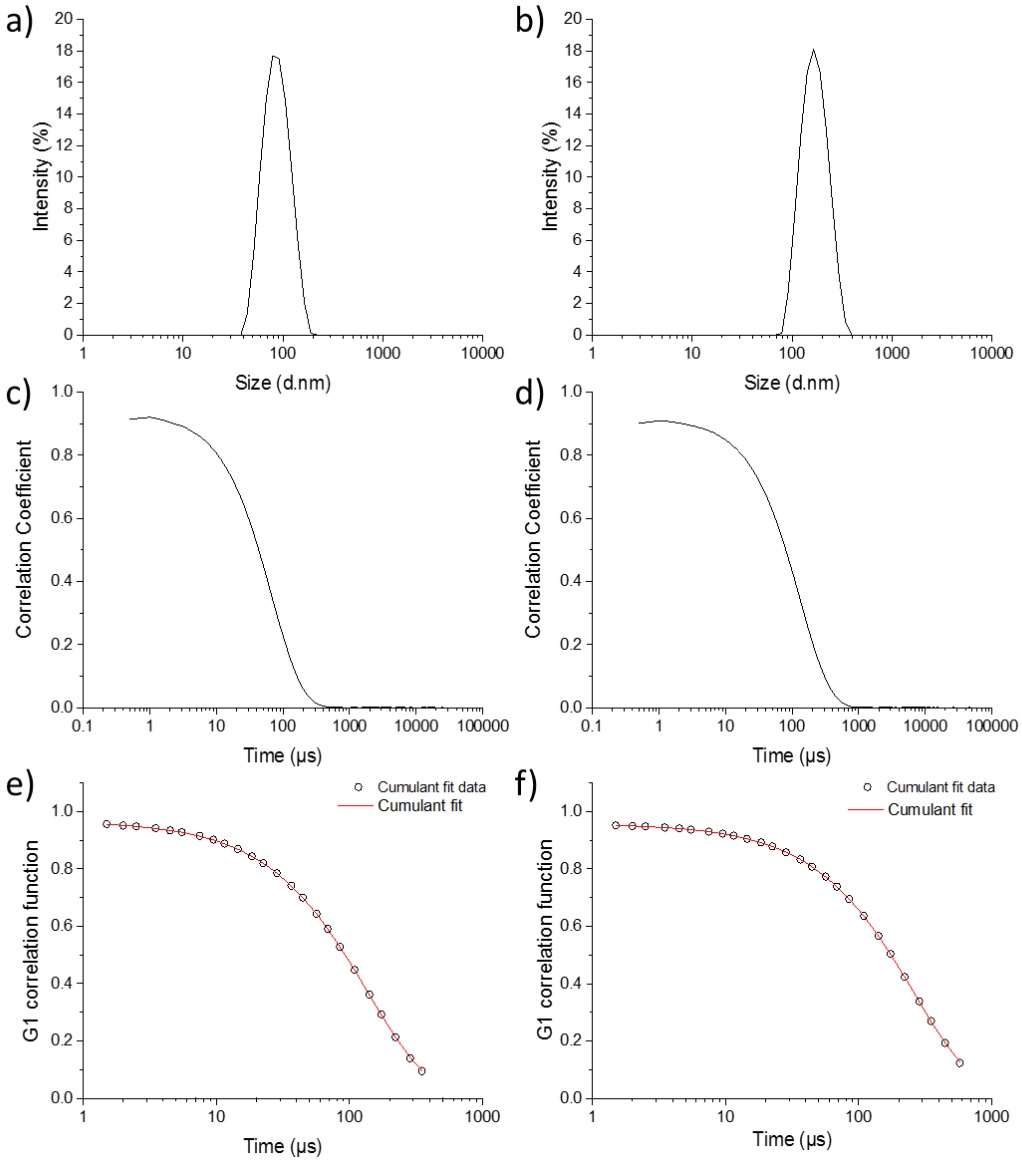

Figure 2.15 DLS data at 50 °C. a) Size distribution by intensity for 1 mg/mL diblock sample; b) Size distribution by intensity for 5 mg/mL diblock sample; c) raw correlation function for 1 mg/mL diblock sample; d) raw correlation function for 5 mg/mL diblock sample; e) Fitting curve using cumulant method for 1 mg/mL sample, empty circles indicate experimental data; f) Fitting curve using cumulant method for 5 mg/mL sample, empty circles indicate experimental data.

The particles formed at 50 °C for diblock samples at 1 mg/mL and 5 mg/mL in water showed monodisperse distribution, with polydispersity indices of 0.079 and 0.067, respectively. The results suggest the system is homogeneous at T > LCST. The correlation function raw data are shown in Figure 2.15c and 2.15d. The G1 correlation function using cumulant fit method are shown in Figure 2.15e and 2.15f. Both curves fit the experimental data nicely.

### 2.5.4 Size Distribution of PEG-CLP and PDEGMEMA Controls

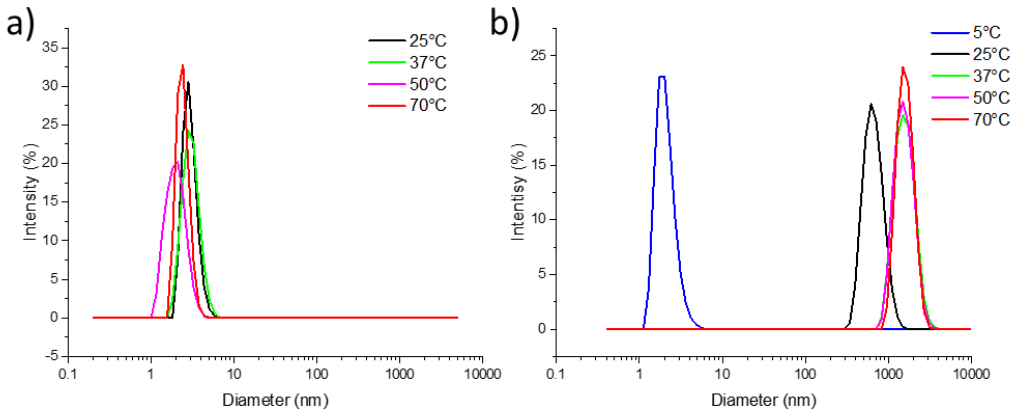


Figure 2.16 Size distribution by number at different temperatures. a) PEG-CLP diblock, 1 mg/mL in water; b) PDEGMEMA, 1 mg/mL in water.

## 2.6 Acknowledgements

This work was funded in part by the National Science Foundation (DMR 0907478 to K.L.K.) and the National Center for Research Resources (NCRR), a component of the National Institutes of Health (P30 GM103519 for instrument resources). This work was also supported in part by the Center for Neutron Science at UD under award (U.S. Department of Commerce) #70NANB7H6178. Its contents are solely the responsibility of the authors and do not necessarily represent the official views of NCRR or NIH. The authors wish to acknowledge Chaoying Ni, Fei Deng, Yingchao Chen, and Darrin Pochan at the University of Delaware for their advice and assistance with TEM. We also thank Rachel Letteri at University of Massachusetts Amherst for conducting GPC, which was supported by the Materials Research Facilities Network (MRFN) of the UMass MRSEC on Polymers (DMR-0820506).

## REFERENCES


1. Kadler, K. E.; Baldock, C.; Bella, J.; Boot-Handford, R. P. *J. Cell Sci.* **2007**, *120*, 1955.

2. Ramachandran, G. N.; Kartha, G. *Nature* **1955**, *176*, 593.

3. Ramshaw, J. A. M.; Shah, N. K.; Brodsky, B. *J. Struct. Biol.* **1998**, *122*, 86.

4. Watanabe, K.; Nishio, Y.; Makiura, R.; Nakahira, A.; Kojima, C. *Int. J. Pharm.* **2013**, *446*, 81.

5. Kojima, C.; Suehiro, T.; Watanabe, K.; Ogawa, M.; Fukuhara, A.; Nishisaka, E.; Harada, A.; Kono, K.; Inui, T.; Magata, Y. *Acta Biomater* **2013**, *9*, 5673.

6. Ruszczak, Z.; Friess, W. *Adv Drug Deliver Rev* **2003**, *55*, 1679.

7. Lee, C. H.; Singla, A.; Lee, Y. *Int. J. Pharm.* **2001**, *221*, 1.

8. Luo, T. Z.; Kiick, K. L. *Eur. Polym. J.* **2013**, *49*, 2998.

9. Yu, S. M.; Li, Y.; Kim, D. *Soft Matter* **2011**, *7*, 7927.

10. Shoulders, M. D.; Raines, R. T. In *Annu. Rev. Biochem.*; Annual Reviews: Palo Alto, 2009; Vol. 78, p 929.

11. Fallas, J. A.; Dong, J. H.; Tao, Y. Z. J.; Hartgerink, J. D. *J. Biol. Chem.* **2012**, *287*, 8039.

12. Persikov, A. V.; Ramshaw, J. A. M.; Brodsky, B. *J. Biol. Chem.* **2005**, *280*, 19343.

13. Boudko, S. P.; Engel, J. *J. Mol. Biol.* **2004**, *335*, 1289.

14. Barth, D.; Kyrieleis, O.; Frank, S.; Renner, C.; Moroder, L. *Chem-Eur J* **2003**, *9*, 3703.

15. Yang, W.; Chan, V. C.; Kirkpatrick, A.; Ramshaw, J. A. M.; Brodsky, B. *J. Biol. Chem.* **1997**, *272*, 28837.

16. He, L. R.; Theato, P. *Eur. Polym. J.* **2013**, *49*, 2986.

17. O'Leary, L. E. R.; Fallas, J. A.; Bakota, E. L.; Kang, M. K.; Hartgerink, J. D. *Nat. Chem.* **2011**, *3*, 821.

18. Przybyla, D. E.; Chmielewski, J. *J Am Chem Soc* **2008**, *130*, 12610.

19. Krishna, O. D.; Kiick, K. L. *Biomacromolecules* **2009**, *10*, 2626.

20. Cejas, M. A.; Kinnney, W. A.; Chen, C.; Vinter, J. G.; Almond, H. R.; Balss, K. M.; Maryanoff, C. A.; Schmidt, U.; Breslav, M.; Mahan, A.; Lacy, E.; Maryanoff, B. E. *P Natl Acad Sci USA* **2008**, *105*, 8513.

21. Cejas, M. A.; Kinney, W. A.; Chen, C.; Leo, G. C.; Tounge, B. A.; Vinter, J. G.; Joshi, P. P.; Maryanoff, B. E. *J Am Chem Soc* **2007**, *129*, 2202.

22. Rele, S.; Song, Y. H.; Apkarian, R. P.; Qu, Z.; Conticello, V. P.; Chaikof, E. L. *J Am Chem Soc* **2007**, *129*, 14780.

23. Pires, M. M.; Przybyla, D. E.; Perez, C. M. R.; Chmielewski, J. *J Am Chem Soc* **2011**, *133*, 14469.

24. Pires, M. M.; Lee, J.; Ernenwein, D.; Chmielewski, J. *Langmuir* **2012**, *28*, 1993.

25. Hsu, W.; Chen, Y. L.; Horng, J. C. *Langmuir* **2012**, *28*, 3194.

26. Perez, C. M. R.; Rank, L. A.; Chmielewski, J. *Chem. Commun.* **2014**, *50*, 8174.

27. Perez, C. M. R.; Panitch, A.; Chmielewski, J. *Macromol. Biosci.* **2011**, *11*, 1426.

28. Hernandez-Gordillo, V.; Chmielewski, J. *Biomaterials* **2014**, *35*, 7363.

29. Wang, A. Y.; Mo, X.; Chen, C. S.; Yu, S. M. *J Am Chem Soc* **2005**, *127*, 4130.

30. Li, Y.; Ho, D.; Meng, H.; Chan, T. R.; An, B.; Yu, H.; Brodsky, B.; Jun, A. S.; Yu, S. M. *Bioconjugate Chem.* **2013**, *24*, 9.

31. Wang, A. Y.; Foss, C. A.; Leong, S.; Mo, X.; Pomper, M. G.; Yu, S. M. *Biomacromolecules* **2008**, *9*, 1755.

32. Li, Y.; Foss, C. A.; Summerfield, D. D.; Doyle, J. J.; Torok, C. M.; Dietz, H. C.; Pomper, M. G.; Yu, S. M. *P Natl Acad Sci USA* **2012**, *109*, 14767.

33. Krishna, O. D.; Jha, A. K.; Jia, X. Q.; Kiick, K. L. *Biomaterials* **2011**, *32*, 6412.

34. Zhang, Z.; Lai, Y. X.; Yu, L.; Ding, J. D. *Biomaterials* **2010**, *31*, 7873.

35. Humtsoe, J. O.; Kim, J. K.; Xu, Y.; Keene, D. R.; Hook, M.; Lukomski, S.; Wary, K. K. *J. Biol. Chem.* **2005**, *280*, 13848.

36. Harris, J. M.; Chess, R. B. *Nat. Rev. Drug Discov.* **2003**, *2*, 214.

37. Klok, H. A. *J. Polym. Sci. Pol. Chem.* **2005**, *43*, 1.

38. Ding, J. X.; Xiao, C. S.; Tang, Z. H.; Zhuang, X. L.; Chen, X. S. *Macromol. Biosci.* **2011**, *11*, 192.

39. Wigenius, J.; Bjork, P.; Hamedi, M.; Aili, D. *Macromol. Biosci.* **2010**, *10*, 836.

40. Shu, J. Y.; Tan, C.; DeGrado, W. F.; Xu, T. *Biomacromolecules* **2008**, *9*, 2111.

41. Sahin, E.; Kiick, K. L. *Biomacromolecules* **2009**, *10*, 2740.

42. Kopecek, J.; Yang, J. Y. *Abstr. Pap. Am. Chem. Soc.* **2011**, *241*.

43. Elder, A. N.; Dangelo, N. M.; Kim, S. C.; Washburn, N. R. *Biomacromolecules* **2011**, *12*, 2610.

44. Lee, O. S.; Liu, Y. M.; Schatz, G. C. *J. Nanopart. Res.* **2012**, *14*.

45. Aluri, S.; Pastuszka, M. K.; Moses, A. S.; MacKay, J. A. *Biomacromolecules* **2012**, *13*, 2645.

46. Grieshaber, S. E.; Farran, A. J. E.; Lin-Gibson, S.; Kiick, K. L.; Jia, X. Q. *Macromolecules* **2009**, *42*, 2532.

47. Grieshaber, S. E.; Farran, A. J. E.; Bai, S.; Kiick, K. L.; Jia, X. Q. *Biomacromolecules* **2012**, *13*, 1774.

48. Chen, Y.; Youn, P.; Furgeson, D. Y. *J Control Release* **2011**, *155*, 175.

49. Yu, Y. C.; Berndt, P.; Tirrell, M.; Fields, G. B. *J Am Chem Soc* **1996**, *118*, 12515.

50. Gore, T.; Dori, Y.; Talmon, Y.; Tirrell, M.; Bianco-Peled, H. *Langmuir* **2001**, *17*, 5352.

51. Luo, J. N.; Tong, Y. W. *Acs Nano* **2011**, *5*, 7739.

52. Krishna, O. D.; Wiss, K. T.; Luo, T. Z.; Pochan, D. J.; Theato, P.; Kiick, K. L. *Soft Matter* **2012**, *8*, 3832.

53. Wiss, K. T.; Krishna, O. D.; Roth, P. J.; Kiick, K. L.; Theato, P. *Macromolecules* **2009**, *42*, 3860.

54. Roth, P. J.; Wiss, K. T.; Zentel, R.; Theato, P. *Macromolecules* **2008**, *41*, 8513.

55. Persikov, A. V.; Ramshaw, J. A. M.; Kirkpatrick, A.; Brodsky, B. *Biochemistry-Us* **2005**, *44*, 1414.

56. Sakakiba.S; Tanaka, N.; Kakudo, M.; Okuyama, K.; Ashida, T.; Kishida, Y. *J. Mol. Biol.* **1972**, *65*, 371.

57. Persikov, A. V.; Ramshaw, J. A. M.; Kirkpatrick, A.; Brodsky, B. *Biochemistry-Us* **2000**, *39*, 14960.

58. Kar, K.; Amin, P.; Bryan, M. A.; Persikov, A. V.; Mohs, A.; Wang, Y. H.; Brodsky, B. *J. Biol. Chem.* **2006**, *281*, 33283.

59. Miles, C. A. *Biopolymers* **2007**, *87*, 51.

60. Cheon, J. B.; Kim, B. C.; Park, Y. H.; Park, J. S.; Moon, J. Y.; Nahm, J. H.; Cho, C. S. *Macromol. Chem. Phys.* **2001**, *202*, 395.

61. Qin, S. H.; Geng, Y.; Discher, D. E.; Yang, S. *Adv. Mater.* **2006**, *18*, 2905.

62. Topp, M. D. C.; Dijkstra, P. J.; Talsma, H.; Feijen, J. *Macromolecules* **1997**, *30*, 8518.

63. Zhang, W. Q.; Shi, L. Q.; Wu, K.; An, Y. G. *Macromolecules* **2005**, *38*, 5743.

64. Isoda, K.; Kanayama, N.; Miyamoto, D.; Takarada, T.; Maeda, M. *React Funct Polym* **2011**, *71*, 367.

65. Zhao, C. W.; Zhuang, X. L.; He, C. L.; Chen, X. S.; Jing, X. B. *Macromol. Rapid Commun.* **2008**, *29*, 1810.

66. Nuhn, H.; Klok, H. A. *Biomacromolecules* **2008**, *9*, 2755.

67. McDaniel, J. R.; Radford, D. C.; Chilkoti, A. *Biomacromolecules* **2013**, *14*, 2866.

68. Cacace, M. G.; Landau, E. M.; Ramsden, J. J. *Q. Rev. Biophys.* **1997**, *30*, 241.

69. Zhang, Y. J.; Cremer, P. S. *Curr. Opin. Chem. Biol.* **2006**, *10*, 658.

70. Ravoo, B. J.; Stuart, M. C. A.; Brisson, A. D. R.; Weringa, W. D.; Engberts, J. *Chem. Phys. Lipids* **2001**, *109*, 63.

71. Wei, H.; Cheng, S. X.; Zhang, X. Z.; Zhuo, R. X. *Prog Polym Sci* **2009**, *34*, 893.

72. Otsuka, I.; Fuchise, K.; Halila, S.; Fort, S.; Aissou, K.; Pignot-Paintrand, I.; Chen, Y. G.; Narumi, A.; Kakuchi, T.; Borsali, R. *Langmuir* **2010**, *26*, 2325.

73. Zhao, Y.; Gao, H. Y.; Liang, G. D.; Zhu, F. M.; Wu, Q. *Polym. Chem.* **2014**, *5*, 962.

74. Marsden, H. R.; Handgraaf, J. W.; Nudelman, F.; Sommerdijk, N.; Kros, A. *J Am Chem Soc* **2010**, *132*, 2370.

75. Koga, T.; Kamiwatari, S.; Higashi, N. *Langmuir* **2013**, *29*, 15477.

76. Bacinello, D.; Garanger, E.; Taton, D.; Tam, K. C.; Lecommandoux, S. *Biomacromolecules* **2014**, *15*, 1882.

77. Pires, M. M.; Ernenwein, D.; Chmielewski, J. *Biomacromolecules* **2011**, *12*, 2429.

78. Li, Y.; Yu, S. M. *Curr. Opin. Chem. Biol.* **2013**, *17*, 968.

79. Meuer, S.; Braun, L.; Schilling, T.; Zentel, R. *Polymer* **2009**, *50*, 154.

80. Brodsky, B.; Persikov, A. V. In *Fibrous Proteins: Coiled-Coils, Collagen and Elastomers*; Parry, D. A. D., Squire, J. M., Eds.; Elsevier Academic Press Inc: San Diego, 2005; Vol. 70, p 301.

81. Olsen, B. D.; Segalman, R. A. *Mater. Sci. Eng. R-Rep.* **2008**, *62*, 37.

82. Holmdahl, R.; Bockermann, R.; Backlund, J.; Yamada, H. *Ageing Res. Rev.* **2002**, *1*, 135.

# Chapter 3

# NONCOVALENT MODULATION OF THE INVERSE TEMPERATURE TRANSITION AND ASSEMBLY OF ELASTIN-*B*-COLLAGEN-LIKE PEPTIDE BIOCONJUGATES

## 3.1 Introduction

In the past few decades, thermoresponsive polymers have been intensely studied to develop new smart materials such as hydrogels, films, and drug nanocarriers. Elastin-like polypeptides (ELPs), in particular, which are derived from the hydrophobic domain of tropoelastin[1] and comprise many copies of the pentapeptide repeat Val-Pro-Gly-Xaa-Gly (VPGXG), have also been very widely studied owing to their LCST-like behavior. With heating above their inverse transition temperature ($T_t$), the ELPs collapse into a coacervate phase,[2] enabling their use as building blocks for temperature-sensitive smart biomaterials. Many studies have demonstrated the outstanding versatility of the $(VPGXG)_n$ consensus repeat for modulating inverse transition temperatures[2-5] and in the formation of a range of drug delivery vehicles that can be targeted to tissues and cells either via passive or peptide- and stimuli-responsive mechanisms.[6-12]

For example, van Hest and coworkers[13] reported a series of ELP−PEG diblock copolymers and miktoarm star polymers, via strain-promoted alkyne−azide cycloaddition (SPAAC), which self-assembled into nanosized micelles (Figure 3.1a), with the ELP domain collapsed in the center and the PEG domain as the corona providing stealth and steric protection on the outside. In addition to synthetic polymer,

peptide was also conjugated with ELPs. For example, MacKay and coworkers[14] conjugated L4F, an alpha helical peptide inspired by the lipid-binding domain of the ApoA1 protein, with elastin like peptide $(VPGAG)_{192}$. The resulting diblock self-assembled into vesicles that are 49 nm in radius with lamellae 8 nm in thickness (Figure 3.1b). The nanoparticles were found to suppress hepatic stellate cell activation. Arias and coworkers[8] investigated the physicochemical properties and immunogenicity of nanovesicles assembled from a genetically engineered elastin-like block corecombinamer (ELbcR) comprising hydrophilic $[(VPGVG)_2\text{-}(VPGEG)\text{-}(VPGVG)_2]_{10}$ ($E_{50}$) and hydrophobic $(VPGIG)_{60}$ ($I_{60}$) domains, with the N terminal functionalized with a major membrane protein sequence (dAg) from *Mycobacterium tuberculosis*. The resulting ELP copolymer exhibited a transition temperature at 15 °C and self-assembled into vesicles with diameter of approximately 60 nm (Figure 3.1c).

In addition to temperature change, some other external stimuli have also been utilized to manipulate the phase transition of ELP containing conjugates. For example, Chilkoti and coworkers[15] conjugated a ligand binding protein domain, calmodulin (CaM), to elastin like polypeptides which were 60 or 180 pentapeptide long. Binding of $Ca^{2+}$ to apoCaM allosterically triggers the LCST transition of the attached ELP, resulting in formation of meso-microscale particles depending upon the chain length of the ELP (Figure 3.1d). Chelation of the bound $Ca^{2+}$ by EDTA reverses the LCST transition. More recently, researchers from the same group reported ELP diblock containing a histidine rich domain.[11] The diblock copolymer self-assembled at 37 °C into spherical micelles that were stabilized by $Zn^{2+}$ and were disrupted as the pH drops from 7.4 to 6.4 (Figure 3.1e).

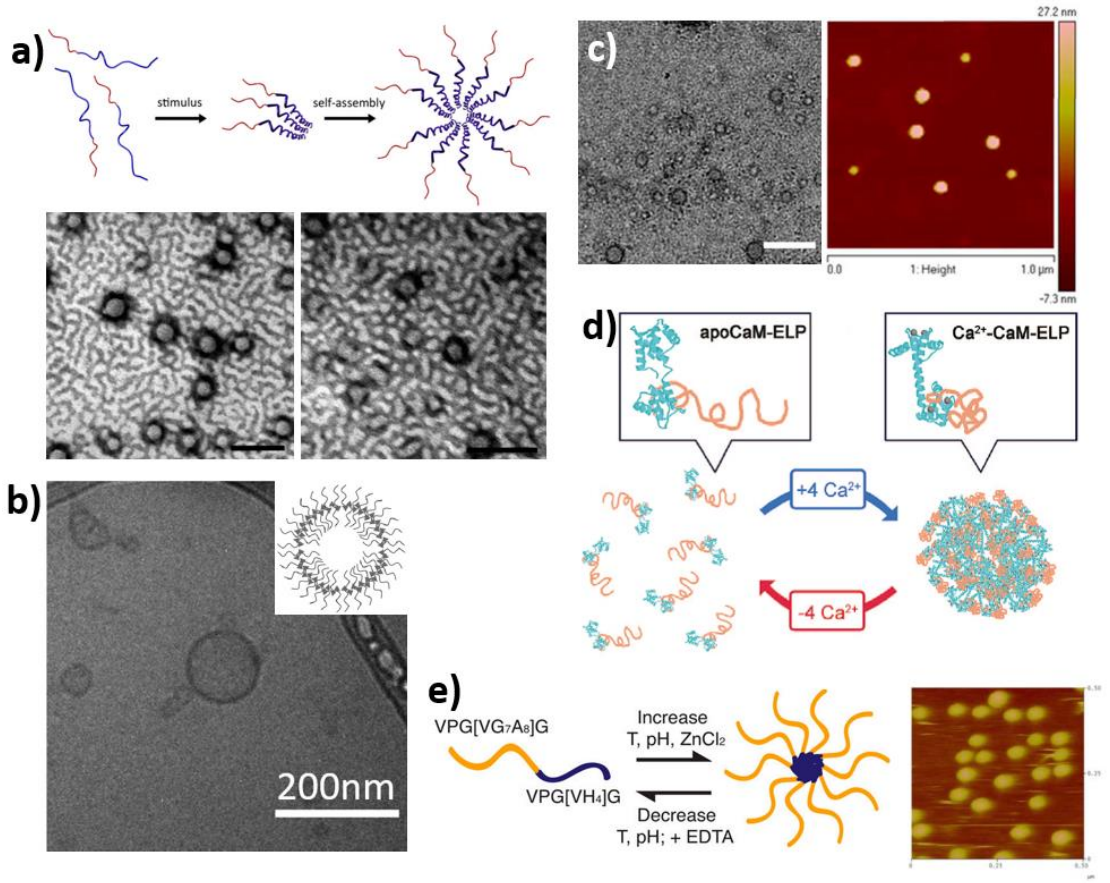


Figure 3.1 Self-assembly of ELP conjugates. a) Self-assembly of ELP-PEG block copolymer into micelles triggered by the phase transition of the ELP domain; bottom two figures are TEM micrographs of self-assembled ELP130 functionalized with one PEG5k chain and two PEG 5k chains respectively. Scale bars = 200 nm; b) Cryo-TEM image of L4F-$(VPGAG)_{192}$ peptide vesicles, with an inserted schematic showing the structure of the vesicle; c) TEM and AFM tapping-mode height image of nanoparticles assembled from dAg-$E_{50}I_{60}$ elastin like corecombinamer. Scale bar = 200 nm; d) Schematic representation of the allosteric, calcium-triggered control of phase transition of CaM-ELP fusion proteins; e) pH responsive histidine-rich elastin like polypeptide block copolymer self-assembles at 37 °C into spherical micelles. (reproduced with permission from ref[8, 11, 13-15])

While these studies illustrate the utility of the ELPs, essentially all of the ELPs employed have been recombinant, comprising tens or even hundreds of pentapeptide repeats. Short synthetic ELPs (*e.g.*, those with fewer than ten pentapeptides) have not been used widely for the thermoresponsive fabrication of nanoparticles, owing to their high transition temperatures.[3, 4, 16] In addition, while many hydrogels and films have been produced from ELPs combined with domains of other structural proteins such as silk and resilin,[17-25] there have been no reports of short ELP-based nanostructures equipped with such domains.

Short synthetic collagen-like peptides (CLPs), on the other hand, have been employed widely in studies aimed at collagen folding and at development of therapeutic matrices and molecules. CLPs have been shown to mimic the triple helix conformation of native collagen,[26-28] and thus have served as model systems for triple helix structure and the stabilization effect of specific amino acid residues in collagens,[29-31] as well as to mimic collagen fibril formation.[32-34] Additionally, recent studies have illustrated that single-stranded CLPs have a strong propensity to bind native collagen via a strand invasion process.[35] The high propensity of CLPs for collagen permits detection of minute quantities of collagen (e.g. 5 ng)[36] with substantial promise for staining collagens in human tissues (e.g. skin; cornea; bone[36]; liver[37]), especially those with high ECM turnover (e.g. prostate tumor xenografts, joints, and articular cartilage[38]). Despite this widespread use, the utilization of CLPs as domains in responsive nanoparticles has been described in only a very limited number of reports.[39, 40]

We postulated that the conjugation of short ELPs with CLP domains would offer significant opportunities in the design and application of thermoresponsive

nanoparticles, and report here the facile chemical production of these conjugates and their unexpected thermally responsive behavior. The CLP sequence $(GPO)_4GFOGER(GPO)_4GG$ was employed, owing to the fact that CLPs with 8 or more GPO repeats exhibit melting temperatures ($T_m$) above 37 °C,[26, 27, 41] which enables formation of stable triple helix at physiological temperature. The peptide sequence GFOGER was employed owing to the fact that it is widely recognized by several kinds of integrins such as $\alpha_1\beta_2$, $\alpha_2\beta_1$, and $\alpha_{11}\beta_1$.[42-44] It has been reported more recently that the introduction of the GFOGER peptide in a PEG-based hydrogel not only provides a better chondrogenic microenvironment compared with that imparted by the RGD peptide, but also enhanced gene expression of type II collagen.[45] Based on these investigations, inclusion of the GFOGER domain should facilitate the binding of these materials with cells in future studies. An ELP with the sequence $(VPGFG)_6$ was introduced as the thermoresponsive domain, as it would be expected to have a $T_t$ below 37 °C,[4] allowing the conjugate to assemble via collapse of the ELP domain at physiological temperature.

## 3.2 Experimental Section

### 3.2.1 Materials

Fmoc-protected amino acids including Fmoc-propargyl glycine, Rink amide MBHA resin, N,N,N',N'-tetramethyl-O-(1H-benzotriazol-1-yl) uronium hexafluorophosphate (HBTU), and piperidine for solid-phase peptide synthesis were purchased from AAPPTEC Inc. (Louisville, KY). HPLC-grade acetonitrile, dimethylformamide (DMF) and copper wire were purchased from Fisher Scientific (Fairlawn, NJ). Copper(I) Acetate, 4-azidobutanoic acid, N-methyl-2-pyrrolidone

(NMP), trifluoroacetic acid (TFA), triisopropylsilane (TIS), triethylamine (TEA), diisopropylethylamine (DIEA) and deuterated DMSO were purchased from Sigma-Aldrich (St. Louis, MO).

### 3.2.2 Peptide synthesis

A collagen-like peptide with the sequence $(GPO)_4GFOGER(GPO)_4GG$ and an elastin-like peptide with sequence $(VPGFG)_6G'$ (G': propargyl glycine) were synthesized via traditional solid-phase peptide synthesis methods (SPPS) using a Focus XC automatic peptide synthesizer (AAPPTec Inc., Louisville, KY). Rink amide MBHA resin with a loading capacity of 0.52 mmol/g was used for the synthesis. The amino acids were activated for coupling with HBTU in the presence of 2 M diisopropylethylamine (DIEA) in NMP. Deprotection of the Fmoc group was conducted using 20% piperidine in DMF. One-hour coupling cycles were used for all the residues. 4-azidobutanoic acid was manually attached to the N-terminus of the CLP on resin. Double coupling with 4:1 amino acid/resin ratio was used for the conjugation. Cleavage of the peptides from the resin was conducted in 95:2.5:2.5 (v:v:v) trifluoroacetic acid (TFA) /triisopropylsilane (TIS) /water for 3 hours. The TFA was mostly evaporated and fthe cleaved peptide was precipitated in cold ether. The peptide was then redissolved in water and lyophilized.

Crude peptides were purified via reverse-phase HPLC (Waters Inc., Milford, MA) on a Waters Xbridge BEH130 Prep C-18 column. The mobile-phase comprised gradients of degassed deionized water with 0.1% TFA and acetonitrile with 0.1% TFA, at a flow rate of 5 ml/min. Peptide was detected by a UV detector at 214 nm; fractions with product were collected and lyophilized. The molecular weight of the peptides was confirmed via electrospray ionization mass spectrometry (ESI-MS, AutospecQ, VG

Analytical, Manchester, UK) and the purity of the peptide was confirmed via analytical scale, reverse-phase HPLC (Waters 2996; Symmetry C18, 3.5 μm, 4.6 x 75 mm).

### 3.2.3 ELP-CLP conjugate synthesis

The synthesis of the conjugate was performed via copper(I)-catalyzed alkyne-azide cycloaddition (CuAAC) "click" reaction.[46] Solutions of CLP (8.57 mg, 3 μmol) in 0.5 mL anhydrous DMF, ELP (9.12 mg, 3 μmol) in 0.5 mL anhydrous DMF, and Cu(I) acetate (0.25 equiv. to alkyne) in 0.5 mL anhydrous DMF were added to a nitrogen-purged vial. DMF was employed for the reaction because in polar aprotic solvents, the CLP and CLP-ELP conjugate are not able to form stable triple helical conformations, which we expected would improve the efficiency of the reaction. In addition, DMF is also a good solvent for the ELP as well, so none of the reactants or products precipitate during the reaction. The mixture was stirred at 80 °C under nitrogen for 24 h. After reaction, the resulting hybrid copolymer was isolated into a 5-fold volume of cold diethyl ether and redissolved in water to remove the catalysts. The diblock solution was then dialyzed against water for 7 days to remove the residual catalyst. A dialysis membrane with MWCO of 1000 Da was used for the process. The product was then collected and lyophilized at nearly 100% yield, indicating that the reaction conditions do not degrade the peptides. Characterization of the products (below) also indicated the stability of the peptides under the coupling reaction conditions. The ELP-CLP diblock showed self-assembly and formed aggregates in aqueous solutions, and similar aggregation was also observed in acetonitrile-based solvents. HPLC therefore could not be performed for the conjugate, and GPC (in

organic solvents)/NMR/FTIR were used to verify the identity and purity of the diblock products.

### 3.2.4 Gel Permeation Chromatography (GPC)

GPC was performed in trifluoroethanol (TFE) with 0.02 M sodium trifluoroacetate at 40 °C using an Agilent 1200 system equipped with an isocratic pump operated at 1 mL/min, one 50 mm x 8 mm PSS PFG guard column (Polymer Standards Service), three 300 mm x 7.5 mm PSS PFG analytical linear M columns with 7 μm particle size (Polymer Standards Service), and a refractive index detector. The system was calibrated with PMMA standards. 100 μL sample was used for each injection.

### 3.2.5 Nuclear Magnetic Resonance Spectrometry (NMR)

$^{1}$H NMR spectra were recorded under standard quantitative conditions on a Bruker AVIII spectrometer operating at 600 MHz, using at least 64 scans. All samples were dissolved in deuterated dimethyl sulfoxide (δ (d6-DMSO) = 2.50 ppm) at a concentration of 2 mg/mL. The resulting spectra were analyzed using Mnova software (Mestrelab Research, Santiago de Compostela, Spain).

### 3.2.6 Fourier Transform Infrared Spectroscopy (FTIR)

FTIR spectra were collected using a Thermo Nicolet Nexus 670 (Thermo Scientific, Waltham, MA, USA) spectrometer with a DuraSamplIR II ATR accessory (Smiths Detection, Danbury, CT, USA). The peptide samples were added as solids onto the silicon ATR crystal and gently pressed down during data acquisition (128 scans at 4 $cm^{-1}$ resolution from 1000 - 4000 $cm^{-1}$). A background of the clean silicon crystal in air was subtracted from all sample spectra.

### 3.2.7 Circular Dichroic Spectroscopy (CD)

Characterization of the secondary structure of the CLP domain was conducted via circular dichroic spectroscopy (Jasco 810 circular dichroism spectropolarimeter, Jasco Inc., Easton, MD, USA). Either CLP, ELP or ELP-CLP conjugate was dissolved at a concentration of 100 μM in PBS (10 mM, pH 7.4, 137 mM NaCl and 2.7 mM KCl) and incubated overnight before measurement. The CD spectra were recorded using quartz cells with a 0.2 cm optical path length.

Full wavelength scans were collected to study the conformation of the peptide domain at selected temperatures. The sample was incubated at each temperature for 10 min before measurement. The scanning rate was 50 nm/min, with a response time of 4 s. The wavelength scans were obtained from 200 nm to 250 nm and were recorded every 1 nm. In order to precisely measure the melting temperature of the CLP domain, variable temperature experiments were conducted at a constant wavelength of 225 nm with a 0.25 °C/min heating rate. Refolding kinetics were studied via temperature-jump experiments. The sample solution was incubated at 80 °C for 30 min followed by quenching to 5 °C in less than 2 minutes. The ellipticity at 225 nm as a function of time was monitored at 5 °C beginning right after the temperature jump. Although in the refolding experiment, the CLP triple helix did not reach a 100% folded state, a 4 hour refolding time was sufficient to allow accurate calculation of the refolding rate constants, as well as to provide a good comparison between the refolding behavior of the CLP and ELP-CLP diblock conjugate.

### 3.2.8 Dynamic Light Scattering (DLS)

Analysis of particle sizes in solution was conducted via dynamic light scattering (DLS) on a ZetaSizer Nano Series (Nano ZS, Malvern Instruments, U.K.) at

a scattering angle of 173°, and data fitting using the cumulant method. CLP, ELP and ELP-CLP conjugate samples were all prepared at 1 mg/mL in deionized water. A CLP (0.5 mg/mL) and ELP (0.5 mg/mL) physical mixture dissolved in water, as well as ELP samples (1 mg/mL) in 0.1 M NaCl and 0.3 NaCl solution were also prepared as controls. All samples were incubated at 4 °C overnight before measurement. The lower critical solution temperature (LCST) of the ELP and ELP-CLP conjugate was assessed by measurement of the average size of particles at temperatures from 5 °C to 80 °C, at an interval of 2 °C. Samples were incubated at each temperature for 2 minutes before measurements. The LCST was assigned as the temperature at which the intensity of scattered light began to increase. For particle size distribution studies at 25 °C, 37 °C, 50 °C, 65 °C and 80 °C, each sample was incubated for 10 min at the desired temperature before measurements. The reported data represent an average of at least three measurements.

### 3.2.9 Transmission Electron Microscopy (TEM)

Samples for TEM were prepared on carbon-coated copper grids (CF300-Cu, Electron Microscopy Sciences Inc.). The grids, pipette tips, and samples were incubated in an isothermal oven (VWR Signature™ Forced Air Safety Ovens, VWR Inc.) at desired temperature (25 °C, 37 °C, 50 °C, 65 °C and 80 °C) for at least 30 min before sample preparation, which was also conducted in the oven. ELP-CLP diblock sample was dissolved in water at concentration of 1 mg/mL (consistent with DLS exeperiments and to prevent precipitation of the PTA stain). 5 μL of the sample solution was drop cast on the grid and blotted after 60 seconds. For staining, 1% phosphotungstic acid (PTA) (pH adjusted to 7.0 using 1 M NaOH) as a negative stain was used. 3 μL of the PTA solution was drop cast on the grid and blotted after 10

seconds. The sample was allowed to dry in the oven at the desired temperature for 30 minutes and then was air-dried for 2 hours. TEM images were taken on a JEM-3010 TEM (JEOL USA Inc., Peabody, MA) at an acceleration voltage of 200 keV.

### 3.2.10 Cryo Transmission Electron Microscopy (Cryo-TEM)

Cryo-TEM was performed in a Tecnai 12 microscope operated at 120 kV. 3 μL of the diblock sample solution at 1 mg/mL dissolved in water was placed on a 300 mesh quantifoil R1.2/1.3 film supported on a copper holey carbon grid (SPI supplies inc., West Chester, PA) within a Vitrobot vitrication system (FEI Inc. Hillsboro, OR). The sample was blotted and quickly plunged into a liquid ethane reservoir cooled by liquid nitrogen. The vitrified samples were transferred to a Gatan 626 cryo-holder and cryo-transfer stage cooled by liquid nitrogen. During observation of the vitrified samples, the cryo-holder temperature was maintained below -176 °C. The images were recorded digitally with a Gatan CCD camera.

## 3.3 Results and Discussion

### 3.3.1 Conjugate synthesis and characterization

Both peptides were synthesized via traditional Fmoc-based, solid-phase peptide synthesis methods (SPPS) (Figure 3.2). An azide was introduced to the N terminal of the CLP and an alkyne group was introduced to the C terminal of the ELP to allow facile conjugation of the two peptides via CuAAC “click” reaction. After purification with reverse-phase HPLC, peptides with purity greater than 90% was obtained (Figure 3.3). The molecular weight of both peptides was verified via ESI-MS (Figure 3.4 and Figure 3.5).For CLP, Mw = 3039 Da, m/z = 1520.6 [$(M + 2H)^{2+}$, calcd

1520.5], m/z = 1014.3 [(M + 3H)$^{3+}$, calcd 1014.0]. For ELP, Mw = 2856 Da, m/z = 1429.3 [(M + 2H)$^{2+}$, calcd 1429.0], m/z= 960.7 [(M + 2H+Na)$^{3+}$, calcd 960.3].

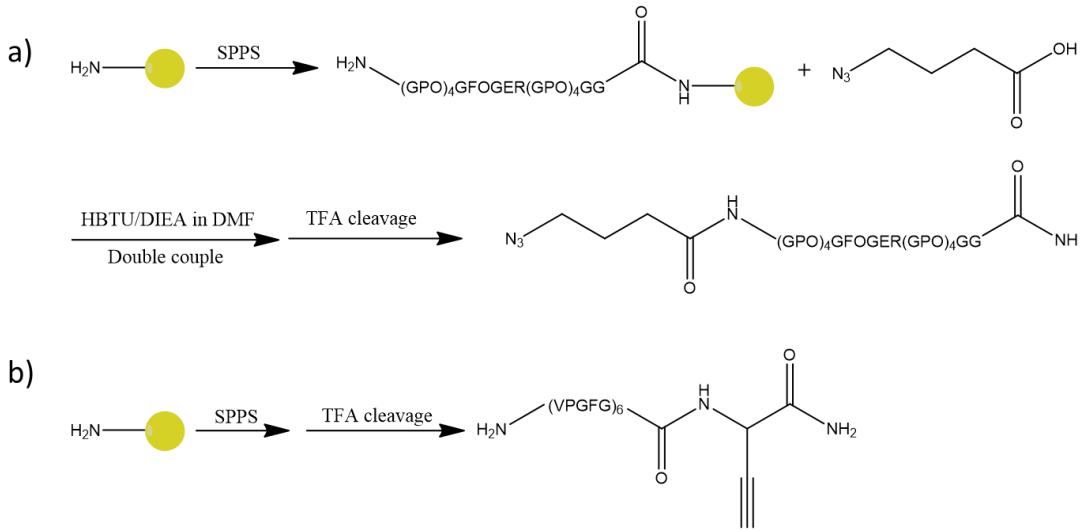


Figure 3.2 Solid phase peptide synthesis and molecular structure of: a) azide functionalized collagen-like peptide; b) alkyne functionalized elastin-like peptide

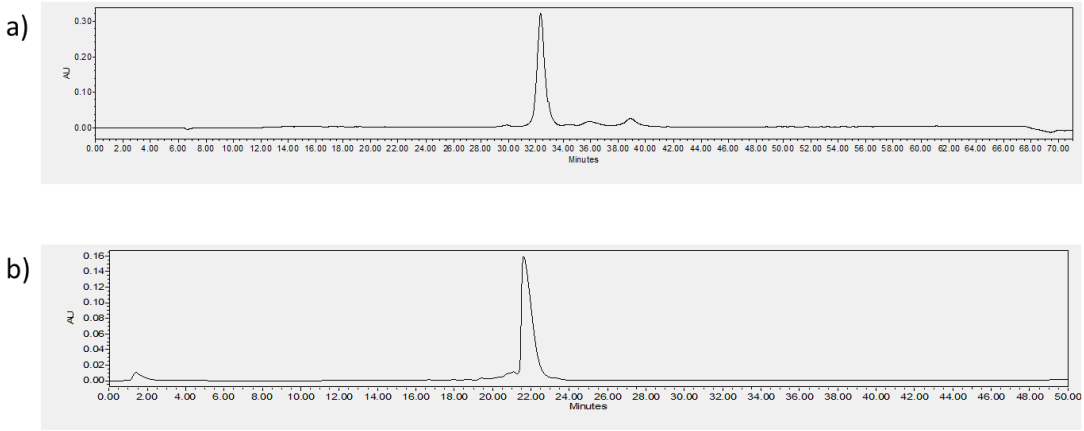


Figure 3.3 RP-HPLC trace of purified peptides: a) collagen-like peptide; b) elastin-like peptide

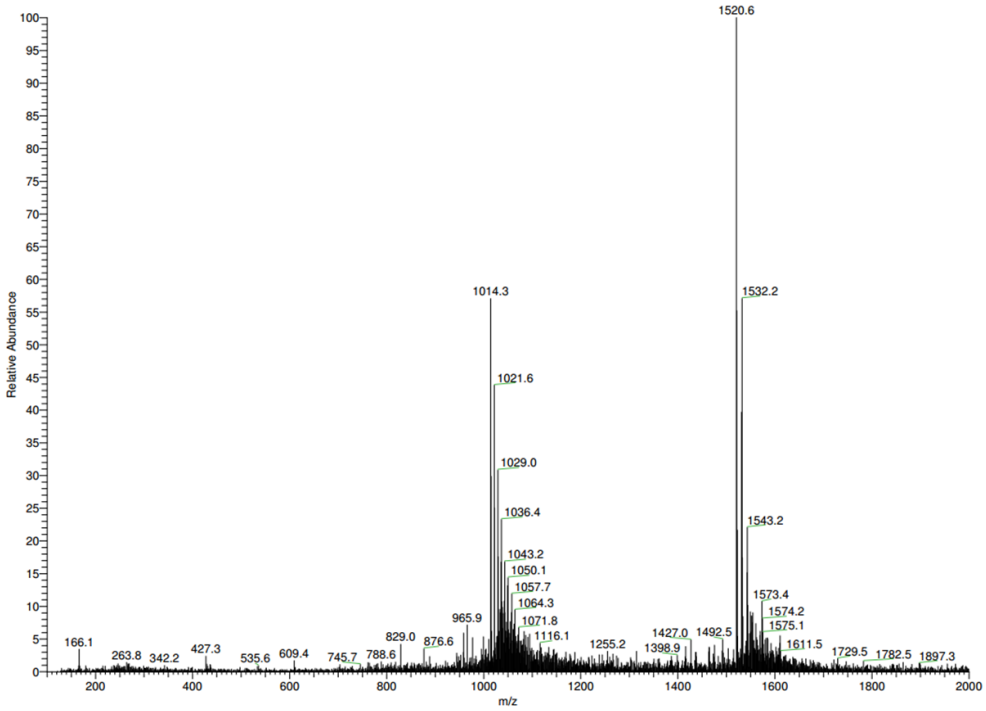


Figure 3.4 ESI-MS of purified CLP.

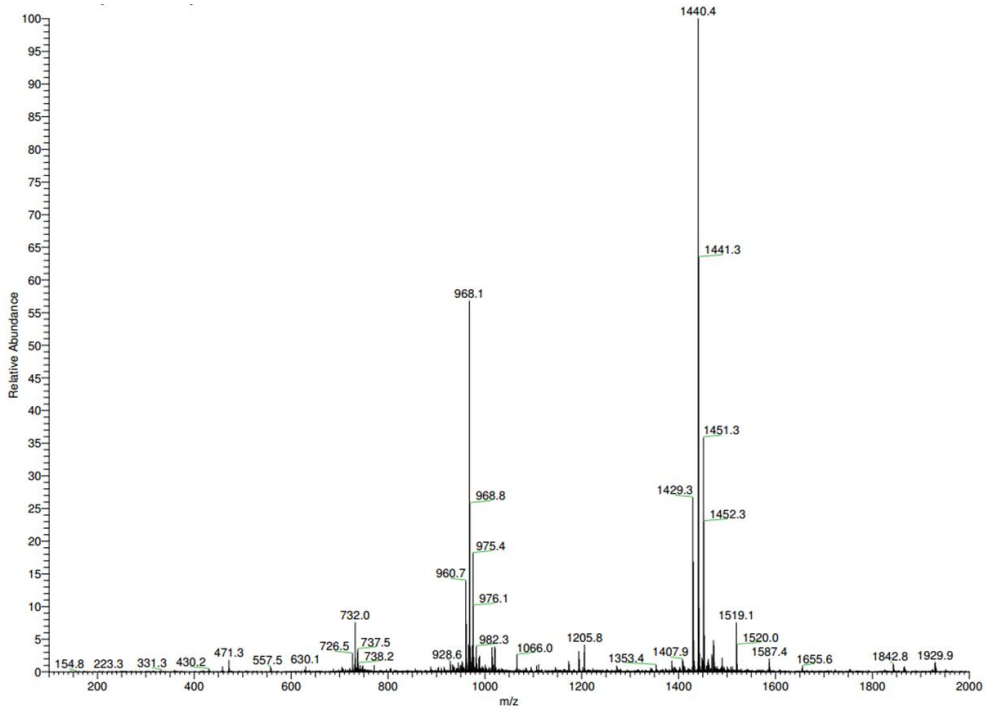


Figure 3.5 ESI-MS of purified ELP.

The alkyne functionalized ELP was conjugated to the azide functionalized CLP via CuAAC "click" reaction (Figure 3.6), employing DMF as a solvent in order to ensure the solubility of all reactants and the ELP-CLP product. The product was collected in nearly 100% yield, indicating the lack of peptide degradation under the reaction conditions. As discussed above, self-assembly and aggregation of the ELP-CLP conjugates in aqueous solutions and in acetonitrile-based solvents precluded characterization of the ELP-CLP conjugates via HPLC. Therefore, GPC (in organic solvents), $^{1}$H NMR, and FTIR were used to verify the identity and purity of the diblock products. The molecular weight distribution of purified products was studied via gel permeation chromatography (GPC) conducted using trifluoroethanol (TFE) as the mobile phase (Figure 3.7). The traces shown were obtained using refractive index

detection and were normalized to give a better comparison between the diblock and starting material. As shown in Figure 3.7, the elution time of the diblock was clearly shifted to the higher molecular weight region compared with the CLP or ELP starting material. The results suggest successful conjugation of the two building blocks and the product peak with a negligible shoulder in the lower molecular region indicates the click reaction was complete and successful removal of excess starting material. An estimation of molecular weight from a calibration employing linear poly (methyl methacrylate) (PMMA) standards yielded a Mw of 11.2 kDa of the ELP-CLP diblock, consistent with the addition of Mw of the ELP 4.8 kDa and the CLP 6.7 kDa. The molecular weights were larger than anticipated, likely due to the potential physicochemical differences between the peptides and PMMA standards, which would affect their mobility and/or hydrodynamic volume in the mobile phase.[47] The smaller shoulder located at 27.5 min likely corresponds to the ELP-CLP trimer. Indeed, circular dichroism full wavelength scan experiments conducted on the diblock sample dissolved in TFE (Figure 3.8) suggested the diblock was partially folded in triple helical conformation under the same conditions as those under which the GPC was performed.

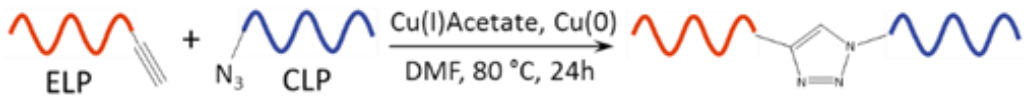


Figure 3.6 Chemical conjugation of ELP and CLP.

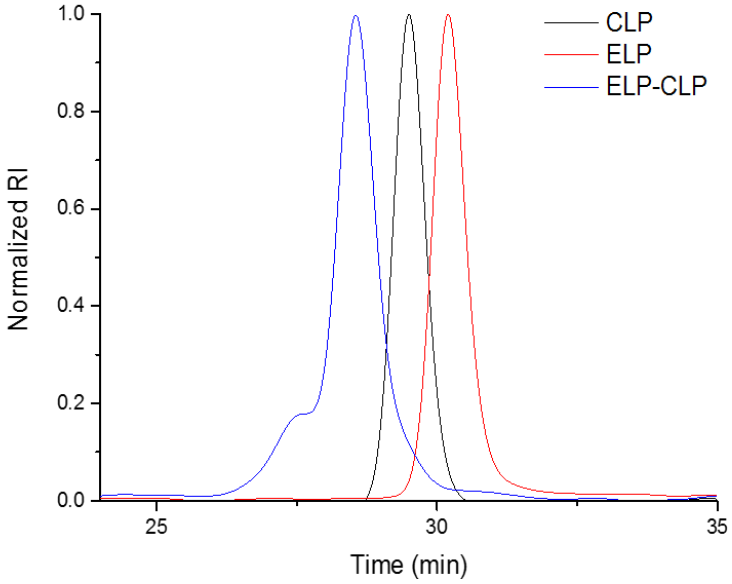


Figure 3.7 GPC trace of ELP-CLP diblock and peptide starting material.

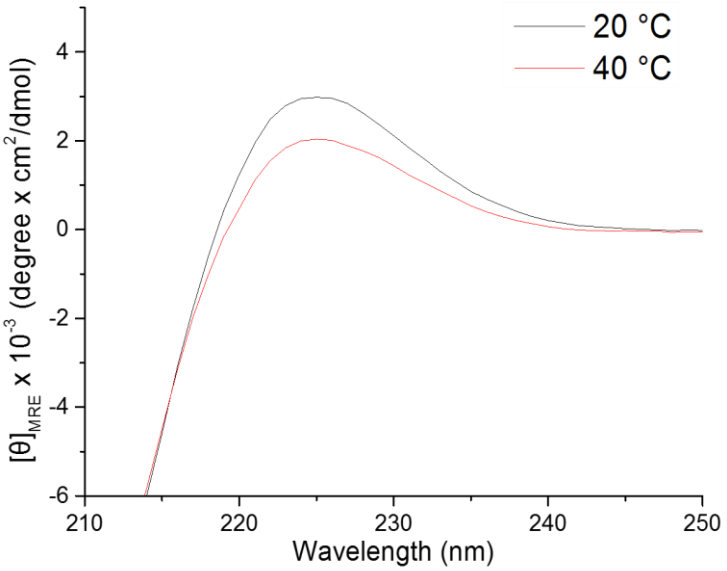


Figure 3.8 CD spectra showing the wavelength scans for the ELP-CLP diblock sample dissolved in TFE at 20 °C and 40 °C. Results suggested the diblock maintained a partially folded triple helical conformation when injected into the column for GPC experiments at 40 °C.

$^{1}$H NMR spectroscopy was utilized to confirm the presence of both the ELP and CLP domain in the diblock product (Figure 3.9). The spectrum of the ELP-CLP diblock, given in Figure 3.9c, showed all corresponding characteristic signals from the ELP as well as the CLP building block. A zoomed in spectrum of the diblock (Figure 3.10) suggested that the alkyne protons from ELP propargyl glycine vanished in the diblock sample, indicating complete consumption of the ELP starting material in the click reaction. FT-IR was used to track the azide group before and after the conjugation reaction. Spectra of the ELP and the azide functionalized CLP as well as the resulting ELP-CLP diblock are shown in Figure 3.11. The strong band at 2094 cm$^{-1}$ is indicative of the azide end groups in the starting CLP.[48] The band was not

observed in the ELP-CLP diblock conjugate, indicating complete consumption of the CLP starting material in the click reaction. The NMR and FT-IR results, together with the higher MW suggested by GPC, suggest successful synthesis and purification of the diblock.

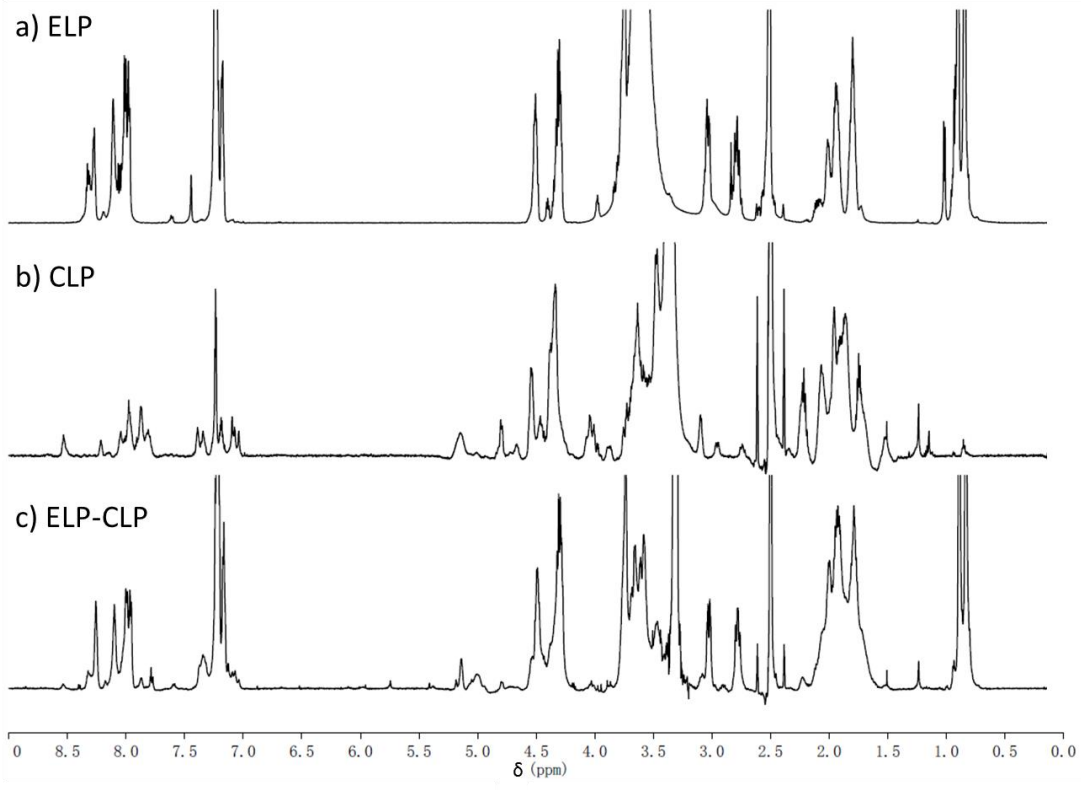


Figure 3.9 $^{1}H$ NMR spectra (600 MHz) of: a) elastin-like peptide; b) collagen-like peptide; c) ELP-CLP diblock in $d_6$-DMSO.

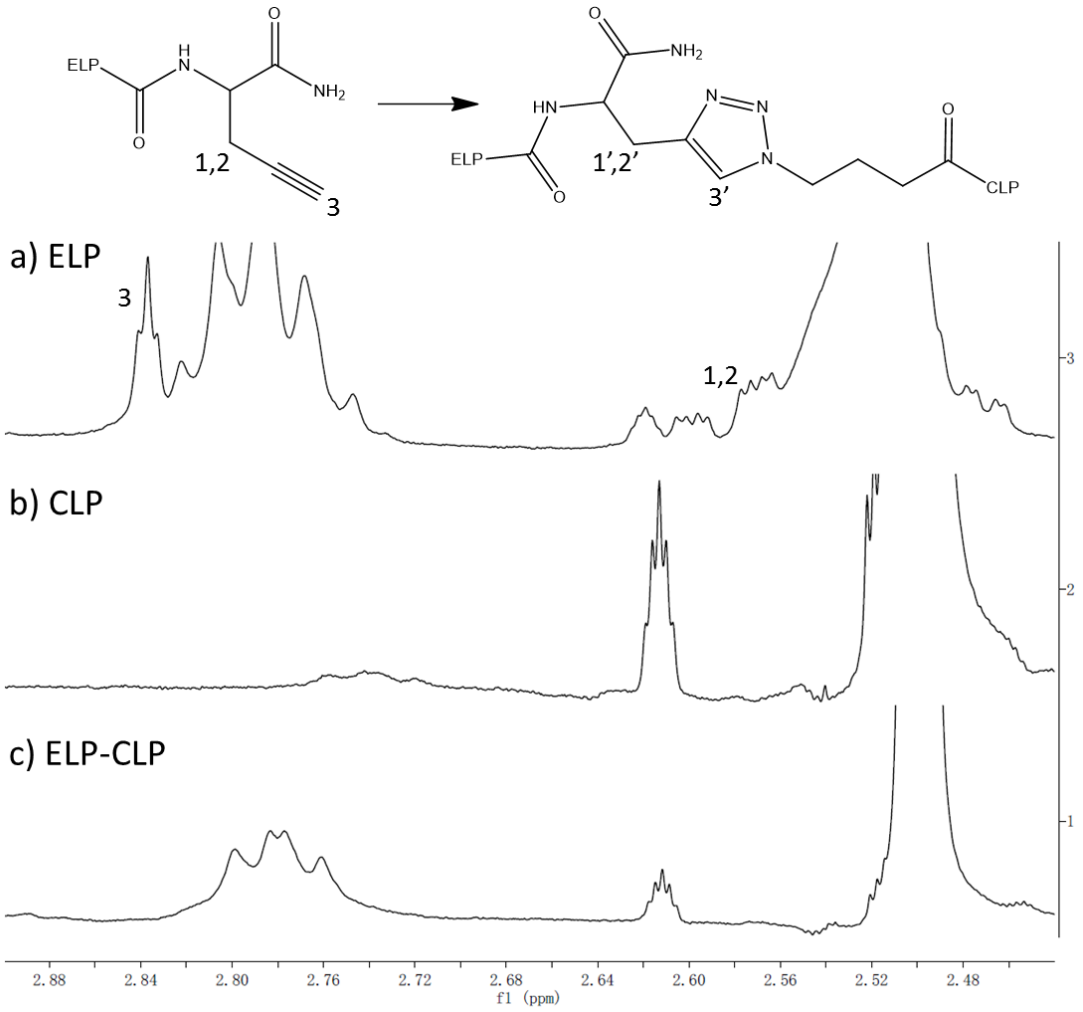


Figure 3.10 Expanded $^{1}$H NMR spectra between 2.4 ppm and 2.9 ppm of: a) elastin-like peptide; b) collagen-like peptide; c) ELP-CLP diblock.

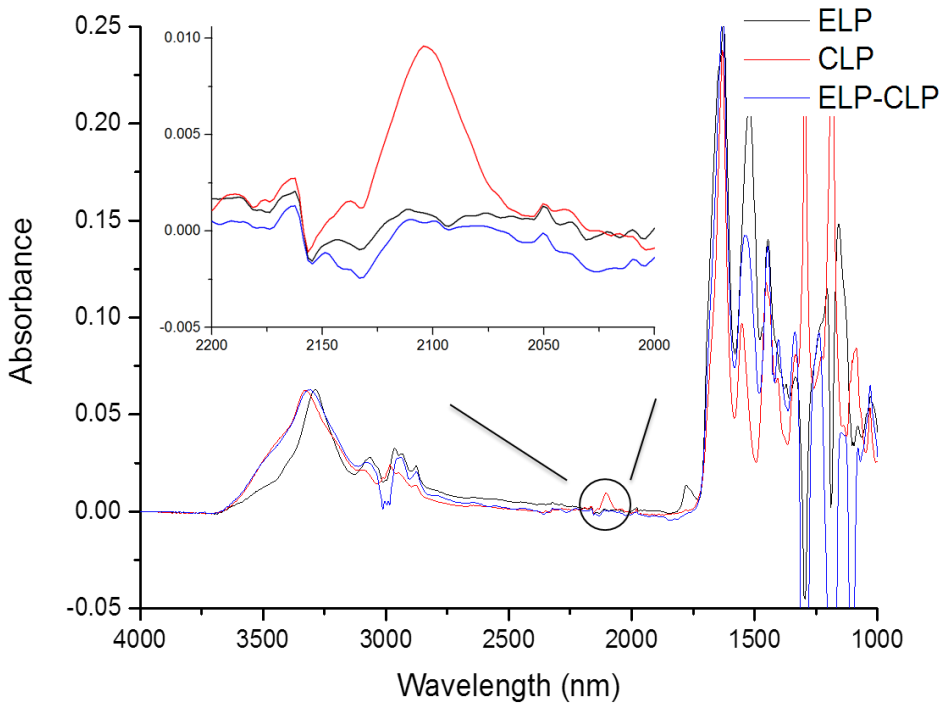


Figure 3.11 ATR-FTIR spectra of the ELP-CLP diblock and peptide starting materials.

### 3.3.2 CLP domain triple helix formation

The ability of the CLP domain to form stable triple helix at physiological temperature while conjugated to the ELP was probed via circular dichroic spectroscopy (CD). The CD spectra of ELP-CLP at temperatures ranging from 5 °C to 80 °C (Figure 3.12) show a clear maximum at ca. 225 nm, indicating that the CLP domain is competent to form triple helical structures after conjugation with ELP. The reduction of the intensity of the peak with increasing temperature (Figure 3.12b) indicates the expected unfolding of the triple helix upon heating, with the first derivative of the melting curve (after correction for the contribution from the ELP,

Figure 3.16) suggesting a $T_m$ of ca. 57 °C for the CLP-ELP conjugate, which is significantly higher than that of the isolated CLP (ca. 50°C, Figure 3.17). Presumably, the collapse of the ELP domain at the elevated temperatures anchors the CLP and stabilizes it against unfolding, similar to our previously reported results for a polymer-conjugated CLP.[40, 49] The refolding of the CLP triple helix (Figures 3.12c and 3.12d) is likewise accelerated by the ELP anchoring of the CLP, owing to the increase in the local concentration of the CLP strands.[39, 40, 49, 50] While a rate constant of $1.14 \times 10^7$ $M^{-2} \cdot s^{-1}$ was observed for the refolding reaction of the CLP, the diblock shows a higher rate constant of $4.63 \times 10^7$ $M^{-2} \cdot s^{-1}$.

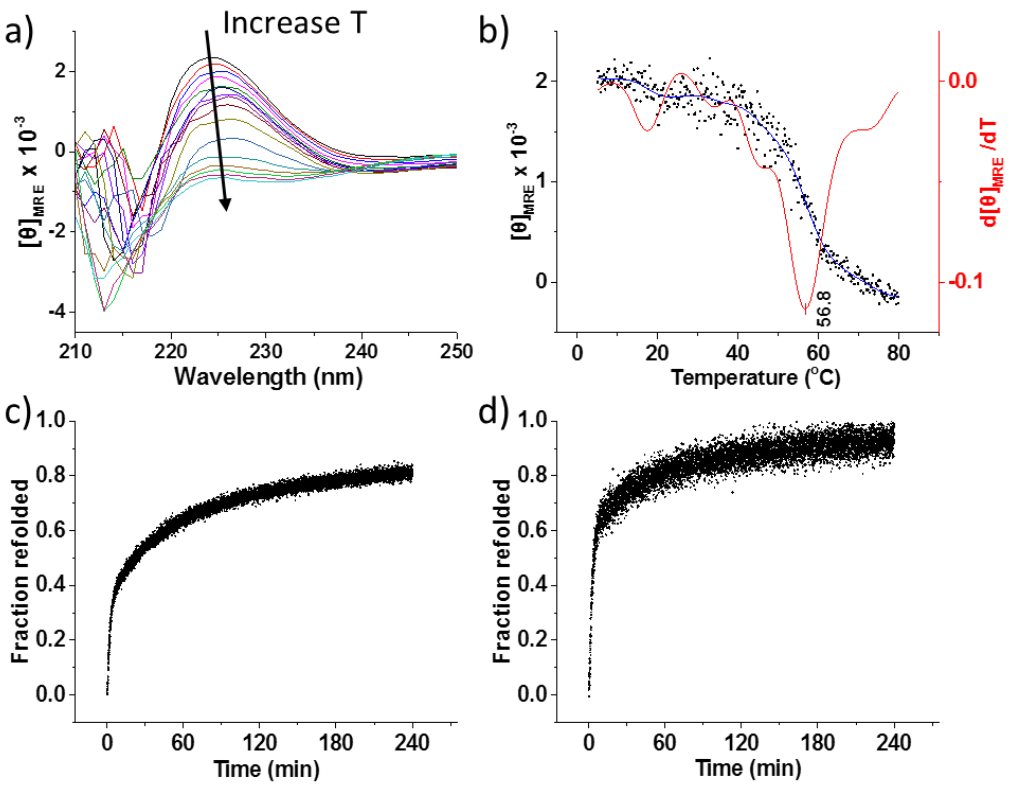


Figure 3.12 a) CD spectra showing representative full-wavelength scans for the ELP-CLP conjugate; b) Thermal unfolding profile for an ELP-CLP conjugate; the first derivative of the unfolding curve with respect to temperature is shown in red; c) Refolding profile of CLP after quenching from 80 °C to 5 °C; d) Refolding profile of the ELP-CLP conjugate after quenching.

### 3.3.3 Thermoresponsive self-assembly

The anticipated assembly of ELP-CLP nanostructures at physiologically relevant temperatures was confirmed via dynamic light scattering (DLS) (Figure 3.13). In contrast to our expectations that nanoparticle formation would be triggered at near physiological temperature, however, the conjugates formed structures with hydrodynamic diameters ($D_h$) that ranged from approximately 50 to 200 nm at all temperatures between 4 °C and 65 °C (Figure 3.13a), with a $D_h$ of approximately 160

nm at 37 °C (Figure 3.13b). These results are counterintuitive based on the expected increase of the transition temperature of thermoresponsive polymers and ELPs with conjugation to a hydrophilic domain.[51-54] Instead, conjugation of the short ELP to a hydrophilic CLP results in a dramatic *reduction* of the $T_t$ of the ELP to below 4 °C; the lack of aggregation of the ELP alone (Figure 3.18) indicates that this reduction exceeds 80 °C.

Just as the CLP triple helix is stabilized at high temperature by the anchoring effect of ELP coacervation, the unexpected assembly of the ELP-CLP conjugates at low temperatures is almost certainly attributable to the anchoring effects of the CLP triple helix, which would serve to locally isolate three ELP domains at concentrations approximately 100-fold higher than that of the ELP monomers in solution. Previous investigations have illustrated that ELPs exhibit lower transition temperatures with increasing concentration and length of the (poly)peptide,[3, 4, 55] as well as with covalent conjugation of short ELPs as sidechains of synthetic graft polymers;[56-58] the colocalization of three ELP chains by the CLP triple helix may thus be expected to show similar trends.

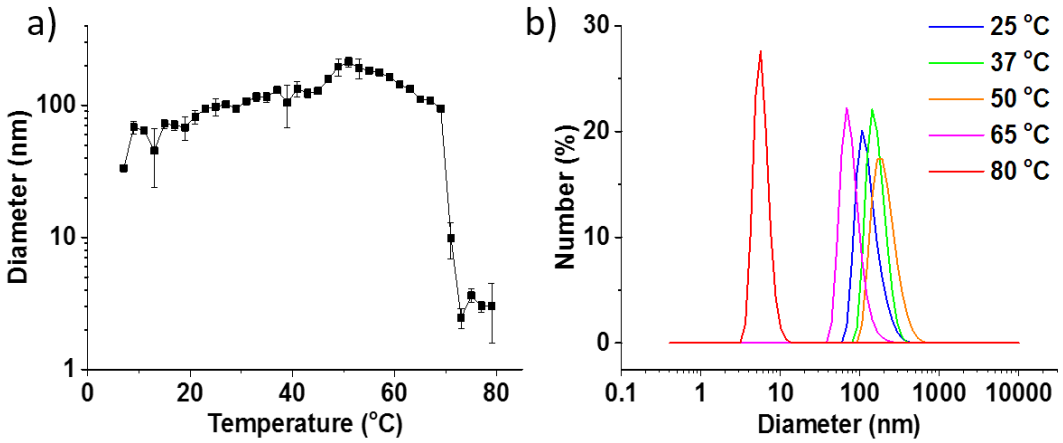


Figure 3.13 Dynamic light scattering characterization of the assembly of ELP-CLP conjugates. a) Hydrodynamic diameter of nanostructures as a function of temperature upon heating; b) Size distributions of ELP-CLP assemblies at select temperatures.

The anchoring of the ELP by the noncovalent formation of CLP triple helix, however, should offer unique and as yet unreported opportunities to reversibly modulate the transition temperatures of the ELP domain and to thus confer dual thermoresponsiveness to the conjugates. Indeed, after an initial increase in the $D_h$ of the ELP-CLP nanoparticles with heating to 50 °C (Figure 3.13), $D_h$ begins to decrease once the sample is heated above this temperature, which is also approximately the melting temperature of the CLP (Figure 3.12b). With additional heating to 80 °C, the CLP unfolds completely (Figure 3.12b), and the nanoparticles become fully solubilized as monomers with an average $D_h$ of only 5.6 nm (Figure 3.13b). Once the triple helix is unfolded and the ELP is no longer anchored, the $T_t$ of the unfolded ELP-CLP conjugate is above 80 °C, which is consistent with our control results (Figure 3.18) and with the expected behavior of the ELP with the addition of a hydrophilic

CLP domain. This behavior is fully reversible (Figure 3.19), thus offering a new avenue for controlling the temperature responsiveness of short ELPs.

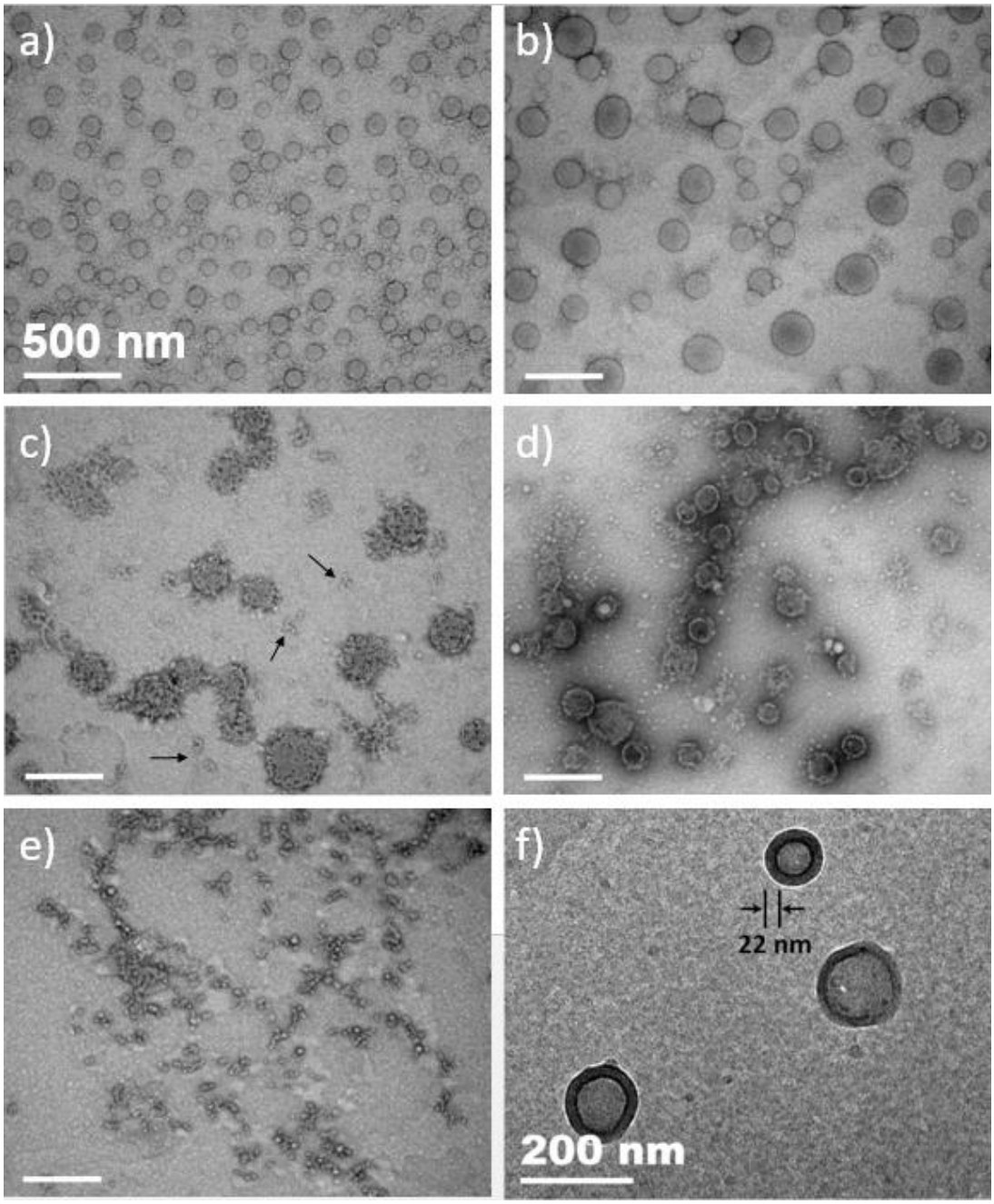


Figure 3.14 a)-e) TEM images of nanoparticles from ELP-CLP conjugates at various temperatures, after negative staining with phosphotungstic acid. Scale bars: 500 nm. a) 25 °C; b) 37 °C; c) 50 °C; d) 65 °C; e) 80 °C. f) Cryo-TEM image of nanoparticles of the ELP-CLP diblock at 25 °C. Scale bar: 200 nm.

Transmission electron microscopy (TEM) was conducted to investigate the morphology of the nanostructures formed at 25 °C, 37 °C, 50 °C, 65 °C and 80 °C (Figure 3.14a-3.14e, respectively). Consistent with the DLS results, nanoparticles with an average diameter of approximately 80 – 100 nm were observed at room temperature, and the diameter of these particles increased to 150 – 250 nm at physiological temperature. Once the sample was heated above the $T_m$ of the collagen domain (50 °C), the nanoparticles showed some changes in morphology and size, with both porosity and apparent monomer (indicated by black arrows) observed at 50 °C (Figure 3.14c), with increasing porosity and decreasing size when the temperature was raised to 65 °C (Figure 3.14d). A vesicular structure is suggested for the nanoparticles, although only at the elevated temperatures, perhaps because the PTA stain was capable of diffusing into the porous nanoparticles and thus accumulating at both the exterior and interior surfaces of the vesicles. At 80 °C (Figure 3.14e), the molecules are soluble and no defined nanostructure was observed.

The vesicular structure of the nanoparticles was further confirmed via cryo-TEM of conjugates incubated at room temperature (Figure 3.14f); vesicles with a diameter of approximately 100 nm were observed. Image analysis indicates that the thickness of the vesicle walls is 22 ± 2 nm, which is consistent with the presence of two CLP triple helices (9.1 nm each) summed with the approximate $R_g$ of the collapsed ELP domains (3.4 nm).[59, 60] The results suggest a bilayer structure of the vesicle walls, with collapsed ELP domains in the center and CLP triple helical domains at both interior and exterior surfaces (Figure 3.15). The presence of a small percentage of unfolded CLP chains is rendered in the schematic, to reflect the unfolding of the CLP domain observed in CD experiments.

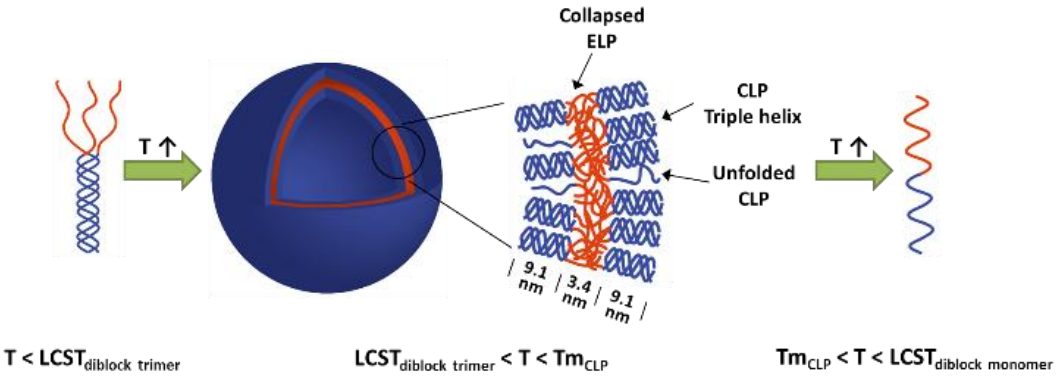


Figure 3.15 Proposed assembly/disassembly and bilayer structure of ELP-CLP vesicles.

## 3.4 Conclusions

The thermally induced assembly of ELP block copolypeptides has been a subject of intense investigation over decades. Essentially all previous reports, however, employ ELP-based recombinant polypeptides that mainly form micellar structures, although there are some reports of larger structures and nanostructures that exhibit additional sensitivity to pH and di-cations.[11, 61-63] There have been very limited reports of thermoresponsive nanostructures that can be assembled from short synthetic ELPs.[16, 64, 65] Our studies illustrate that this barrier can be overcome by simply anchoring three ELP chains to a collagen triple helix. This not only exploits the reversibility of triple helix formation to modulate the transition temperature of the molecules over a wide range, but should also permit manipulation of the size of the vesicles. In addition, there are few reports of the assembly of thermoresponsive collagen-like peptide containing copolymers,[39] and none to our knowledge in which nanovesicles are produced. The likely location of the collagen domain at the exterior surface of the vesicles may serve as a means to localize nanoparticles in collagen-containing tissues, hydrogels, and films.[38, 66, 67]

Simple variations in the relative lengths of the ELP and CLP domains, as well as variations in the sequences of the domains, offer a wide range of options for tailoring the thermoresponsive behavior of these systems. For example, preliminary studies of ELP-CLP conjugates with shorter ELP sequences ($(VPGFG)_{3-5}$) suggest that the transition temperature of nanoparticle formation and disassembly can be tuned to fall within the physiological range for the $(VPGFG)_5$-CLP (Figure 3.20). The large size and polydispersity of the aggregates, however, suggests that the hydrophobic interactions of the shorter $(VPGFG)_5$ are insufficient to form well defined nanoparticles. Changes to the stability of the CLP block, when balanced with the hydrophobicity of the ELP domain, could also be employed to impart triggered assembly/disassembly under select conditions. The prospects are promising for these approaches in drug delivery, imaging, and materials modification.

## 3.5 Supporting Information

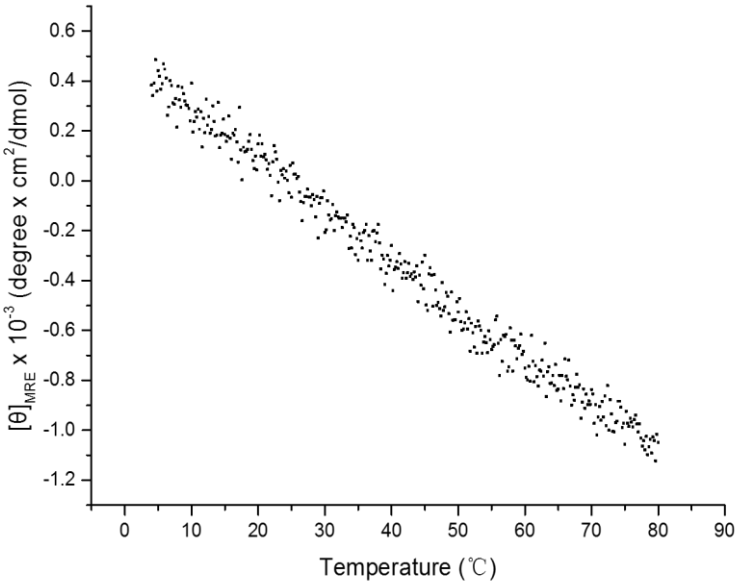


Figure 3.16 Thermal unfolding profile for ELP plotted as $[\theta]_{MRE225nm}$ versus temperature.It was subtracted from the diblock unfolding profile to remove the contribution from ELP domain.

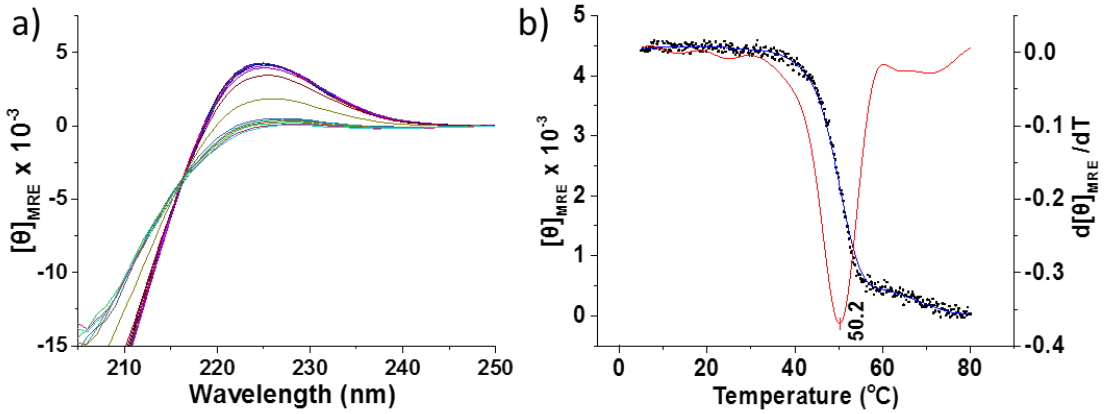


Figure 3.17 a) CD spectra showing the wavelength scans for the collagen like peptide; b) Blue curve with dots (Y axis on the left side): thermal unfolding profile for CLP; red curve (Y axis on the right side): first derivative of the unfolding curve with respect to temperature;

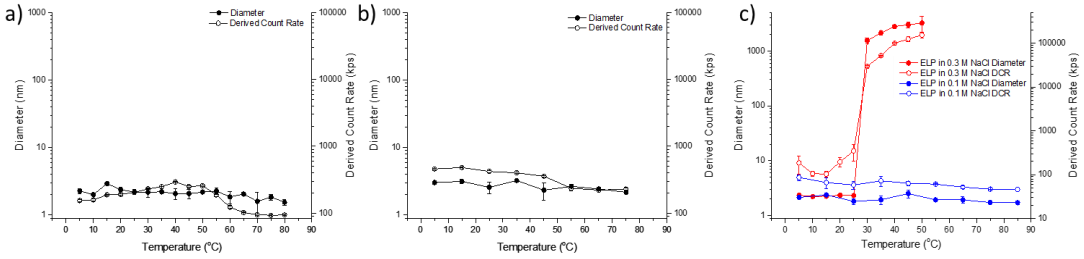


Figure 3.18 Hydrodynamic diameter of assemblies as a function of temperature upon heating. a) ELP at 1 mg/mL in water; b) ELP and CLP physical mixture at 0.5 mg/mL each in water; c) ELP at 1 mg/mL in NaCl aqueous solution

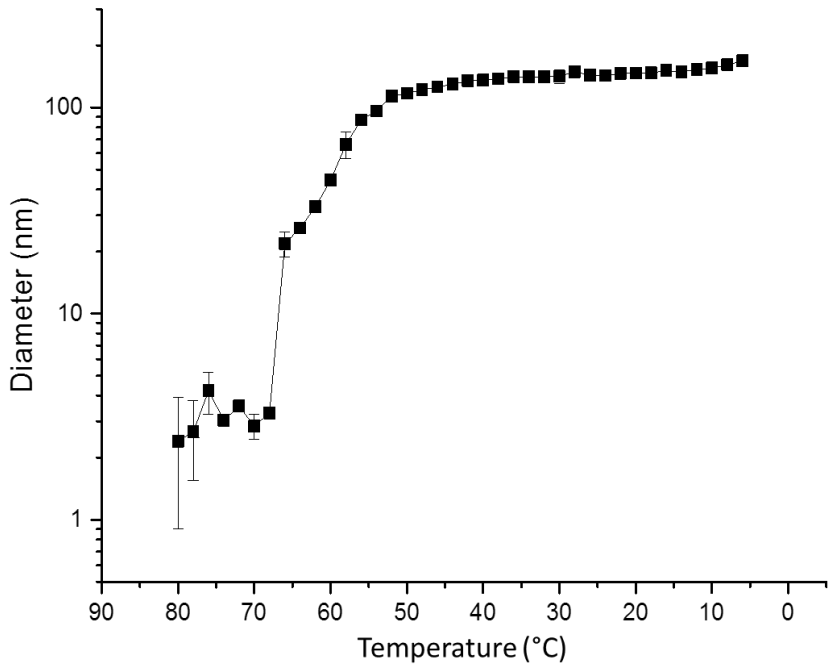


Figure 3.19 Hydrodynamic diameter of ELP-CLP diblock assemblies as a function of temperature upon cooling

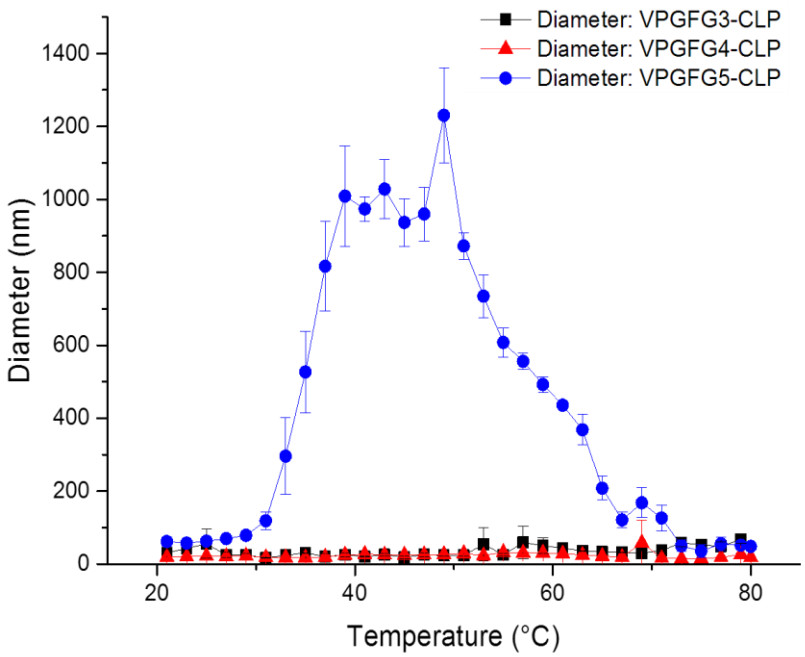


Figure 3.20 Hydrodynamic diameter of VPGFG$_{3\text{-}5}$-CLP diblock assemblies as a function of temperature upon heating

### 3.6 Acknowledgements

This work was funded in part by the National Science Foundation (DMR 0907478 to K.L.K.) and the National Center for Research Resources (NCRR), a component of the National Institutes of Health (1 P30 GM103519 and 1 P30 GM110758-01 for instrument resources). We thank Chaoying Ni, Fei Deng, Yingchao Chen, and Darrin Pochan at the University of Delaware for advice and assistance with TEM, and Rachel Letteri at University of Massachusetts Amherst for conducting GPC (supported by the Materials Research Facilities Network (MRFN) of the UMass MRSEC on Polymers (DMR-0820506)).

## REFERENCES


1. J.A. Foster, E. Bruenger, W.R. Gray, L.B. Sandberg, ISOLATION AND AMINO-ACID SEQUENCES OF TROPOELASTIN PEPTIDES. *J. Biol. Chem.* **1973,** *248* (8), 2876-2879.

2. D.W. Urry, Physical chemistry of biological free energy transduction as demonstrated by elastic protein-based polymers. *J. Phys. Chem. B* **1997,** *101* (51), 11007-11028.

3. J.R. McDaniel, D.C. Radford, A. Chilkoti, A Unified Model for De Novo Design of Elastin-like Polypeptides with Tunable Inverse Transition Temperatures. *Biomacromolecules* **2013,** *14* (8), 2866-2872.

4. H. Nuhn, H.A. Klok, Secondary Structure Formation and LCST Behavior of Short Elastin-Like Peptides. *Biomacromolecules* **2008,** *9* (10), 2755-2763.

5. F.G. Quiroz, A. Chilkoti, Sequence heuristics to encode phase behaviour in intrinsically disordered protein polymers. *Nat. Mater.* **2015,** *14*, 1164-1171.

6. L. Martin, E. Castro, A. Ribeiro, M. Alonso, J.C. Rodriguez-Cabello, Temperature-Triggered Self-Assembly of Elastin-Like Block Co-Recombinamers: The Controlled Formation of Micelles and Vesicles in an Aqueous Medium. *Biomacromolecules* **2012,** *13* (2), 293-298.

7. W.M. Park, J.A. Champion, Thermally Triggered Self-Assembly of Folded Proteins into Vesicles. *J Am Chem Soc* **2014,** *136* (52), 17906-17909.

8. C. Garcia-Arevalo, J.F. Bermejo-Martin, L. Rico, V. Iglesias, L. Martin, J.C. Rodriguez-Cabello, F.J. Arias, Immunomodulatory Nanoparticles from Elastin-Like Recombinamers: Single-Molecules for Tuberculosis Vaccine Development. *Mol. Pharm.* **2013,** *10* (2), 586-597.

9. Y. Fujita, M. Mie, E. Kobatake, Construction of nanoscale protein particle using temperature-sensitive elastin-like peptide and polyaspartic acid chain. *Biomaterials* **2009,** *30* (20), 3450-3457.

10. P. Shi, J.A. Gustafson, J.A. MacKay, Genetically engineered nanocarriers for drug delivery. *Int. J. Nanomed.* **2014,** *9*, 1617-1626.

11. D.J. Callahan, W.E. Liu, X.H. Li, M.R. Dreher, W. Hassouneh, M. Kim, P. Marszalek, A. Chilkoti, Triple Stimulus-Responsive Polypeptide Nanoparticles That Enhance Intratumoral Spatial Distribution. *Nano Lett.* **2012,** *12* (4), 2165-2170.

12. M.R. Dreher, A.J. Simnick, K. Fischer, R.J. Smith, A. Patel, M. Schmidt, A. Chilkoti, Temperature triggered self-assembly of polypeptides into multivalent spherical micelles. *J Am Chem Soc* **2008,** *130* (2), 687-694.

13. M.B. van Eldijk, F.C.M. Smits, N. Vermue, M.F. Debets, S. Schoffelen, J.C.M. van Hest, Synthesis and Self-Assembly of Well-Defined Elastin-Like Polypeptide-Poly(ethylene glycol) Conjugates. *Biomacromolecules* **2014,** *15* (7), 2751-2759.

14. M.K. Pastuszk, X.D. Wang, L.L. Lock, S.M. Janib, H.G. Cui, L.D. DeLeve, J.A. MacKay, An amphipathic alpha-helical peptide from apolipoprotein A1 stabilizes protein polymer vesicles. *J Control Release* **2014,** *191*, 15-23.

15. B. Kim, A. Chilkoti, Allosteric Actuation of Inverse Phase Transition of a Stimulus-Responsive Fusion Polypeptide by Ligand Binding. *J Am Chem Soc* **2008,** *130* (52), 17867-17873.

16. M.B. van Eldijk, J.C.Y. Wang, I.J. Minten, C.L. Li, A. Zlotnick, R.J.M. Nolte, J. Cornelissen, J.C.M. van Hest, Designing Two Self-Assembly Mechanisms into One Viral Capsid Protein. *J Am Chem Soc* **2012,** *134* (45), 18506-18509.

17. J.S. Haghpanah, R. Tu, S. Da Silva, D. Yan, S. Mueller, C. Weder, E.J. Foster, I. Sacui, J.W. Gilman, J.K. Montclare, Bionanocomposites: Differential Effects of Cellulose Nanocrystals on Protein Diblock Copolymers. *Biomacromolecules* **2013,** *14* (12), 4360-4367.

18. J.C. Liu, D.A. Tirrell, Cell Response to RGD Density in Cross-Linked Artificial Extracellular Matrix Protein Films. *Biomacromolecules* **2008,** *9* (11), 2984-2988.

19. A.A. Dinerman, J. Cappello, M. El-Sayed, S.W. Hoag, H. Ghandehari, Influence of Solute Charge and Hydrophobicity on Partitioning and Diffusion in a Genetically Engineered Silk-Elastin-Like Protein Polymer Hydrogel. *Macromol. Biosci.* **2010,** *10* (10), 1235-1247.

20. P.J. Nowatzki, D.A. Tirrell, Physical properties of artificial extracellular matrix protein films prepared by isocyanate crosslinking. *Biomaterials* **2004,** *25* (7-8), 1261-1267.

21. J.A. Gustafson, R.A. Price, K. Greish, J. Cappello, H. Ghandehari, Silk-Elastin-like Hydrogel Improves the Safety of Adenovirus-Mediated Gene-Directed Enzyme-Prodrug Therapy. *Mol. Pharm.* **2010,** *7* (4), 1050-1056.

22. J.A. Gustafson, H. Ghandehari, Silk-elastinlike protein polymers for matrix-mediated cancer gene therapy. *Adv Drug Deliver Rev* **2010,** *62* (15), 1509-1523.

23. K. Trabbic-Carlson, L.A. Setton, A. Chilkoti, Swelling and mechanical behaviors of chemically cross-linked hydrogels of elastin-like polypeptides. *Biomacromolecules* **2003,** *4* (3), 572-580.

24. M.K. McHale, L.A. Setton, A. Chilkoti, Synthesis and in vitro evaluation of enzymatically cross-linked elastin-like polypeptide gels for cartilaginous tissue repair. *Tissue Engineering* **2005,** *11* (11-12), 1768-1779.

25. A. Bracalello, V. Santopietro, M. Vassalli, G. Marletta, R. Del Gaudio, B. Bochicchio, A. Pepe, Design and Production of a Chimeric Resilin-, Elastin-, and Collagen-Like Engineered Polypeptide. *Biomacromolecules* **2011,** *12* (8), 2957-2965.

26. T.Z. Luo, K.L. Kiick, Collagen-like peptides and peptide-polymer conjugates in the design of assembled materials. *Eur. Polym. J.* **2013,** *49* (10), 2998-3009.

27. S.M. Yu, Y. Li, D. Kim, Collagen mimetic peptides: progress towards functional applications. *Soft Matter* **2011,** *7* (18), 7927-7938.

28. M.D. Shoulders, R.T. Raines, Collagen Structure and Stability. In *Annu. Rev. Biochem.*, Annual Reviews: Palo Alto, 2009; Vol. 78, pp 929-958.

29. J.A. Fallas, J.H. Dong, Y.Z.J. Tao, J.D. Hartgerink, Structural Insights into Charge Pair Interactions in Triple Helical Collagen-like Proteins. *J. Biol. Chem.* **2012,** *287* (11), 8039-8047.

30. A.V. Persikov, J.A.M. Ramshaw, B. Brodsky, Prediction of collagen stability from amino acid sequence. *J. Biol. Chem.* **2005,** *280* (19), 19343-19349.

31. L.R. He, P. Theato, Collagen and collagen mimetic peptide conjugates in polymer science. *Eur. Polym. J.* **2013,** *49* (10), 2986-2997.

32. L.E.R. O'Leary, J.A. Fallas, E.L. Bakota, M.K. Kang, J.D. Hartgerink, Multi-hierarchical self-assembly of a collagen mimetic peptide from triple helix to nanofibre and hydrogel. *Nat. Chem.* **2011,** *3* (10), 821-828.

33. S. Rele, Y.H. Song, R.P. Apkarian, Z. Qu, V.P. Conticello, E.L. Chaikof, D-periodic collagen-mimetic microfibers. *J Am Chem Soc* **2007,** *129* (47), 14780-14787.

34. O.D. Krishna, K.L. Kiick, Supramolecular Assembly of Electrostatically Stabilized, Hydroxyproline-Lacking Collagen-Mimetic Peptides. *Biomacromolecules* **2009,** *10* (9), 2626-2631.

35. A.Y. Wang, X. Mo, C.S. Chen, S.M. Yu, Facile modification of collagen directed by collagen mimetic peptides. *J Am Chem Soc* **2005,** *127* (12), 4130-4131.

36. Y. Li, D. Ho, H. Meng, T.R. Chan, B. An, H. Yu, B. Brodsky, A.S. Jun, S.M. Yu, Direct Detection of Collagenous Proteins by Fluorescently Labeled Collagen Mimetic Peptides. *Bioconjugate Chem.* **2013,** *24* (1), 9-16.

37. A.Y. Wang, C.A. Foss, S. Leong, X. Mo, M.G. Pomper, S.M. Yu, Spatio-temporal modification of collagen scaffolds mediated by triple helical propensity. *Biomacromolecules* **2008,** *9* (7), 1755-1763.

38. Y. Li, C.A. Foss, D.D. Summerfield, J.J. Doyle, C.M. Torok, H.C. Dietz, M.G. Pomper, S.M. Yu, Targeting collagen strands by photo-triggered triple-helix hybridization. *P Natl Acad Sci USA* **2012,** *109* (37), 14767-14772.

39. J.N. Luo, Y.W. Tong, Self-Assembly of Collagen-Mimetic Peptide Amphiphiles into Biofunctional Nanofiber. *Acs Nano* **2011,** *5* (10), 7739-7747.

40. O.D. Krishna, K.T. Wiss, T.Z. Luo, D.J. Pochan, P. Theato, K.L. Kiick, Morphological transformations in a dually thermoresponsive coil-rod-coil bioconjugate. *Soft Matter* **2012,** *8* (14), 3832-3840.

41. B. Brodsky, A.V. Persikov, Molecular structure of the collagen triple helix. In *Fibrous Proteins: Coiled-Coils, Collagen and Elastomers*, D.A.D. Parry, J.M. Squire, Eds. Elsevier Academic Press Inc: San Diego, 2005; Vol. 70, pp 301-+.

42. C.G. Knight, L.F. Morton, A.R. Peachey, D.S. Tuckwell, R.W. Farndale, M.J. Barnes, The collagen-binding A-domains of integrins alpha(1)beta(1) and alpha(2)beta(1) recognize the same specific amino acid sequence, GFOGER, in native (triple-helical) collagens. *J. Biol. Chem.* **2000,** *275* (1), 35-40.

43. W.M. Zhang, J. Kapyla, J.S. Puranen, C.G. Knight, C.F. Tiger, O.T. Pentikainen, M.S. Johnson, R.W. Farndale, J. Heino, D. Gullberg, alpha(11)beta(1) integrin recognizes the GFOGER sequence in interstitial collagens. *J. Biol. Chem.* **2003,** *278* (9), 7270-7277.

44. C.D. Reyes, A.J. Garcia, Engineering integrin-specific surfaces with a triple-helical collagen-mimetic peptide. *J. Biomed. Mater. Res. Part A* **2003,** *65A* (4), 511-523.

45. R. Mhanna, E. Ozturk, Q. Vallmajo-Martin, C. Millan, M. Muller, M. Zenobi-Wong, GFOGER-Modified MMP-Sensitive Polyethylene Glycol Hydrogels Induce Chondrogenic Differentiation of Human Mesenchymal Stem Cells. *Tissue Eng. Part A* **2014,** *20* (7-8), 1165-1174.

46. S.E. Grieshaber, B.A. Paik, S. Bai, K.L. Kiick, X.Q. Jia, Nanoparticle formation from hybrid, multiblock copolymers of poly(acrylic acid) and a VPGVG peptide. *Soft Matter* **2013,** *9* (5), 1589-1599.

47. S.E. Grieshaber, A.J.E. Farran, S. Lin-Gibson, K.L. Kiick, X.Q. Jia, Synthesis and Characterization of Elastin-Mimetic Hybrid Polymers with Multiblock, Alternating Molecular Architecture and Elastomeric Properties. *Macromolecules* **2009,** *42* (7), 2532-2541.

48. W. Agut, R. Agnaou, S. Lecommandoux, D. Taton, Synthesis of block copolypeptides by click chemistry. *Macromol. Rapid Commun.* **2008,** *29* (12-13), 1147-1155.

49. T.Z. Luo, L.R. He, P. Theato, K.L. Kiick, Thermoresponsive Self-Assembly of Nanostructures from a Collagen-Like Peptide-Containing Diblock Copolymer. *Macromol. Biosci.* **2015,** *15* (1), 111-123.

50. Y.C. Yu, P. Berndt, M. Tirrell, G.B. Fields, Self-assembling amphiphiles for construction of protein molecular architecture. *J Am Chem Soc* **1996,** *118* (50), 12515-12520.

51. K. Isoda, N. Kanayama, D. Miyamoto, T. Takarada, M. Maeda, RAFT-generated poly(N-isopropylacrylamide)-DNA block copolymers for temperature-responsive formation of polymer micelles. *React Funct Polym* **2011,** *71* (3), 367-371.

52. C.W. Zhao, X.L. Zhuang, C.L. He, X.S. Chen, X.B. Jing, Synthesis of Novel Thermo- and pH-Responsive Poly(L-lysine)-Based Copolymer and its Micellization in Water. *Macromol. Rapid Commun.* **2008,** *29* (22), 1810-1816.

53. A. Chilkoti, M.R. Dreher, D.E. Meyer, Design of thermally responsive, recombinant polypeptide carriers for targeted drug delivery. *Adv Drug Deliver Rev* **2002,** *54* (8), 1093-1111.

54. J.A. MacKay, D.J. Callahan, K.N. FitzGerald, A. Chilkoti, Quantitative Model of the Phase Behavior of Recombinant pH-Responsive Elastin-Like Polypeptides. *Biomacromolecules* **2010,** *11* (11), 2873-2879.

55. D.E. Meyer, A. Chilkoti, Genetically encoded synthesis of protein-based polymers with precisely specified molecular weight and sequence by recursive directional ligation: Examples from the elastin-like polypeptide system. *Biomacromolecules* **2002,** *3* (2), 357-367.

56. F. Fernandez-Trillo, A. Dureault, J.P.M. Bayley, J.C.M. van Hest, J.C. Thies, T. Michon, R. Weberskirch, N.R. Cameron, Elastin-based side-chain polymers: Improved synthesis via RAFT and stimulus responsive behavior. *Macromolecules* **2007,** *40* (17), 6094-6099.

57. R.M. Conrad, R.H. Grubbs, Tunable, Temperature-Responsive Polynorbornenes with Side Chains Based on an Elastin Peptide Sequence. *Angew. Chem.-Int. Edit.* **2009,** *48* (44), 8328-8330.

58. L. Ayres, K. Koch, P. Adams, J.C.M. van Hest, Stimulus responsive behavior of elastin-based side chain polymers. *Macromolecules* **2005,** *38* (5), 1699-1704.

59. R.K. Ainavarapu, J. Brujic, H.H. Huang, A.P. Wiita, H. Lu, L.W. Li, K.A. Walther, M. Carrion-Vazquez, H.B. Li, J.M. Fernandez, Contour length and refolding rate of a small protein controlled by engineered disulfide bonds. *Biophys. J.* **2007,** *92* (1), 225-233.

60. G. Stirnemann, D. Giganti, J.M. Fernandez, B.J. Berne, Elasticity, structure, and relaxation of extended proteins under force. *P Natl Acad Sci USA* **2013,** *110* (10), 3847-3852.

61. W.Y. Kim, J.T. Xiao, E.L. Chaikof, Recombinant Amphiphilic Protein Micelles for Drug Delivery. *Langmuir* **2011,** *27* (23), 14329-14334.

62. W. Kim, J. Thevenot, E. Ibarboure, S. Lecommandoux, E.L. Chaikof, Self-Assembly of Thermally Responsive Amphiphilic Diblock Copolypeptides into Spherical Micellar Nanoparticles. *Angew. Chem.-Int. Edit.* **2010,** *49* (25), 4257-4260.

63. B.C. Dash, S. Mahor, O. Carroll, A. Mathew, W.X. Wang, K.A. Woodhouse, A. Pandit, Tunable elastin-like polypeptide hollow sphere as a high payload and controlled delivery gene depot. *J Control Release* **2011,** *152* (3), 382-392.

64. M. Pechar, J. Brus, L. Kostka, C. Konak, M. Urbanova, M. Slouf, Thermoresponsive self-assembly of short elastin-like polypentapeptides and their poly(ethylene glycol) derivatives. *Macromol. Biosci.* **2007,** *7* (1), 56-69.

65. M. Dai, J. Haghpanah, N. Singh, E.W. Roth, A. Liang, R.S. Tu, J.K. Montclare, Artificial Protein Block Polymer Libraries Bearing Two SADs: Effects of Elastin Domain Repeats. *Biomacromolecules* **2011,** *12* (12), 4240-4246.

66. X. Mo, Y.J. An, C.S. Yun, S.M. Yu, Nanoparticle-assisted visualization of binding interactions between collagen mimetic peptide and collagen fibers. *Angew. Chem.-Int. Edit.* **2006,** *45* (14), 2267-2270.

67. M.A. Urello, K.L. Kiick, M.O. Sullivan, A CMP-based method for tunable, cell-mediated gene delivery from collagen scaffolds. *J. Mat. Chem. B* **2014,** *2* (46), 8174-8185.

# Chapter 4

# THERMORESPONSIVE ELASTIN-*b*-COLLAGEN-LIKE PEPTIDE BIOCONJUGATE NANOPARTICLES FOR TARGETED DRUG DELIVERY IN COLLAGEN CONTAINING MATRICES

## 4.1 Introduction

Collagen is the main component of the extracellular matrix (ECM) in humans. Comprising 29 different types, collagens are widely located in tendon, ligament, skin, cartilage and bone, with widespread functions such as mediating cell adhesion, migration, tissue scaffolding and repairing.[1] Although the roles of collagens vary widely, they all share the same tertiary structure – collagen triple helix, which comprises three polyproline-II type helices twisted together in a right-handed form.[2] Synthetic model collagens, named as collagen-like peptides (CLPs) or collagen-mimetic peptides (CMPs), are short synthetic (poly)peptides, which mimic the triple helical conformation of native collagens.[3-5] Unlike native collagens, folding and unfolding of CLP triple helices are reversible, possibly attributed to their relatively low molecular mass (<5 kDa).[5]

In the past two decades, these peptides have been widely employed to elucidate the triple helix structure and the stabilization effect of different amino acid residues in collagens,[6-10] as well as to produce higher-order supramolecular structures.[11-15] More recently, Wang et al. have reported that single-stranded CLPs have a strong propensity to bind native collagen via a strand invasion process.[16] The high propensity of CLPs for collagen permits the utilization of CLPs as staining reagent to

detect minute quantities of collagens in human tissues including skin, cornea, bone[17] and liver.[18] *In vivo* studies suggest that CLPs are able to permeate and accumulate in regions with high MMP activities, such as prostate tumor xenografts, joints and articular cartilage.[19] Despite the great potential of using CLPs as novel biomaterial for tracking pathogenic collagens, research on the utilization of these peptides as building blocks in generating nanosized drug carriers are very limited.[20, 21]

On the other hand, elastin-like polypeptides (ELPs), derived from the hydrophobic domain of tropoelasin,[22] are synthetic polypeptides comprising many copies of the pentapeptide repeat Val-Pro-Gly-Xaa-Gly (VPGXG). Due to their LCST -like behavior called inverse temperature transition, the ELPs are widely used to develop new smart materials including drug delivery vehicles that can be targeted to tissues and cells either via passive or peptide- and stimuli-responsive mechanisms.[23-29] However, essentially all of the ELPs employed in current research activities are recombinantly synthesized, with tens or even hundreds of pentapeptide repeats. Thermoresponsive drug delivery systems comprising short synthetic ELPs (fewer than ten pentapeptides) have rarely reported, possibly due to their high transition temperatures.[30-32]

In our previous work,[33] we successfully overcame this limitation by conjugating short ELPs with a triple-helix-forming collagen-like peptide. The resulting ELP-CLP conjugates exhibited a remarkable reduction in the inverse transition temperature of the ELP domain upon formation of the CLP triple helix. The lower transition temperature of the conjugate enables the facile formation of well-defined vesicles at physiological temperature and the unexpected resolubilization of the vesicles at *elevated* temperatures upon unfolding of the CLP domain.

We hypothesized that the interactions between CLPs on the surface of the vesicles and natural collagens[16] could be exploited to target these vesicles to collagen containing substrates via triple helix hybridization. In this work, the hypothesis was corroborated by retention experiments of the nanoparticles on type II collagen films. Additionally, we believe the resolubilization of the ELP domain and dissociation of the vesicles at elevated temperatures may endow these nanoparticles with great potential for temperature controlled drug release. Fluorescein, as a modelled drug, was encapsulated into the nanoparticles. A sustained release of clinically relevant amount of cargo was observed within a period of 3 weeks. As expected, a burst release was triggered by dissociation of the vehicles via unfolding of the CLP domain upon heating. Cytocompatibility of the ELP-CLP nanoparticles was evaluated by measuring cell viability *in vitro*, using NIH-3T3 fibroblasts, ATDC5 chondrocytes as well as RAW 264.7 macrophages. In addition, for macrophages incubated with the nanoparticles, essentially no TNF-α expression above the level of a negative control was observed, illustrating the lack of an inflammatory response initiated by the nanoparticles. Endowed with the collagen targeting ability from the CLP domain, thermoresposiveness from the ELP domain, controlled long term drug release, cytocompatibility, and non-immune responsiveness, these ELP-CLP nanoparticles shows great potential for targeted drug delivery applications, especially for diseases associated with high MMP activity such as cancer,[34-36] general autoimmune connective tissue disorders (such as rheumatoid arthritis),[37-39] Marfan syndrome,[19, 40] and osteogenesis imperfecta.[41]

## 4.2 Materials and Methods

### 4.2.1 ELP-CLP diblock synthesis and characterization

As described in our previous paper,[33] elastin-like polypeptide (ELP) with sequence $(VPGFG)_6$ and collagen-like peptide (CLP) with sequence $(GPO)_4GFOGER(GPO)_4GG$ were synthesized via solid phase peptide synthesis (SPPS) and purified via reverse phase high pressure liquid chromatography (HPLC). The synthesis of the ELP-CLP conjugate was performed via copper(I)-catalyzed alkyne-azide cycloaddition (CuAAC) "click" reaction. The purity of the diblock was verified via gel permeation chromatography (GPC), nuclear magnetic resonance spectrometry (NMR) and Fourier transform infrared spectroscopy (FTIR). The ability of the CLP domain to retain triple helical conformation was studied using circular dichroic spectroscopy (CD).

### 4.2.2 Thermoresponsive drug release from ELP-CLP nanoparticles

#### 4.2.2.1 Preparation of drug loaded nanoparticles

To investigate the feasibility of the ELP-CLP nanoparticles as potential drug carriers, fluorescein was used as a modelled drug and encapsulated into the nanoparticles. Briefly, 0.5 mg ELP-CLP diblock and 1 mg fluorescein were dissolved in 0.5 mL PBS (10 mM, pH 7.4) at 80 °C. The sample was then incubated at 37 °C for 1 hour to allow the nanoparticle formation and simultaneous encapsulation of fluorescein. Nanoparticle solutions were then concentrated by centrifugation using Amicon Ultra-0.5 mL Centrifugal Filters (3 kDa, Billerica, MA) and washed with fresh PBS for at least 10 times, until no fluorescence was detected in the wash solution. Concentrated nanoparticle solutions were then diluted using fresh PBS to yield 1

mg/mL nanoparticle working solutions for subsequent studies. For transmission electron microscopy (TEM) studies, instead of using PBS, nanoparticles were prepared in deionized water to prevent the precipitation of phosphotungstic acid (PTA) stain.

#### 4.2.2.2 Particle size distribution

Analysis of particle sizes prior to and after fluorescein encapsulation was conducted via dynamic light scattering (DLS) on a ZetaSizer Nano Series (Nano ZS, Malvern Instruments, U.K.) at a scattering angle of 173°, and data fitting using the cumulant method. Size distribution studies were performed at both 37 °C and 80 °C. Each sample was incubated for 10 min at the desired temperature before measurements. The reported data represent an average of at least three measurements.

#### 4.2.2.3 Morphology

Morphology of the nanoparticles, prior to and after fluorescein encapsulation was studied via transmission electron microscopy (TEM). Samples were prepared on carbon-coated copper grids (CF300-Cu, Electron Microscopy Sciences Inc.). The grids, pipette tips, and samples were all incubated in an isothermal oven (VWR Signature™ Forced Air Safety Ovens, VWR Inc.) at desired temperature (37 °C or 80 °C) for at least 30 min before sample preparation, which was also conducted in the oven. 5 μL of the sample solution was drop cast on the grid and blotted after 60 seconds. For staining, 1% phosphotungstic acid (PTA) (pH adjusted to 7.0 using 1 M NaOH) as a negative stain was used. 3 μL of the PTA solution was drop cast on the grid and blotted after 10 seconds. The sample was then allowed to dry in the oven at the desired temperature for 30 minutes and then was air-dried for 2 hours. TEM images were

taken on a JEM-3010 TEM (JEOL USA Inc., Peabody, MA) at an acceleration voltage of 300 keV.

#### 4.2.2.4 Release profile

0.5 mL Fluorescein loaded nanoparticle solution at 1 mg/mL in PBS (10 mM, pH 7.4) was dialyzed against 14 mL PBS using a 0.5 mL Slide-A-Lyzer™ MINI Dialysis Device (MWCO 3.5 kDa) (Thermo Fisher Scientific Inc, Waltham, MA). 3 mL PBS was removed and replenished at predetermined time points. The release of fluorescein was monitored by measuring the fluorescence intensity of the removed buffer using a PerkinElmer Fusion microplate reader (Waltham, MA, USA), with excitation/emission wavelengths of 485/535 nm. At day 21, the nanoparticle solution was heated and incubated at 80 °C for one hour to fully dissociate the nanoparticles and the amount of residual encapsulated fluorescein was measured. The reported data represent an average of three repeats. Figure S1 shows a schematic of the experiment.

### 4.2.3 Nanoparticle retention on collagen films

Type II collagen from chicken sternal cartilage was purchased from Sigma-Aldrich (St. Louis, MO) and dissolved at 5 mg/mL in 0.25% v/v acetic acid overnight. The pH of the collagen solution was adjusted to 7-8 using 10x PBS and 1 M NaOH. Instead of physical encapsulation of fluorescein into the nanoparticles, carboxyfluorescein was covalently conjugated with the N-terminal amine of the ELP. The fluorescein labelled ELP-CLP nanoparticles (210 µg/mL in PBS, pH 7.4) were then incubated briefly at 65 °C for 10 minutes to partially unfold the CLP triple helices; nanoparticles remain intact during this heating owing to the collapse of the ELP domain (Figure S2). A control sample was run in which this heating step at 65 °C

was not conducted. For each sample, 30 µL nanoparticle solution was added into 600 µL collagen solution to obtain a final nanoparticle concentration of 10 µg/mL. The samples were then incubated at 4 °C for 3 hours to allow the nanoparticles to bind with the collagen membrane via strand invasion. The nanoparticle incorporated collagen solution were gelled at 37 °C for 1 hour and dried overnight at room temperature to form a thin layer of collagen film. The collagen films were then washed with PBS repeatedly until no fluorescence was detected in the wash to ensure all unembedded nanoparticles were removed. Figure S3 shows the procedure of the experiment.

For the release of the nanoparticles from collagen films, 500 µL 1x PBS was added on the top of each film as a reservoir for the release. 200 µL sample was collected and 200 µL fresh PBS was added to each well at desired time intervals. Fluorescence of nanoparticles in the collected samples was analyzed using a PerkinElmer Fusion microplate reader (Waltham, MA, USA), with excitation/emission wavelengths of 485/535 nm. Results were reported as an average of 4 repeats for the preheated samples and an average of 3 repeats for the non-preheated controls. At day 10, the samples were heated up and incubated at 80 °C for 1 hour to completely dissolve the film and dissociate the nanoparticles. Solutions became clear after incubation. 200 µL solution was then immediately collected from each sample and the fluorescence intensity was measured.

### 4.2.4 Inflammatory response

RAW264.7 murine macrophages were purchased from American Type Culture Collection (ATCC) and were cultured in DMEM (Sigma Aldrich) supplemented with 10% heat-inactivated fetal bovine serum (MediaTech), 10 mM HEPES (GIBCO), 55

μM β-mercaptoethanol (GIBCO), and 1% antibiotic/antimycotic (GIBCO) at 37°C with 5% $CO_2$. Upon reaching 60-80% confluency, cells were lifted off the plates by gentle scraping and seeded on a 96-well plate at a density of 5 x $10^4$ cells per well in 200 μL cell culture media. After an overnight incubation and media change, cells were treated with various concentrations of ELP-CLP nanoparticles (50, 150, 500, and 1000 μg/mL) in medium. Cells treated with lipopolysaccharide (LPS, 50 ng/mL) were served as a positive control, while cells in culture medium without the nanoparticles were utilized as a negative control. After 8 h of incubation, the supernatant was collected and stored at -20 °C until further analysis. Cell metabolism post-treatment was assayed using PrestoBlue Viability Assay (Life Technologies), which provides a fluorescence measurement of the overall reductive capability of the cells, according to the manufacturer's instructions. Briefly, 20 μL of reagent was added to 100 μL of cells and medium. After 2 h of incubation at 37 °C, the medium was collected and analyzed using a PerkinElmer VICTOR3 1420 Multilabel Plate Reader (PerkinElmer, Waltham, MA) at excitation/emission wavelengths of 570 nm/615 nm. TNF-α concentration in collected media samples was measured via an enzyme-linked immunosorbent assay (ELISA) (BD Bioscience), according to the manufacturer's instructions.

### 4.2.5 Fibroblast viability

The cytotoxicity of the ELP-CLP nanoparticles was assessed *in vitro* for the murine embryotic fibroblast (NIH-3T3) cell line. Cells were cultured in a 12-well corning cellgro® tissue culture plate (plating density of 10,000 cells/cm^2, working volume of 1 mL) in the presence of Dulbecco's Modified Eagle's Media (DMEM) supplemented with 10% v/v fetal bovine serum (FBS) and 1% v/v penicillin

streptomycin (PS) for 24 hours, and then washed with Dulbecco's phosphate buffered saline (DPBS). The cells were then incubated in fully supplemented DMEM media for 24 hours, with the addition of preformed ELP-CLP nanoparticles at final concentrations of 0 ug/mL, 500 µg/mL and 1000 µg/mL. The cells were then washed again with DPBS, stained with non-supplemented DMEM containing 0.1% v/v of Calcein AM and 0.1% v/v of Propidium Iodide for 45 minutes, and imaged using a Leica DMI-6000B fluorescent microscope.

### 4.2.6 Chondrocyte viability and proliferation

ATDC5 cells, murine chondrocyte cell line, were plated into 12-well culture dishes at a density of 10,000 cells/cm^2, cultured for 24 hours in the presence of DMEM/F-12 (1:1 mixture) containing 10% FBS and 1% PS, and then washed in 1x HBSS. Preformed ELP-CLP nanoparticles in culture media were added to the wells at 0, 50, 150, 500, and 1000 ug/mL. Following 24 or 72 hours of incubation with ELP-CLP nanoparticles, the culture medium was removed, washed with 1x HBSS, and then Calcien-AM (2mM; live cells) and EtDH-1 (4mM; dead cells) were added to the wells for 40 minutes to perform live-dead staining, assessed via fluorescent microscopy using a Axio Observer Z1. To quantitate cell viability, the number of live and dead ATDC5 cells were counted. ATDC5 cell proliferation was measured longitudinally (0- through 72 hours) by assessing areal cell coverage (area of covered by cells/total area of image) over time using an object detection method (Laplace of Gaussian Filter) in MATLAB, similarly to previous methods using ImageJ.[42]

## 4.3 Results

### 4.3.1 Thermoresponsive drug release from ELP-CLP nanoparticles

Diblock copolymers consisting of one thermoresponsive block and one hydrophilic block were expected to exhibit reversible self-assembly behaviors as temperature changes. The diblock in this work consists of a hydrophilic CLP block and a thermoresponsive ELP block. In our previous study,[33] the diblock was reported to undergo self-assembly into hollowed nanovesicles in aqueous conditions at physiological temperature. More interestingly, when the diblock sample was heated above the melting temperature ($T_m$) of the CLP domain, the nanoparticles became fully resolubilized, attributed to the unfolding of the CLP triple helices. We think this unusual thermoresponsive dissociation of the nanoparticles may endow the diblock with potential for temperature controlled drug release. Thus drug releasing and loading experiment were performed. Fluorescein, which is one of the most commonly used fluorophore for biological research, has been widely employed as a fluorescent probe and hydrophobic modelled drug, both *in vitro*[43-45] and *in vivo*.[46-48] To evaluate the potential of the ELP-CLP diblock nanoparticles as drug carriers for controlled delivery, fluorescein-loaded nanoparticles were prepared.

#### 4.3.1.1 Nanoparticle characterization

Dynamic light scattering (DLS) was conducted to study the size distribution of the ELP-CLP nanoparticles, with or without fluorescein encapsulated. Figure 1a shows the size distributions for the diblock sample at 37 °C and 80 °C. Figure 1d shows the size distributions for the fluorescein loaded diblock sample at 37 °C and 80 °C. In both cases, nanostructures with an average diameter of approximately 100 - 200 nm were observed. As expected, while the CLP domain completely unfolds at

80 °C, the nanostructures dissociated into small objects with diameters of approximately 5 - 10 nm, which were attributed to the soluble diblock, consistent with previous reports.[33, 49]

To obtain insight into the morphologies of the nanostructures observed via DLS, transmission electron microscopy (TEM) measurements were also conducted on the drug free (Figure 1b and 1c) and drug loaded nanoparticles (Figure 1e and 1f) at 37 °C and 80 °C. To better visualize the nanostructures, 1% PTA (pH adjusted to 7.0 using NaOH) aqueous solution was used as negative stain. Similar to the drug free diblock nanoparticles (Figure 1b),[33] at physiological temperature, the fluorescein loaded ELP-CLP diblock nanoparticles were still able to maintain the vesicular structure (Figure 1e). Statistical analysis using ImageJ software suggests the thickness of the vesicle layer to be of approximately 21.8 ± 2.9 nm (based on 112 nanoparticle within 8 images), consistent with that of the drug free vesicles.[33] As expected, when heated above the $T_m$ of the CLP domain, the drug loaded nanoparticles were resolubilized and dissociated into monomers, with no well-defined structure observed via microscopy (Figure 1c and 1f), which were also consistent with the DLS results. These results suggest that after encapsulation of the drug, the ELP-CLP diblock is still able to form stable nanovesicles at physiological temperature and these nanoparticles can be resolubilized at elevated temperatures, which may trigger the release of encapsulated drugs.

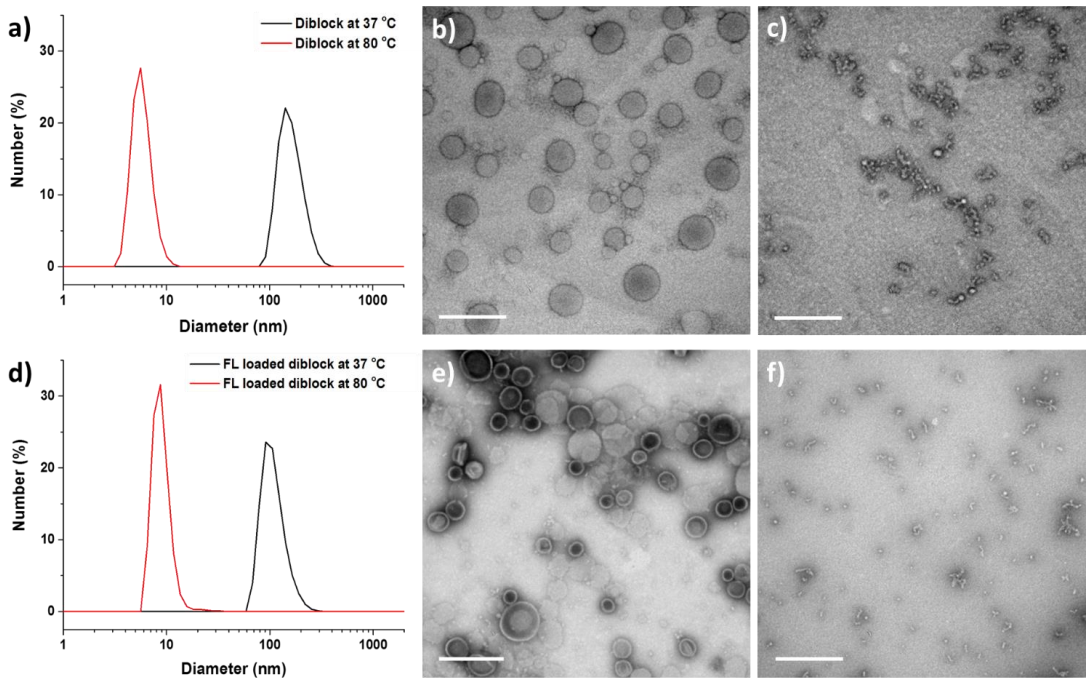


Figure 4.1 Nanoparticle characterization. a) Size distributions of ELP−CLP assemblies. b) TEM image of nanoparticles from ELP−CLP conjugates at 37 °C. c) TEM image of nanoparticles from ELP−CLP conjugates at 80 °C. d) Size distributions of fluorescein loaded ELP−CLP assemblies. e) TEM image of fluorescein loaded nanoparticles from ELP−CLP conjugates at 37 °C. c) TEM image of fluorescein loaded nanoparticles from ELP−CLP conjugates at 80 °C. Scale bars = 500 nm.

#### 4.3.1.2 Release profile

The release of fluorescein from the nanoparticle was monitored as a function of time at 37 °C in PBS (Figure 2), via measurement of the fluorescence intensity of the buffer in which the nanoparticles were dialyzed against. From the release profile shown in Figure 2, a burst release of approximately 45% percent of encapsulated drug was observed in the first 48 hours, followed by a sustained release of total 50% encapsulated drug within 21 days. As expected, when the sample was heated up to 80 °C at day 21, a burst release was observed, likely attributed to the dissociation of

the nanoparticles at elevated temperatures (Figure 1d and 1f). The amount of fluorescein encapsulated was calculated to be 181.8 ng, which exceeds, by approximately 10-fold, the $IC_{50}$ values reported for a range of hydrophobic osteoarthritis drugs (1.2 – 99.8 ng),[50-52] suggesting that these nanoparticles will be useful for such intended applications.

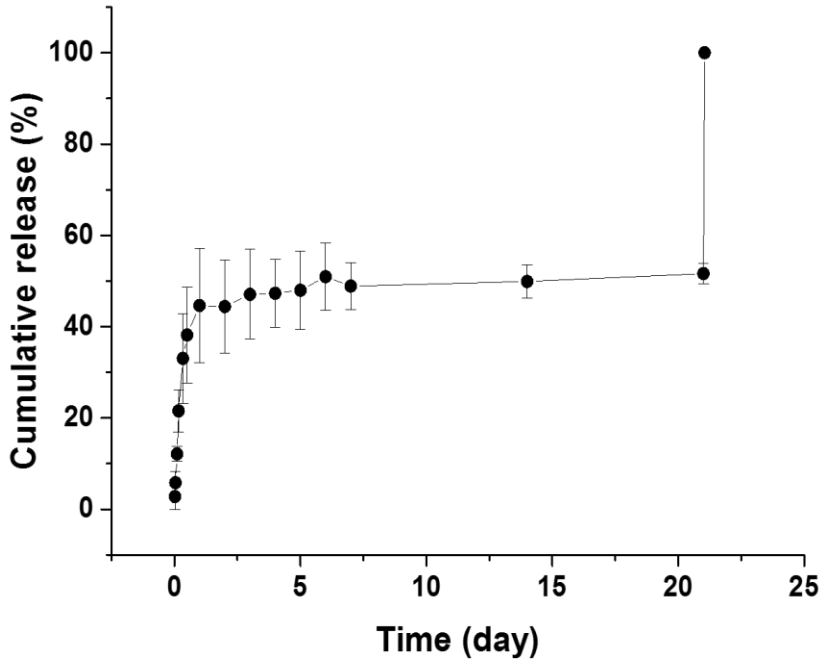


Figure 4.2 Cumulative release of fluorescein from ELP-CLP nanoparticles as a function of time. The amount of released fluorescein was calculated by measuring the fluorescence at 535 nm using a fluorescein calibration curve. At day 21, the sample was heated at 80 °C before measurement. Each data point represents the mean ± standard deviation for a total of three separately prepared and analyzed samples.

### 4.3.2 Collagen retention

To determine whether the ELP-CLP diblock nanoparticle could be immobilized on collagen containing matrices, nanoparticle binding and retention studies were conducted on type II collagen films. Since the retention and releasing of nanoparticles were quantified via fluorescence measurements and the nanoparticles were releasing encapsulated fluorescein as well, in order to distinguish the two different kinds of release, instead of physical encapsulation of the fluorescent probe, the ELP-CLP diblock was covalently functionalized with fluorescein at the N terminal. DLS results suggest the fluorescein labelled diblock was still able to self-assemble into nanoparticles with similar size and thermoresponsive behavior (Figure S2).

To improve the binding affinity with collagen substrate via triple helix hybridization, the fluorescein labelled nanoparticles were pre-incubated at 65 °C for 15 minutes to allow the CLP triple helix domain to be partially unfolded before adding to the collagen films. A non-preheated sample was used as negative control. The release profile of preheated sample *vs.* unpreheated control was shown in Figure 4. For both the preheated sample and unpreheated control, only a very small amount of release was observed within 10 days, illustrating that the fluorescently labelled ELP-CLP nanoparticles were strongly retained in the collagen film. At day 10, the collagen films were dissolved at elevated temperatures, resulting in a burst release for both samples. While a total of approximately 0.201 μg/cm$^2$ nanoparticles were initially retained on the film for the control, collagen films embedded with preheated nanoparticles showed improved initial retention of 0.629 ug/cm$^2$, which was approximately 3-fold higher compared with the control, likely attributed to the specific binding via triple helix hybridization. The strong binding, high retention and thermoresponsive release of the ELP-CLP nanoparticles from collagen films endows

these vehicles with potential to serve as drug delivery vehicles for targeting collagen containing matrices such as articular cartilage of the knee joints, as well as the tumor sites.

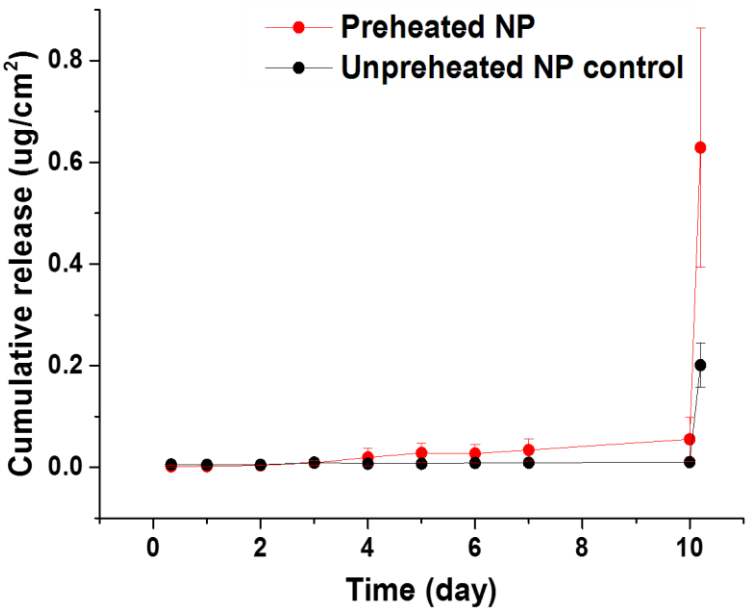


Figure 4.3 Cumulative release of fluorescent labelled ELP-CLP nanoparticles from type II collagen film as a function of time. Sample (red curve) was pre-heated at 65 °C to partially unfold the CLP triple helix, so that the sample would be able to bind to the collagen film via strand invasion. A non-preheated nanoparticle control (black) was also used. The amount of released nanoparticles was calculated by measuring the fluorescence at 535 nm using a FELP-CLP nanoparticle calibration curve. At day 10, the film was heated at 80 °C before measurement. Each data point for the preheated nanoparticle sample represents the mean ± standard deviation for a total of five separately prepared and analyzed samples. Data for the unpreheated nanoparticle sample represents three samples.

### 4.3.3 Inflammatory response of ELP-CLP nanoparticles

Biomaterial application within tissues can evoke inflammatory reactions, cause abnormal wound healing, and potentially damage host tissue.[53] Inflammation is a complex process mediated by multiple cell types and signaling molecules. In particular, macrophages play a critical role in the inflammation process by secreting pro-inflammatory cytokines (e.g. TNF-α) that are heavily involved in tissue repair and foreign body reactions.[54] Therefore, to gauge the suitability of ELP-CLP nanoparticles for *in vivo* applications, we evaluated the inflammatory potential of our materials against murine-derived RAW264.7 macrophage-like cells. Following culture, macrophage metabolic activity was similar across cultures following treatment, indicating that the ELP-CLP nanoparticles were not toxic at any of the concentrations tested (Figure S4). To further evaluate the potential of the ELP-CLP nanoparticles to evoke an inflammatory response, the production of TNF-α, a proinflammatory cytokine that is heavily involved in the inflammatory cascade, was examined. RAW264.7 macrophages produced negligible amounts of TNF-α following culture with 50, 150, 500, or 1000 μg/mL of ELP-CLP nanoparticles, similar to the activation level displayed by control macrophages exposed to medium only (Figure 4), which is also consistent with responses observed with other particulate systems and ELP-based biomaterials [55-57]. Conversely, RAW264.7 cells exposed to 50 ng/mL LPS positive control exhibited a nearly 100-fold increase in TNF-α production compared to controls. The lack of significant activation of macrophages by the ELP-CLP nanoparticles suggests their potential as a biocompatible drug delivery system.

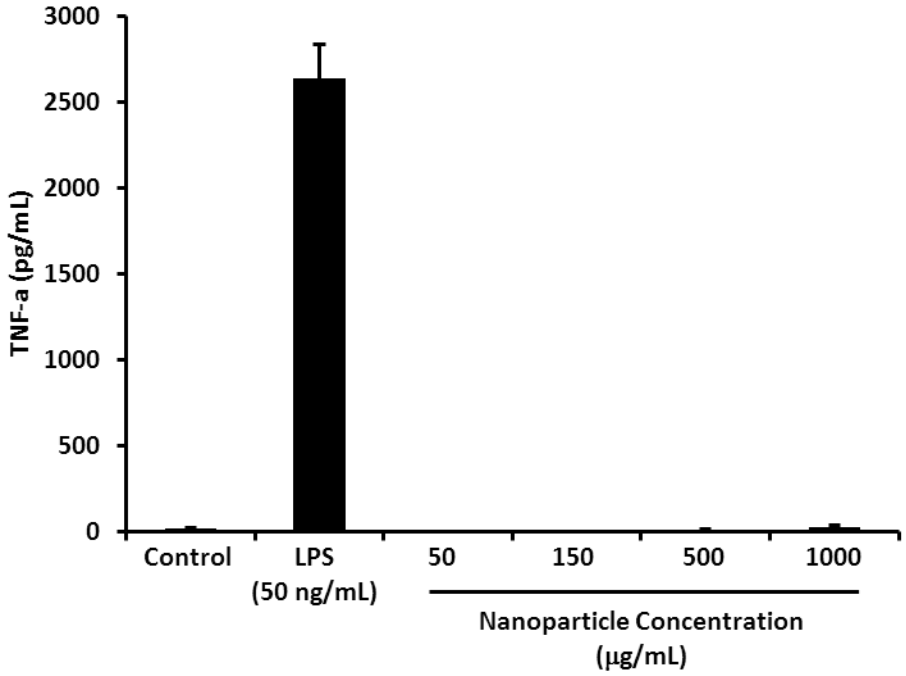


Figure 4.4 Activation of murine-derived RAW264.7 macrophages treated with ELP-CLP nanoparticles. RAW264.7 macrophages were cultured on TCPS and incubated with medium only (control), 50 ng/mL LPS, or various concentrations of ELP-CLP nanoparticles for 8 hrs prior to evaluation of TNF-α secretion by macrophage. N=3.

### 4.3.4 Fibroblast viability

Considering the critical role of fibroblasts in the synthesis of collagen in the ECM, cytotoxicity of the ELP-CLP nanoparticles was assessed with murine embryotic fibroblasts (NIH-3T3 cell line). Cells were plated using standard cell culture procedures and incubated with preformed nanoparticles for 24 hours, after which they were subjected to live and dead stains (Calcein AM and propidium iodide respectively) and assessed for viability with fluorescent microscopy. Results for untreated cell control are shown in Figure 5a,b and results for cells treated with 1 mg/mL concentration of nanoparticles were shown in Figure 5c,d, respectively. Similar

experiments were also performed for cells cultured with nanoparticles at lower concentrations (Figure S5). Both phase images seen in Figure 5 have apparent healthy morphologies for both the treated and untreated cells. The favorable viability of both treated and untreated cells are seen in the fluorescent images. The presence of the live stain (green) and the absence of the dead stain are indicative of successful metabolization of Calcein acetoxymethyl to Calcein fluorescent dye, as well as the lack of permeable cell membranes, respectively. The distinct similarities seen between the untreated control and the nanoparticle treated cells, suggests that the nanoparticles are not cytotoxic to murine fibroblast cells after 24 hours of exposure at concentrations well above that of therapeutically relevant doses.

The lack of cytotoxicity of these nanoparticles from NIH-3T3 fibroblasts are in good agreement with the other cell lines discussed later in this manuscript. There have been many studies that have looked at the interaction of mouse fibroblasts with various materials.[58-61] Most notably similar nanoparticle drug delivery vehicles such as silver, gold, and polymer based nanoparticles all have varying degrees of increased cytotoxicity and unfavorable cell morphologies with respect to our studies seen here. [62-68] The apparent lack of cytotoxicity of our peptide nanoparticles offers a viable and risk free means for drug delivery.

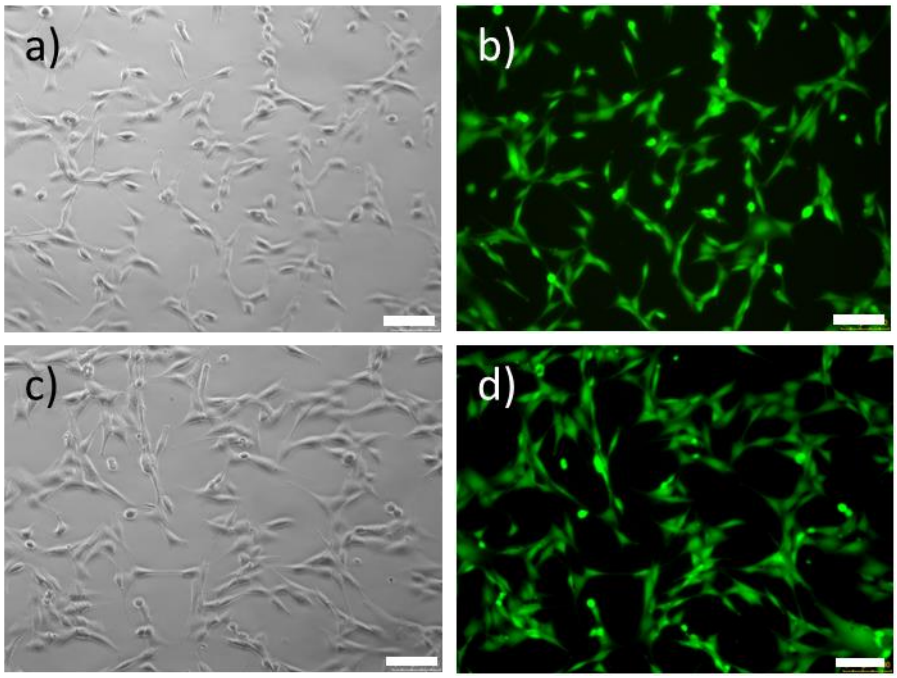


Figure 4.5 Cell viability results after 24 hour incubation with serum. All images are with a 10x objective. a,b) phase image and Calcien AM live stain (respectively) of 0 ug/mL NP control; c,d) phase image and Calcien AM live stain of 1000 ug/mL NPs. Scale bars = 100 µm.

### 4.3.5 Chondrocyte viability and proliferation

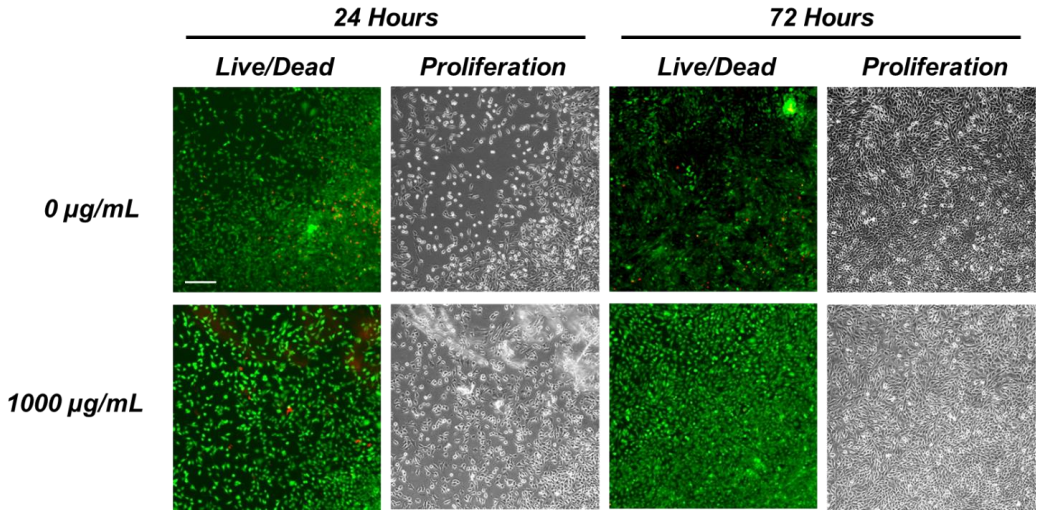


Figure 4.6 ADTC5 viability and proliferation in the presence of ELP-CLP nanoparticles in vitro. Representative images of ATDC5 cell viability via live (green fluorescence)/dead (red fluorescence) assay and proliferation (differential interference contrast microscopy) at 24 hour and 72 hours post- ELP-CLP nanoparticles application (0 and 1000 ug/mL shown at top and bottom panel, respectively). Application of ELP-CLP nanoparticles does not appear to cause ATDC5 death or change in cell proliferation. Scale bar = 200 µm and applies to all images.

Previous *In vivo* studies conducted by Yu and coworkers suggested that, through triple helix hybridization, collagen like peptides could permeate and accumulate in regions with high MMP and collagen remodeling actives including tumor, joint and articular cartilage.[19] Equipped with a CLP layer on the exterior surface of the vesicles, the ELP-CLP nanoparticles should thus offer particular promise for targeted drug delivery into these regions. Considering the critical role of chondrocytes in producing and maintaining the collagen and proteoglycans matrix in the cartilage, the compatibility of the nanoparticles with ATDC5 cell line was

investigated. Characterized as a chondrogenic cell ATDC5 cells are regarded as a promising *in vitro* model to study the factors that influence cell behaviors during chondrogenesis.[69]

To determine the effect of ELP-CLP nanoparticle concentration on ATDC5 cells, changes in cell viability and proliferation were quantified via live/dead assay and area coverage, respectively, over time. It was observed that application of ELP-CLP did not induce increased ATDC5 cell death at either 24- or 72 hours for any of the ELP-CLP concentration tested compared to untreated cells (Figure 6), with the percent of live cells observed at all ELP-CLP concentrations and timepoints not being significantly different from untreated cells (Figure 7A). Cell proliferation, as well, did not appear to be influenced by any of the ELP-CLP concentrations tested (Figure 6). As expected, quantitative assessment of the degree of areal cell coverage increased in all groups with time (Figure 7B), capturing the natural growth and proliferation of ADTC5 cells *in vitro*. In addition, areal cell coverage at all timepoints was similar among all groups, indicating that the presence of ELP-CLP nanoparticles did not significantly influence ATDC5 cell proliferation. These results suggest that ELP-CLP nanoparticles may be used as viable, biocompatible delivery mechanism for targeting joint regions, in the treatment of a series of diseases with high collagen disorders such as osteoarthritis, rheumatoid arthritis and Marfan syndrome.[19, 37-40]

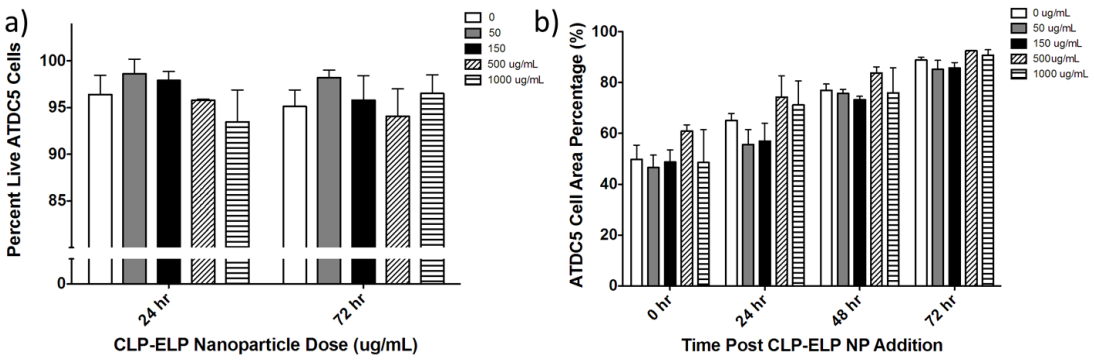


Figure 4.7 Quantitative analysis of ATDC5 viability and proliferation following application of ELP-CLP nanoparticles in vitro. a) ATDC5 cell viability (% live cells) and b) cell proliferation (cell area fraction) following application of 0, 50, 150, 500, and 1000 µg/mL of ELP-CLP nanoparticles. Cell viability and proliferation is unaltered by application of ELP-CLP nanoparticles at any concentration. Results are presented as mean ± SD (n = 3-5 /timepoint/concentration).

## 4.4 Conclusions

In our previous work,[33] an ELP-CLP diblock bioconjugate was synthesized via CuAAC click reaction. The resulting ELP-CLP conjugate exhibited a remarkable reduction in the inverse transition temperature of the ELP domain, attributed to the formation of the CLP triple helix. The diblock self-assembled into well-defined nanovesicles at physiological temperature and the nanoparticles were observed to dissociate at *elevated* temperatures, likely triggered by the unfolding of the CLP domain. In this work, to assess the potential of utilizing the ELP-CLP nanoparticles as drug delivery vehicles targeting collagen containing matrices, fluorescein, as a modelled drug, was encapsulated into the nanoparticles and a sustained release of clinically relevant amount of cargo was observed within a period of 3 weeks. As expected, a burst release was also observed, likely triggered by the dissociation of the vehicles at higher temperatures. Nanoparticle retention experiments conducted on type

II collagen film suggested high binding affinity with native collagens, due to the strand invasion ability of the partially unfolded CLP domain. By measuring cell viability and proliferation *in vitro*, these ELP-CLP nanoparticles found to be cytocompatible with both NIH-3T3 fibroblasts and ATDC5 chondrocytes. Additionally, almost no TNF- α expression was observed from macrophages incubated with the nanoparticles, suggesting that the ELP-CLP nanoparticles were non-inflammatory responsive. Endowed with collagen targeting ability, thermoresposiveness, cytocompatibility, and non-immune responsiveness, we believe the ELP-CLP nanoparticles are promising candidates as drug delivery vehicles for targeting collagen containing matrices.

## 4.5 Supporting Information

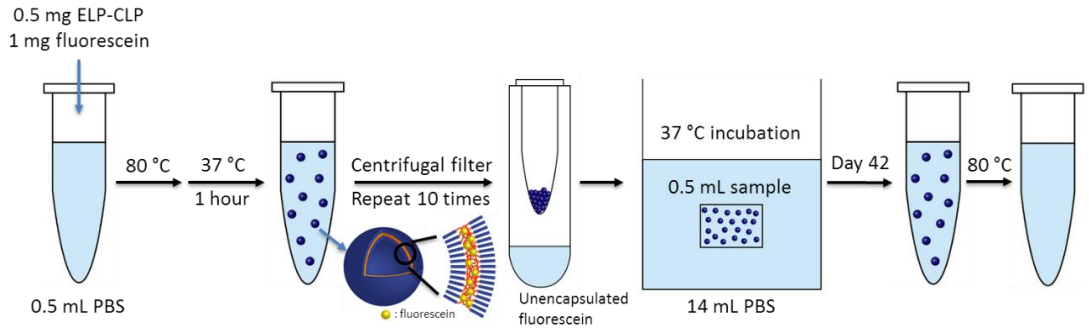


Figure 4.8 Schematic illustration of fluorescein loading and releasing from the ELP-CLP nanoparticles.

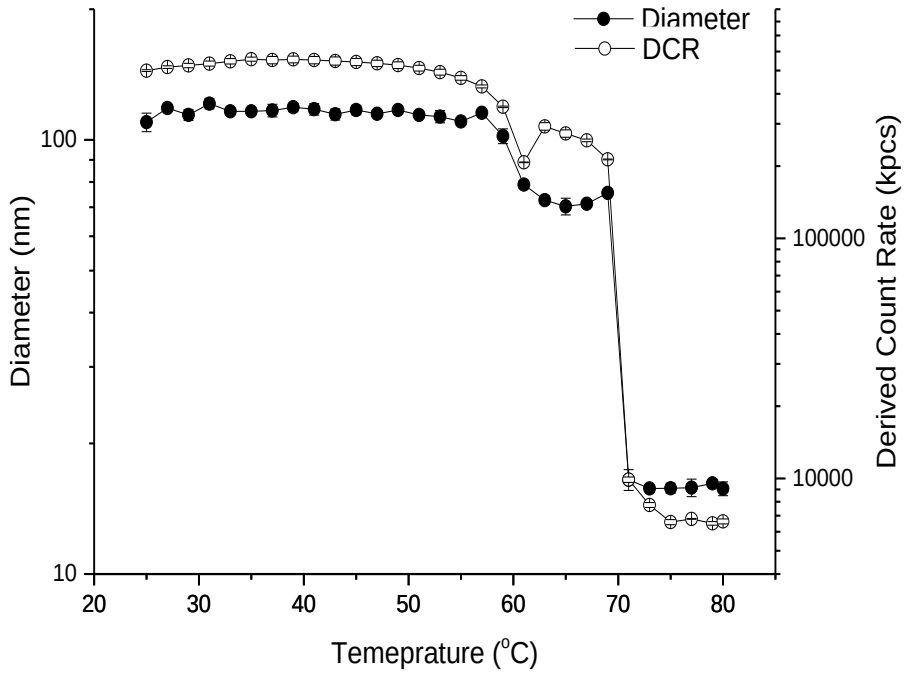


Figure 4.9 Dynamic light scattering characterization of the assembly of fluorescein labelled ELP−CLP conjugates. Hydrodynamic diameter of nanostructures (solid spheres) and derived count rate of the scattering light (hollow spheres) were plotted as a function of temperature upon heating.

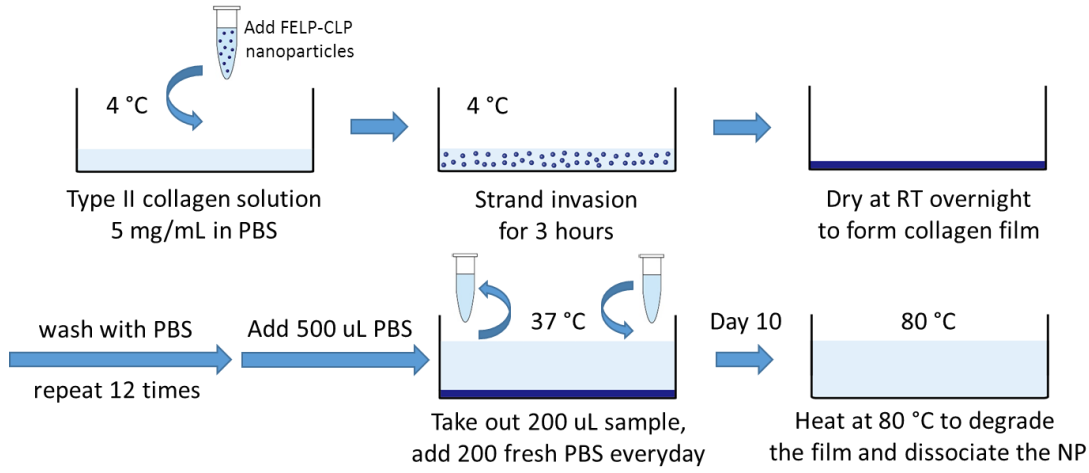


Figure 4.10 Schematic illustration of ELP-CLP nanoparticle retention experiment on type II collagen films.

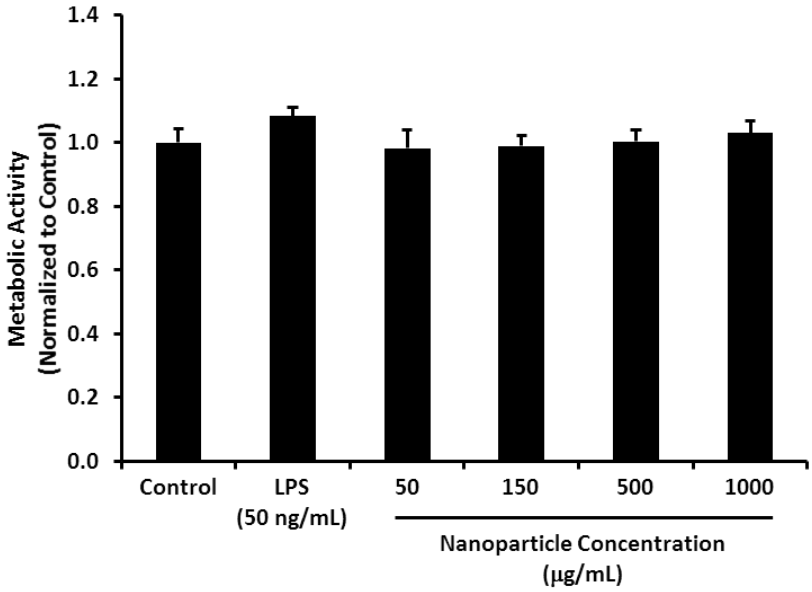


Figure 4.11 Normalized metabolic activity of RAW264.7 macrophages cultured with ELP-CLP nanoparticles at various concentrations, calculated via fluorescence measurement of the overall reductive capability of the cells. The data was normalized with the results from cells in culture medium without the nanoparticles. Each set of data represents the mean ± standard deviation for a total of at least three separately prepared samples.

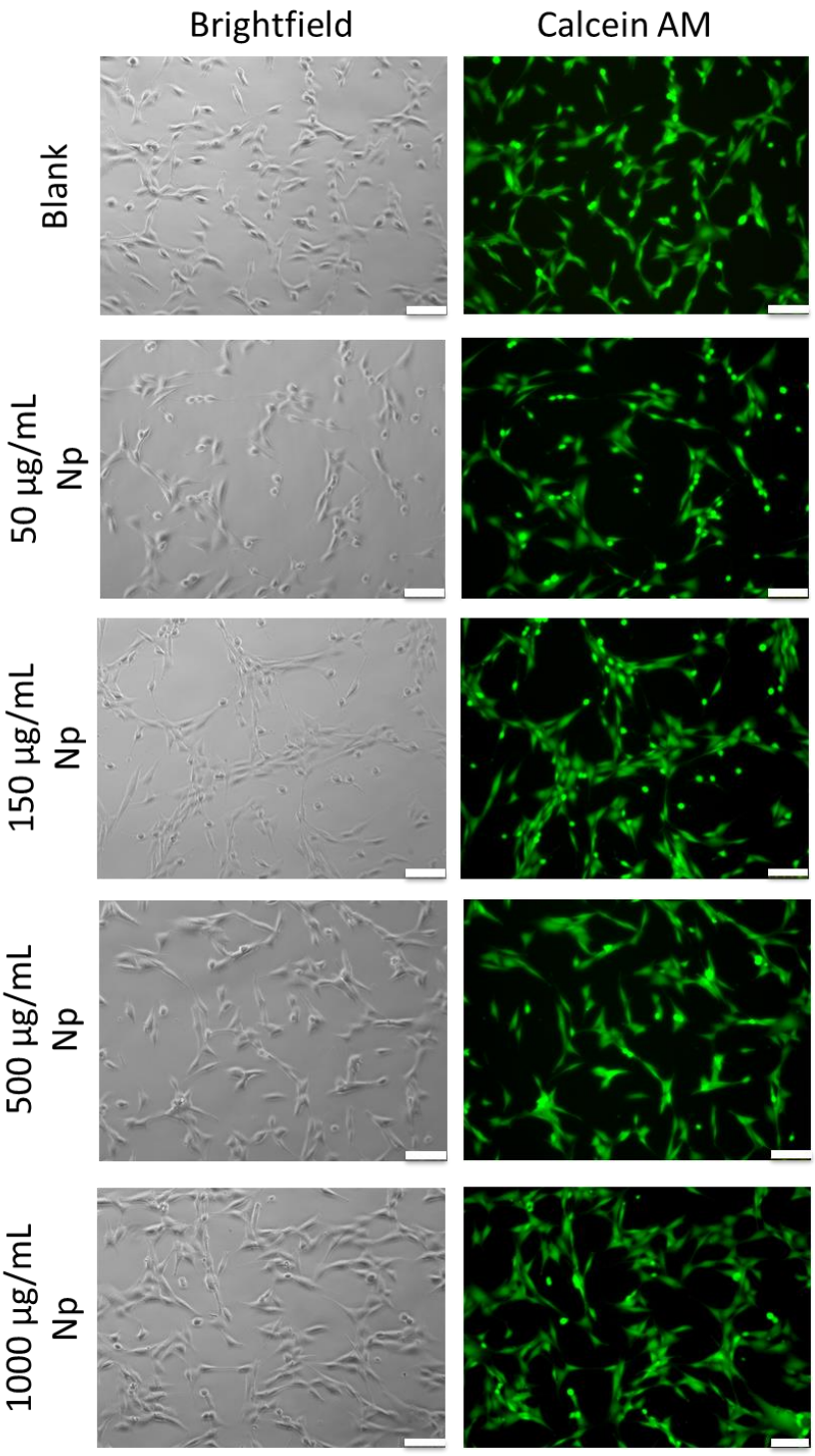


Figure 4.12 NIH-3T3 fibroblast viability after 24-hour incubation with the ELP-CLP nanoparticles. All images are with a 10x objective. Scale bars = 100 µm.

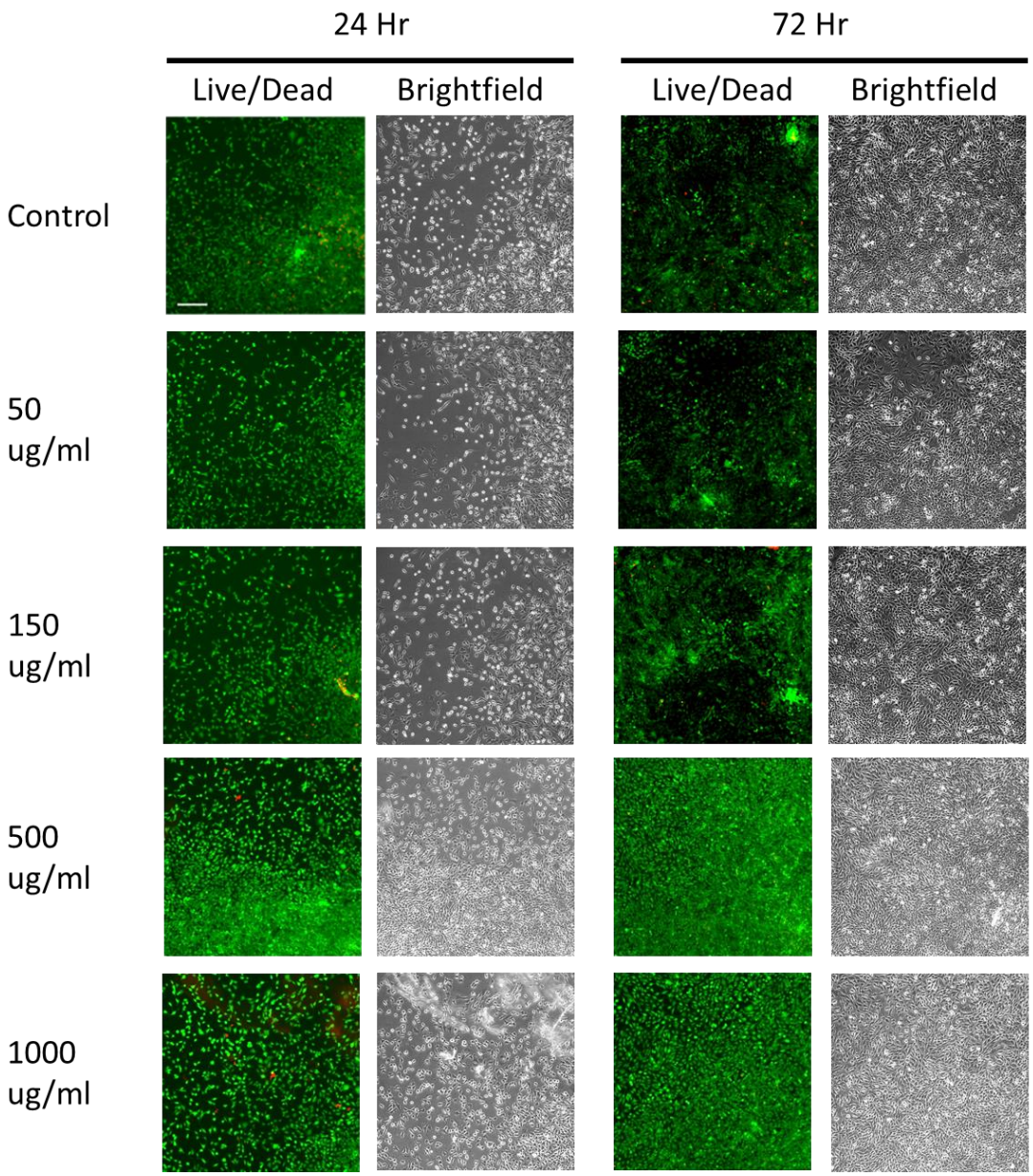


Figure 4.13 ADTC5 viability and proliferation in the presence of ELP-CLP nanoparticles in vitro. Representative images of ATDC5 cell viability via live (green fluorescence)/dead (red fluorescence) assay and proliferation (differential interference contrast microscopy) at 24 hour and 72 hours post- ELP-CLP nanoparticles. Application of ELP-CLP nanoparticles does not appear to cause ATDC5 death or change in cell proliferation. Scale bar = 200 µm and applies to all images.

## REFERENCES


1. K.E. Kadler, C. Baldock, J. Bella, R.P. Boot-Handford, Collagens at a glance. *J. Cell Sci.* **2007,** *120* (12), 1955-1958.

2. G.N. Ramachandran, G. Kartha, STRUCTURE OF COLLAGEN. *Nature* **1955,** *176* (4482), 593-595.

3. T.Z. Luo, K.L. Kiick, Collagen-like peptides and peptide-polymer conjugates in the design of assembled materials. *Eur. Polym. J.* **2013,** *49* (10), 2998-3009.

4. S.M. Yu, Y. Li, D. Kim, Collagen mimetic peptides: progress towards functional applications. *Soft Matter* **2011,** *7* (18), 7927-7938.

5. M.D. Shoulders, R.T. Raines, Collagen Structure and Stability. In *Annu. Rev. Biochem.*, Annual Reviews: Palo Alto, 2009; Vol. 78, pp 929-958.

6. J.A. Fallas, J.H. Dong, Y.Z.J. Tao, J.D. Hartgerink, Structural Insights into Charge Pair Interactions in Triple Helical Collagen-like Proteins. *J. Biol. Chem.* **2012,** *287* (11), 8039-8047.

7. A.V. Persikov, J.A.M. Ramshaw, B. Brodsky, Prediction of collagen stability from amino acid sequence. *J. Biol. Chem.* **2005,** *280* (19), 19343-19349.

8. S.P. Boudko, J. Engel, Structure formation in the C terminus of type III collagen guides disulfide cross-linking. *J. Mol. Biol.* **2004,** *335* (5), 1289-1297.

9. D. Barth, O. Kyrieleis, S. Frank, C. Renner, L. Moroder, The role of cystine knots in collagen folding and stability, part II. Conformational properties of (Pro-Hyp-Gly)(n) model trimers with N- and C-terminal collagen type III cystine knots. *Chem-Eur J* **2003,** *9* (15), 3703-3714.

10. W. Yang, V.C. Chan, A. Kirkpatrick, J.A.M. Ramshaw, B. Brodsky, Gly-Pro-Arg confers stability similar to Gly-Pro-Hyp in the collagen triple-helix of host-guest peptides. *J. Biol. Chem.* **1997,** *272* (46), 28837-28840.

11. M.M. Pires, J. Lee, D. Ernenwein, J. Chmielewski, Controlling the Morphology of Metal-Promoted Higher Ordered Assemblies of Collagen Peptides with Varied Core Lengths. *Langmuir* **2012,** *28* (4), 1993-1997.

12. M.M. Pires, D.E. Przybyla, C.M.R. Perez, J. Chmielewski, Metal-Mediated Tandem Coassembly of Collagen Peptides into Banded Microstructures. *J Am Chem Soc* **2011,** *133* (37), 14469-14471.

13. L.E.R. O'Leary, J.A. Fallas, E.L. Bakota, M.K. Kang, J.D. Hartgerink, Multi-hierarchical self-assembly of a collagen mimetic peptide from triple helix to nanofibre and hydrogel. *Nat. Chem.* **2011,** *3* (10), 821-828.

14. D.E. Przybyla, J. Chmielewski, Metal-triggered radial self-assembly of collagen peptide fibers. *J Am Chem Soc* **2008,** *130* (38), 12610-+.

15. O.D. Krishna, K.L. Kiick, Supramolecular Assembly of Electrostatically Stabilized, Hydroxyproline-Lacking Collagen-Mimetic Peptides. *Biomacromolecules* **2009,** *10* (9), 2626-2631.

16. A.Y. Wang, X. Mo, C.S. Chen, S.M. Yu, Facile modification of collagen directed by collagen mimetic peptides. *J Am Chem Soc* **2005,** *127* (12), 4130-4131.

17. Y. Li, D. Ho, H. Meng, T.R. Chan, B. An, H. Yu, B. Brodsky, A.S. Jun, S.M. Yu, Direct Detection of Collagenous Proteins by Fluorescently Labeled Collagen Mimetic Peptides. *Bioconjugate Chem.* **2013,** *24* (1), 9-16.

18. A.Y. Wang, C.A. Foss, S. Leong, X. Mo, M.G. Pomper, S.M. Yu, Spatio-temporal modification of collagen scaffolds mediated by triple helical propensity. *Biomacromolecules* **2008,** *9* (7), 1755-1763.

19. Y. Li, C.A. Foss, D.D. Summerfield, J.J. Doyle, C.M. Torok, H.C. Dietz, M.G. Pomper, S.M. Yu, Targeting collagen strands by photo-triggered triple-helix hybridization. *P Natl Acad Sci USA* **2012,** *109* (37), 14767-14772.

20. J.N. Luo, Y.W. Tong, Self-Assembly of Collagen-Mimetic Peptide Amphiphiles into Biofunctional Nanofiber. *Acs Nano* **2011,** *5* (10), 7739-7747.

21. O.D. Krishna, K.T. Wiss, T.Z. Luo, D.J. Pochan, P. Theato, K.L. Kiick, Morphological transformations in a dually thermoresponsive coil-rod-coil bioconjugate. *Soft Matter* **2012,** *8* (14), 3832-3840.

22. J.A. Foster, E. Bruenger, W.R. Gray, L.B. Sandberg, ISOLATION AND AMINO-ACID SEQUENCES OF TROPOELASTIN PEPTIDES. *J. Biol. Chem.* **1973,** *248* (8), 2876-2879.

23. L. Martin, E. Castro, A. Ribeiro, M. Alonso, J.C. Rodriguez-Cabello, Temperature-Triggered Self-Assembly of Elastin-Like Block Co-Recombinamers: The Controlled Formation of Micelles and Vesicles in an Aqueous Medium. *Biomacromolecules* **2012,** *13* (2), 293-298.

24. W.M. Park, J.A. Champion, Thermally Triggered Self-Assembly of Folded Proteins into Vesicles. *J Am Chem Soc* **2014,** *136* (52), 17906-17909.

25. C. Garcia-Arevalo, J.F. Bermejo-Martin, L. Rico, V. Iglesias, L. Martin, J.C. Rodriguez-Cabello, F.J. Arias, Immunomodulatory Nanoparticles from Elastin-Like Recombinamers: Single-Molecules for Tuberculosis Vaccine Development. *Mol. Pharm.* **2013,** *10* (2), 586-597.

26. Y. Fujita, M. Mie, E. Kobatake, Construction of nanoscale protein particle using temperature-sensitive elastin-like peptide and polyaspartic acid chain. *Biomaterials* **2009,** *30* (20), 3450-3457.

27. P. Shi, J.A. Gustafson, J.A. MacKay, Genetically engineered nanocarriers for drug delivery. *Int. J. Nanomed.* **2014,** *9*, 1617-1626.

28. D.J. Callahan, W.E. Liu, X.H. Li, M.R. Dreher, W. Hassouneh, M. Kim, P. Marszalek, A. Chilkoti, Triple Stimulus-Responsive Polypeptide Nanoparticles That Enhance Intratumoral Spatial Distribution. *Nano Lett.* **2012,** *12* (4), 2165-2170.

29. M.R. Dreher, A.J. Simnick, K. Fischer, R.J. Smith, A. Patel, M. Schmidt, A. Chilkoti, Temperature triggered self-assembly of polypeptides into multivalent spherical micelles. *J Am Chem Soc* **2008,** *130* (2), 687-694.

30. J.R. McDaniel, D.C. Radford, A. Chilkoti, A Unified Model for De Novo Design of Elastin-like Polypeptides with Tunable Inverse Transition Temperatures. *Biomacromolecules* **2013,** *14* (8), 2866-2872.

31. H. Nuhn, H.A. Klok, Secondary Structure Formation and LCST Behavior of Short Elastin-Like Peptides. *Biomacromolecules* **2008,** *9* (10), 2755-2763.

32. M.B. van Eldijk, J.C.Y. Wang, I.J. Minten, C.L. Li, A. Zlotnick, R.J.M. Nolte, J. Cornelissen, J.C.M. van Hest, Designing Two Self-Assembly Mechanisms into One Viral Capsid Protein. *J Am Chem Soc* **2012,** *134* (45), 18506-18509.

33. T.Z. Luo, K.L. Kiick, Noncovalent Modulation of the Inverse Temperature Transition and Self-Assembly of Elastin-b-Collagen-like Peptide Bioconjugates. *J Am Chem Soc* **2015,** *137* (49), 15362-15365.

34. M. Sameni, J. Dosescu, K.M. Yamada, B.F. Sloane, D. Cavallo-Medved, Functional Live-Cell Imaging Demonstrates that beta(1)-Integrin Promotes Type IV Collagen Degradation by Breast and Prostate Cancer Cells. *Mol. Imaging* **2008,** *7* (5), 199-213.

35. H.E. Jin, R. Farr, S.W. Lee, Collagen mimetic peptide engineered M13 bacteriophage for collagen targeting and imaging in cancer. *Biomaterials* **2014,** *35* (33), 9236-9245.

36. T.A. Ngobili, H. Shah, J.P. Park, K.W. Kwist, B. Inskeep, K.J.L. Burg, B.W. Booth, Remodeling of Tannic Acid Cross linked Collagen Type I Induces Apoptosis in ER+ Breast Cancer Cells. *Anticancer Res.* **2015,** *35* (3), 1285-1290.

37. M.J. Rowley, D.J. Williamson, I.R. Mackay, EVIDENCE FOR LOCAL SYNTHESIS OF ANTIBODIES TO DENATURED COLLAGEN IN THE SYNOVIUM IN RHEUMATOID-ARTHRITIS. *Arthritis Rheum.* **1987,** *30* (12), 1420-1425.

38. G.R. Dodge, I. Pidoux, A.R. Poole, THE DEGRADATION OF TYPE-II COLLAGEN IN RHEUMATOID-ARTHRITIS - AN IMMUNOELECTRON MICROSCOPIC STUDY. *Matrix* **1991,** *11* (5), 330-338.

39. P.E. Van Den Steen, P. Proost, B. Grillet, D.D. Brand, A.H. Kang, J. Van Damme, G. Opdenakker, Cleavage of denatured natural collagen type II by neutrophil gelatinase B reveals enzyme specificity, post-translational modifications in the substrate, and the formation of remnant epitopes in rheumatoid arthritis. *Faseb J.* **2002,** *16* (3), 11.

40. J.H.N. Lindeman, B.A. Ashcroft, J.W.M. Beenakker, M. van Es, N.B.R. Koekkoek, F.A. Prins, J.F. Tielemans, H. Abdul-Hussien, R.A. Bank, T.H. Oosterkamp, Distinct defects in collagen microarchitecture underlie vessel-wall failure in advanced abdominal aneurysms and aneurysms in Marfan syndrome. *P Natl Acad Sci USA* **2010,** *107* (2), 862-865.

41. N.V. Kuznetsova, D.J. McBride, S. Leikin, Changes in thermal stability and microunfolding pattern of collagen helix resulting from the loss of alpha 2(I) chain in osteogenesis imperfecta murine. *J. Mol. Biol.* **2003,** *331* (1), 191-200.

42. S. Busschots, S. O'Toole, J.J. O'Leary, B. Stordal, Non-invasive and non-destructive measurements of confluence in cultured adherent cell lines. *MethodsX* **2015,** *2*, 8-13.

43. R. Iurie, Cell drug delivery of fluorescein loaded ApoB100 functionalized liposomes. *Biointerface Res. Appl. Chem.* **2015,** *5* (6), 1007-1010.

44. X.C. Chen, H.M. Chen, C. Tripisciano, A. Jedrzejewska, M.H. Rummeli, R. Klingeler, R.J. Kalenczuk, P.K. Chu, E. Borowiak-Palen, Carbon-Nanotube-Based Stimuli-Responsive Controlled-Release System. *Chem-Eur J* **2011,** *17* (16), 4454-4459.

45. B.S. Bleier, D. Preena, R.J. Schlosser, R.J. Harvey, Dose quantification of topical drug delivery to the paranasal sinuses by fluorescein luminosity calculation. *Int. Forum Allergy Rhinol.* **2012,** *2* (4), 316-320.

46. S.T. Ku, F. Yan, Y. Wang, Y.L. Sun, N. Yang, L. Ye, The blood-brain barrier penetration and distribution of PEGylated fluorescein-doped magnetic silica nanoparticles in rat brain. *Biochem. Biophys. Res. Commun.* **2010,** *394* (4), 871-876.

47. H. Park, H. Tsutsumi, H. Mihara, Cell-selective intracellular drug delivery using doxorubicin and alpha-helical peptides conjugated to gold nanoparticles. *Biomaterials* **2014,** *35* (10), 3480-3487.

48. C. Muller, G. Perera, V. Konig, A. Bernkop-Schnurch, Development and in vivo evaluation of papain-functionalized nanoparticles. *Eur. J. Pharm. Biopharm.* **2014,** *87* (1), 125-131.

49. T.Z. Luo, L.R. He, P. Theato, K.L. Kiick, Thermoresponsive Self-Assembly of Nanostructures from a Collagen-Like Peptide-Containing Diblock Copolymer. *Macromol. Biosci.* **2015,** *15* (1), 111-123.

50. A.R. Johnson, A.G. Pavlovsky, D.F. Ortwine, F. Prior, C.F. Man, D.A. Bornemeier, C.A. Banotai, W.T. Mueller, P. McConnell, C. Yan, V. Baragi, C. Lesch, W.H. Roark, M. Wilson, K. Datta, R. Guzman, H.K. Han, R.D. Dyer, Discovery and characterization of a novel inhibitor of matrix metalloprotease-13 that reduces cartilage damage in vivo without joint fibroplasia side effects. *J. Biol. Chem.* **2007,** *282* (38), 27781-27791.

51. M.P.H. Le Graverand-Gastineau, Disease Modifying Osteoarthritis Drugs: Facing Development Challenges and Choosing Molecular Targets. *Curr. Drug Targets* **2010,** *11* (5), 528-535.

52. M. Sabatini, C. Lesur, M. Thomas, A. Chomel, P. Anract, G. de Nanteuil, P. Pastoureau, Effect of inhibition of matrix metalloproteinases on cartilage loss in vitro and in a guinea pig model of osteoarthritis. *Arthritis Rheum.* **2005,** *52* (1), 171-180.

53. Z. Sheikh, P. Brooks, O. Barzilay, N. Fine, M. Glogauer, Macrophages, Foreign Body Giant Cells and Their Response to Implantable Biomaterials. *Materials* **2015,** *8* (9), 5269.

54. X. Zhidao, T.T. James, A review on macrophage responses to biomaterials. *Biomedical Materials* **2006,** *1* (1), R1.

55. A.M. Kosinski, J.L. Brugnano, B.L. Seal, F.C. Knight, A. Panitch, Synthesis and characterization of a poly(lactic-co-glycolic acid) core + poly(N-isopropylacrylamide) shell nanoparticle system. *Biomatter* **2012,** *2* (4), 195-201.

56. A.C. Rincón, I.T. Molina-Martinez, B. de las Heras, M. Alonso, C. Baílez, J.C. Rodríguez-Cabello, R. Herrero-Vanrell, Biocompatibility of elastin-like polymer poly(VPAVG) microparticles: in vitro and in vivo studies. *Journal of Biomedical Materials Research Part A* **2006,** *78A* (2), 343-351.

57. Y.-N. Zhang, R.K. Avery, Q. Vallmajo-Martin, A. Assmann, A. Vegh, A. Memic, B.D. Olsen, N. Annabi, A. Khademhosseini, A Highly Elastic and Rapidly Crosslinkable Elastin-Like Polypeptide-Based Hydrogel for Biomedical Applications. *Advanced functional materials* **2015,** *25* (30), 4814-4826.

58. M. Theiszova, S. Jantova, J. Dragunova, P. Grznarova, M. Palou, Comparison the cytotoxicity of hydroxyapatite measured by direct cell counting and MTT test in murine fibroblast NIH-3T3 cells. *Biomedical Papers (Olomouc)* **2005,** *149* (2), 393-396.

59. T. Yeung, P.C. Georges, L.A. Flanagan, B. Marg, M. Ortiz, M. Funaki, N. Zahir, W.Y. Ming, V. Weaver, P.A. Janmey, Effects of substrate stiffness on cell morphology, cytoskeletal structure, and adhesion. *Cell Motil. Cytoskeleton* **2005,** *60* (1), 24-34.

60. X.Z. Shu, K. Ghosh, Y.C. Liu, F.S. Palumbo, Y. Luo, R.A. Clark, G.D. Prestwich, Attachment and spreading of fibroblasts on an RGD peptide-modified injectable hyaluronan hydrogel. *J. Biomed. Mater. Res. Part A* **2004,** *68A* (2), 365-375.

61. S.R. Ryoo, Y.K. Kim, M.H. Kim, D.H. Min, Behaviors of NIH-3T3 Fibroblasts on Graphene/Carbon Nanotubes: Proliferation, Focal Adhesion, and Gene Transfection Studies. *Acs Nano* **2010,** *4* (11), 6587-6598.

62. C.M. Goodman, C.D. McCusker, T. Yilmaz, V.M. Rotello, Toxicity of gold nanoparticles functionalized with cationic and anionic side chains. *Bioconjugate Chem.* **2004,** *15* (4), 897-900.

63. C. Lherm, R.H. Muller, F. Puisieux, P. Couvreur, ALKYLCYANOACRYLATE DRUG CARRIERS .2. CYTOTOXICITY OF CYANOACRYLATE NANOPARTICLES WITH DIFFERENT ALKYL CHAIN-LENGTH. *Int. J. Pharm.* **1992,** *84* (1), 13-22.

64. D. Fischer, Y.X. Li, B. Ahlemeyer, J. Krieglstein, T. Kissel, In vitro cytotoxicity testing of polycations: influence of polymer structure on cell viability and hemolysis. *Biomaterials* **2003,** *24* (7), 1121-1131.

65. P.V. AshaRani, G.L.K. Mun, M.P. Hande, S. Valiyaveettil, Cytotoxicity and Genotoxicity of Silver Nanoparticles in Human Cells. *Acs Nano* **2009,** *3* (2), 279-290.

66. Y.H. Lee, F.Y. Cheng, H.W. Chiu, J.C. Tsai, C.Y. Fang, C.W. Chen, Y.J. Wang, Cytotoxicity, oxidative stress, apoptosis and the autophagic effects of silver nanoparticles in mouse embryonic fibroblasts. *Biomaterials* **2014,** *35* (16), 4706-4715.

67. Y. Pan, S. Neuss, A. Leifert, M. Fischler, F. Wen, U. Simon, G. Schmid, W. Brandau, W. Jahnen-Dechent, Size-dependent cytotoxicity of gold nanoparticles. *Small* **2007,** *3* (11), 1941-1949.

68. H.K. Patra, S. Banerjee, U. Chaudhuri, P. Lahiri, A.K. Dasgupta, Cell selective response to gold nanoparticles. *Nanomed.-Nanotechnol. Biol. Med.* **2007,** *3* (2), 111-119.

69. Y.C. Yao, Y.J. Wang, ATDC5: An excellent in vitro model cell line for skeletal development. *J. Cell. Biochem.* **2013,** *114* (6), 1223-1229.

# Chapter 5

# CONCLUSIONS

In this work, a new class of thermoresponsive diblock conjugates, containing collagen-like peptides and a thermoresponsive polymer, namely poly(diethylene glycol methyl ether methacrylate) (PDEGMEMA), is introduced. The CLP domain maintains its triple helix conformation after conjugation with the polymer. The engineered LCST of these conjugates has enabled temperature-induced assembly under aqueous conditions, at physiologically relevant temperatures, into well-defined vesicles with diameters of approximately 50-200 nm. The formation of nanostructures was driven by the coil/globule conformational transition of the PDEGMEMA building block above its LCST with stabilization of the nanostructures by the hydrophilic CLP. To the best of our knowledge, this is the first report on such assembled nanostructures from collagen-like peptide containing copolymers. Due to the strong propensity for CLPs to bind to natural collagen via strand invasion processes, these nanosized vesicles may be used as drug carriers for targeted delivery.

In addition to synthetic polymers, the collagen like peptide is also conjugated with a thermoresponsive elastin-like peptide (ELP). The resulting ELP-CLP diblock conjugates show a remarkable reduction in the inverse transition temperature of the ELP domain, attributed to the anchoring effect of the CLP triple helix. The lower transition temperature of the conjugate enables facile formation of well-defined vesicles at physiological temperature and the unexpected resolubilization of the vesicles at *elevated* temperatures upon unfolding of the CLP domain. Given the

demonstrated ability of CLPs to modify collagens, this work provides not only a simple and versatile avenue for controlling the inverse transition behavior of elastin-like peptides, but also suggest future opportunities for these thermoresponsive nanostructures in biologically relevant environments.

The potential of using the ELP-CLP nanoparticles as drug delivery vehicles for targeting collagen containing matrices is then evaluated. A sustained release of clinically relevant amount of encapsulated modelled drug is achieved within three weeks, followed by a thermally controlled burst release. As expected, the ELP-CLP nanoparticles show strong retention on collagen substrate, via specific binding through collagen triple helix hybridization. Additionally, cell viability and proliferation studies using fibroblasts and chondrocytes suggest the nanoparticles are non-cytotoxic. Additionally, almost no TNF-α expression from macrophages is observed, suggesting that the nanoparticles do not initiate inflammatory response. Endowed with specific collagen binding, controlled thermoresposiveness, excellent cytocompatibility, and non-immune responsiveness, we believe the ELP-CLP nanoparticles are promising candidates as drug delivery vehicles for targeting collagen containing matrices.

Considering the critical role of collagens in extracellular matrix and the unique ability of the CLP to target native collagens, our work offers significant opportunities for the design of collagen-like peptides and their bioconjugates for targeted drug delivery application in the biomedical arena.

# Appendix A

# PERMISSION LETTERS

## A.1 Elsevier License Terms and Conditions

Oct 21, 2016

---

---

This Agreement between Tianzhi Luo ("You") and Elsevier ("Elsevier") consists of your license details and the terms and conditions provided by Elsevier and Copyright Clearance Center.

| | |
|---|---|
| License Number | 3973860021378 |
| License date | Oct 21, 2016 |
| Licensed Content Publisher | Elsevier |
| Licensed Content Publication | European Polymer Journal |
| Licensed Content Title | Collagen-like peptides and peptide–polymer conjugates in the design of assembled materials |
| Licensed Content Author | Tianzhi Luo,Kristi L. Kiick |
| Licensed Content Date | October 2013 |
| Licensed Content Volume Number | 49 |
| Licensed Content Issue Number | 10 |
| Licensed Content Pages | 12 |
| Start Page | 2998 |
| End Page | 3009 |
| Type of Use | reuse in a thesis/dissertation |
| Portion | full article |
| Format | both print and electronic |
| Are you the author of this | Yes |

| | |
|---|---|
| Elsevier article? | |
| Will you be translating? | No |
| Order reference number | |
| Title of your thesis/dissertation | Collagen Like Peptide Bioconjugates for Targeted Drug Delivery Applications |
| Expected completion date | Oct 2016 |
| Estimated size (number of pages) | 200 |
| Elsevier VAT number | GB 494 6272 12 |
| Requestor Location | Tianzhi Luo<br>201 Dupont Hall<br>University of Delaware<br><br>Newark, DE 19716<br>United States<br>Attn: Tianzhi Luo |
| Total | 0.00 USD |
| Terms and Conditions | |

## INTRODUCTION

1. The publisher for this copyrighted material is Elsevier. By clicking "accept" in connection with completing this licensing transaction, you agree that the following terms and conditions apply to this transaction (along with the Billing and Payment terms and conditions established by Copyright Clearance Center, Inc. ("CCC"), at the time that you opened your Rightslink account and that are available at any time at http://myaccount.copyright.com).

## GENERAL TERMS

2. Elsevier hereby grants you permission to reproduce the aforementioned material subject to the terms and conditions indicated.
3. Acknowledgement: If any part of the material to be used (for example, figures) has appeared in our publication with credit or acknowledgement to another source, permission must also be sought from that source. If such permission is not obtained then that material may not be included in your publication/copies. Suitable acknowledgement to the source must be made, either as a footnote or in a reference list at the end of your publication, as follows:
"Reprinted from Publication title, Vol /edition number, Author(s), Title of article / title of chapter, Pages No., Copyright (Year), with permission from Elsevier [OR APPLICABLE SOCIETY COPYRIGHT OWNER]." Also Lancet special credit - "Reprinted from The Lancet, Vol. number, Author(s), Title of article, Pages No., Copyright (Year), with permission from Elsevier."
4. Reproduction of this material is confined to the purpose and/or media for which permission is hereby given.

5. Altering/Modifying Material: Not Permitted. However figures and illustrations may be altered/adapted minimally to serve your work. Any other abbreviations, additions, deletions and/or any other alterations shall be made only with prior written authorization of Elsevier Ltd. (Please contact Elsevier at permissions@elsevier.com)
6. If the permission fee for the requested use of our material is waived in this instance, please be advised that your future requests for Elsevier materials may attract a fee.
7. Reservation of Rights: Publisher reserves all rights not specifically granted in the combination of (i) the license details provided by you and accepted in the course of this licensing transaction, (ii) these terms and conditions and (iii) CCC's Billing and Payment terms and conditions.
8. License Contingent Upon Payment: While you may exercise the rights licensed immediately upon issuance of the license at the end of the licensing process for the transaction, provided that you have disclosed complete and accurate details of your proposed use, no license is finally effective unless and until full payment is received from you (either by publisher or by CCC) as provided in CCC's Billing and Payment terms and conditions. If full payment is not received on a timely basis, then any license preliminarily granted shall be deemed automatically revoked and shall be void as if never granted. Further, in the event that you breach any of these terms and conditions or any of CCC's Billing and Payment terms and conditions, the license is automatically revoked and shall be void as if never granted. Use of materials as described in a revoked license, as well as any use of the materials beyond the scope of an unrevoked license, may constitute copyright infringement and publisher reserves the right to take any and all action to protect its copyright in the materials.
9. Warranties: Publisher makes no representations or warranties with respect to the licensed material.
10. Indemnity: You hereby indemnify and agree to hold harmless publisher and CCC, and their respective officers, directors, employees and agents, from and against any and all claims arising out of your use of the licensed material other than as specifically authorized pursuant to this license.
11. No Transfer of License: This license is personal to you and may not be sublicensed, assigned, or transferred by you to any other person without publisher's written permission.
12. No Amendment Except in Writing: This license may not be amended except in a writing signed by both parties (or, in the case of publisher, by CCC on publisher's behalf).
13. Objection to Contrary Terms: Publisher hereby objects to any terms contained in any purchase order, acknowledgment, check endorsement or other writing prepared by you, which terms are inconsistent with these terms and conditions or CCC's Billing and Payment terms and conditions. These terms and conditions,

together with CCC's Billing and Payment terms and conditions (which are incorporated herein), comprise the entire agreement between you and publisher (and CCC) concerning this licensing transaction. In the event of any conflict between your obligations established by these terms and conditions and those established by CCC's Billing and Payment terms and conditions, these terms and conditions shall control.

14. Revocation: Elsevier or Copyright Clearance Center may deny the permissions described in this License at their sole discretion, for any reason or no reason, with a full refund payable to you. Notice of such denial will be made using the contact information provided by you. Failure to receive such notice will not alter or invalidate the denial. In no event will Elsevier or Copyright Clearance Center be responsible or liable for any costs, expenses or damage incurred by you as a result of a denial of your permission request, other than a refund of the amount(s) paid by you to Elsevier and/or Copyright Clearance Center for denied permissions.

**LIMITED LICENSE**

The following terms and conditions apply only to specific license types:

15. **Translation**: This permission is granted for non-exclusive world **English** rights only unless your license was granted for translation rights. If you licensed translation rights you may only translate this content into the languages you requested. A professional translator must perform all translations and reproduce the content word for word preserving the integrity of the article.

16. **Posting licensed content on any Website**: The following terms and conditions apply as follows: Licensing material from an Elsevier journal: All content posted to the web site must maintain the copyright information line on the bottom of each image; A hyper-text must be included to the Homepage of the journal from which you are licensing at http://www.sciencedirect.com/science/journal/xxxxx or the Elsevier homepage for books at http://www.elsevier.com; Central Storage: This license does not include permission for a scanned version of the material to be stored in a central repository such as that provided by Heron/XanEdu.

Licensing material from an Elsevier book: A hyper-text link must be included to the Elsevier homepage at http://www.elsevier.com . All content posted to the web site must maintain the copyright information line on the bottom of each image.

**Posting licensed content on Electronic reserve**: In addition to the above the following clauses are applicable: The web site must be password-protected and made available only to bona fide students registered on a relevant course. This permission is granted for 1 year only. You may obtain a new license for future website posting.

17. **For journal authors:** the following clauses are applicable in addition to the above:

**Preprints:**
A preprint is an author's own write-up of research results and analysis, it has not been peer-reviewed, nor has it had any other value added to it by a publisher (such as formatting, copyright, technical enhancement etc.).
Authors can share their preprints anywhere at any time. Preprints should not be added to or enhanced in any way in order to appear more like, or to substitute for, the final versions of articles however authors can update their preprints on arXiv or RePEc with their Accepted Author Manuscript (see below).
If accepted for publication, we encourage authors to link from the preprint to their formal publication via its DOI. Millions of researchers have access to the formal publications on ScienceDirect, and so links will help users to find, access, cite and use the best available version. Please note that Cell Press, The Lancet and some society-owned have different preprint policies. Information on these policies is available on the journal homepage.
**Accepted Author Manuscripts:** An accepted author manuscript is the manuscript of an article that has been accepted for publication and which typically includes author-incorporated changes suggested during submission, peer review and editor-author communications.
Authors can share their accepted author manuscript:

- – immediately
    - via their non-commercial person homepage or blog
    - by updating a preprint in arXiv or RePEc with the accepted manuscript
    - via their research institute or institutional repository for internal institutional uses or as part of an invitation-only research collaboration work-group
    - directly by providing copies to their students or to research collaborators for their personal use
    - for private scholarly sharing as part of an invitation-only work group on commercial sites with which Elsevier has an agreement
- – after the embargo period
    - via non-commercial hosting platforms such as their institutional repository
    - via commercial sites with which Elsevier has an agreement

In all cases accepted manuscripts should:

- – link to the formal publication via its DOI
- – bear a CC-BY-NC-ND license - this is easy to do
- – if aggregated with other manuscripts, for example in a repository or other site, be shared in alignment with our hosting policy not be added to or enhanced in any way to appear more like, or to substitute for, the

published journal article.

**Published journal article (JPA):** A published journal article (PJA) is the definitive final record of published research that appears or will appear in the journal and embodies all value-adding publishing activities including peer review co-ordination, copy-editing, formatting, (if relevant) pagination and online enrichment.

Policies for sharing publishing journal articles differ for subscription and gold open access articles:

**Subscription Articles:** If you are an author, please share a link to your article rather than the full-text. Millions of researchers have access to the formal publications on ScienceDirect, and so links will help your users to find, access, cite, and use the best available version.

Theses and dissertations which contain embedded PJAs as part of the formal submission can be posted publicly by the awarding institution with DOI links back to the formal publications on ScienceDirect.

If you are affiliated with a library that subscribes to ScienceDirect you have additional private sharing rights for others' research accessed under that agreement. This includes use for classroom teaching and internal training at the institution (including use in course packs and courseware programs), and inclusion of the article for grant funding purposes.

**Gold Open Access Articles:** May be shared according to the author-selected end-user license and should contain aCrossMark logo, the end user license, and a DOI link to the formal publication on ScienceDirect.

Please refer to Elsevier's posting policy for further information.

18. **For book authors** the following clauses are applicable in addition to the above: Authors are permitted to place a brief summary of their work online only. You are not allowed to download and post the published electronic version of your chapter, nor may you scan the printed edition to create an electronic version. **Posting to a repository:** Authors are permitted to post a summary of their chapter only in their institution's repository.

19. **Thesis/Dissertation**: If your license is for use in a thesis/dissertation your thesis may be submitted to your institution in either print or electronic form. Should your thesis be published commercially, please reapply for permission. These requirements include permission for the Library and Archives of Canada to supply single copies, on demand, of the complete thesis and include permission for Proquest/UMI to supply single copies, on demand, of the complete thesis. Should your thesis be published commercially, please reapply for permission. Theses and dissertations which contain embedded PJAs as part of the formal submission can be posted publicly by the awarding institution with DOI links back to the formal publications on ScienceDirect.

**Elsevier Open Access Terms and Conditions**

commercial reuse of Open Access articles published with a CC BY NC SA or CC BY NC ND license requires permission from Elsevier and will be subject to a fee. Commercial reuse includes:

- – Associating advertising with the full text of the Article
- – Charging fees for document delivery or access
- – Article aggregation
- – Systematic distribution via e-mail lists or share buttons

Posting or linking by commercial companies for use by customers of those companies.

20. **Other Conditions**:

v1.8

**Questions? customercare@copyright.com or +1-855-239-3415 (toll free in the US) or +1-978-646-2777.**

## A.2 John Wiley and Sons License Terms and Conditions

Oct 21, 2016

---

This Agreement between Tianzhi Luo ("You") and John Wiley and Sons ("John Wiley and Sons") consists of your license details and the terms and conditions provided by John Wiley and Sons and Copyright Clearance Center.

| | |
|---|---|
| License Number | 3973930396844 |
| License date | Oct 21, 2016 |
| Licensed Content Publisher | John Wiley and Sons |
| Licensed Content Publication | Macromolecular Bioscience |
| Licensed Content Title | Thermoresponsive Self-Assembly of Nanostructures from a Collagen-Like Peptide-Containing Diblock Copolymer |
| Licensed Content Author | Tianzhi Luo,Lirong He,Patrick Theato,Kristi L. Kiick |
| Licensed Content Date | Nov 13, 2014 |
| Licensed Content Pages | 13 |
| Type of use | Dissertation/Thesis |
| Requestor type | Author of this Wiley article |
| Format | Print and electronic |
| Portion | Full article |
| Will you be translating? | No |
| Title of your thesis / dissertation | Collagen Like Peptide Bioconjugates for Targeted Drug Delivery Applications |
| Expected completion date | Oct 2016 |
| Expected size (number of pages) | 200 |
| Requestor Location | Tianzhi Luo<br>201 Dupont Hall<br>University of Delaware<br><br>Newark, DE 19716<br>United States<br>Attn: Tianzhi Luo |
| Publisher Tax ID | EU826007151 |
| Billing Type | Invoice |

| | |
|---|---|
| Billing Address | Tianzhi Luo<br>201 Dupont Hall<br>University of Delaware<br><br>Newark, DE 19716<br>United States<br>Attn: Tianzhi Luo |
| Total | 0.00 USD |

Terms and Conditions

**TERMS AND CONDITIONS**

This copyrighted material is owned by or exclusively licensed to John Wiley & Sons, Inc. or one of its group companies (each a"Wiley Company") or handled on behalf of a society with which a Wiley Company has exclusive publishing rights in relation to a particular work (collectively "WILEY"). By clicking "accept" in connection with completing this licensing transaction, you agree that the following terms and conditions apply to this transaction (along with the billing and payment terms and conditions established by the Copyright Clearance Center Inc., ("CCC's Billing and Payment terms and conditions"), at the time that you opened your RightsLink account (these are available at any time at http://myaccount.copyright.com).

**Terms and Conditions**

- The materials you have requested permission to reproduce or reuse (the "Wiley Materials") are protected by copyright.

- You are hereby granted a personal, non-exclusive, non-sub licensable (on a stand-alone basis), non-transferable, worldwide, limited license to reproduce the Wiley Materials for the purpose specified in the licensing process. This license, **and any CONTENT (PDF or image file) purchased as part of your order,** is for a one-time use only and limited to any maximum distribution number specified in the license. The first instance of republication or reuse granted by this license must be completed within two years of the date of the grant of this license (although copies prepared before the end date may be distributed thereafter). The Wiley Materials shall not be used in any other manner or for any other purpose, beyond what is granted in the license. Permission is granted subject to an appropriate acknowledgement given to the author, title of the material/book/journal and the publisher. You shall also duplicate the copyright notice that appears in the Wiley publication in your use of the Wiley Material. Permission is also granted on the understanding that nowhere in the text is a previously published source acknowledged for all

or part of this Wiley Material. Any third party content is expressly excluded from this permission.

- With respect to the Wiley Materials, all rights are reserved. Except as expressly granted by the terms of the license, no part of the Wiley Materials may be copied, modified, adapted (except for minor reformatting required by the new Publication), translated, reproduced, transferred or distributed, in any form or by any means, and no derivative works may be made based on the Wiley Materials without the prior permission of the respective copyright owner.**For STM Signatory Publishers clearing permission under the terms of the STM Permissions Guidelines only, the terms of the license are extended to include subsequent editions and for editions in other languages, provided such editions are for the work as a whole in situ and does not involve the separate exploitation of the permitted figures or extracts,**You may not alter, remove or suppress in any manner any copyright, trademark or other notices displayed by the Wiley Materials. You may not license, rent, sell, loan, lease, pledge, offer as security, transfer or assign the Wiley Materials on a stand-alone basis, or any of the rights granted to you hereunder to any other person.

- The Wiley Materials and all of the intellectual property rights therein shall at all times remain the exclusive property of John Wiley & Sons Inc, the Wiley Companies, or their respective licensors, and your interest therein is only that of having possession of and the right to reproduce the Wiley Materials pursuant to Section 2 herein during the continuance of this Agreement. You agree that you own no right, title or interest in or to the Wiley Materials or any of the intellectual property rights therein. You shall have no rights hereunder other than the license as provided for above in Section 2. No right, license or interest to any trademark, trade name, service mark or other branding ("Marks") of WILEY or its licensors is granted hereunder, and you agree that you shall not assert any such right, license or interest with respect thereto

- NEITHER WILEY NOR ITS LICENSORS MAKES ANY WARRANTY OR REPRESENTATION OF ANY KIND TO YOU OR ANY THIRD PARTY, EXPRESS, IMPLIED OR STATUTORY, WITH RESPECT TO THE MATERIALS OR THE ACCURACY OF ANY INFORMATION CONTAINED IN THE MATERIALS, INCLUDING, WITHOUT LIMITATION, ANY IMPLIED WARRANTY OF MERCHANTABILITY, ACCURACY, SATISFACTORY QUALITY, FITNESS FOR A PARTICULAR PURPOSE, USABILITY, INTEGRATION OR NON-INFRINGEMENT AND ALL SUCH WARRANTIES

ARE HEREBY EXCLUDED BY WILEY AND ITS LICENSORS AND WAIVED BY YOU.

- WILEY shall have the right to terminate this Agreement immediately upon breach of this Agreement by you.

- You shall indemnify, defend and hold harmless WILEY, its Licensors and their respective directors, officers, agents and employees, from and against any actual or threatened claims, demands, causes of action or proceedings arising from any breach of this Agreement by you.

- IN NO EVENT SHALL WILEY OR ITS LICENSORS BE LIABLE TO YOU OR ANY OTHER PARTY OR ANY OTHER PERSON OR ENTITY FOR ANY SPECIAL, CONSEQUENTIAL, INCIDENTAL, INDIRECT, EXEMPLARY OR PUNITIVE DAMAGES, HOWEVER CAUSED, ARISING OUT OF OR IN CONNECTION WITH THE DOWNLOADING, PROVISIONING, VIEWING OR USE OF THE MATERIALS REGARDLESS OF THE FORM OF ACTION, WHETHER FOR BREACH OF CONTRACT, BREACH OF WARRANTY, TORT, NEGLIGENCE, INFRINGEMENT OR OTHERWISE (INCLUDING, WITHOUT LIMITATION, DAMAGES BASED ON LOSS OF PROFITS, DATA, FILES, USE, BUSINESS OPPORTUNITY OR CLAIMS OF THIRD PARTIES), AND WHETHER OR NOT THE PARTY HAS BEEN ADVISED OF THE POSSIBILITY OF SUCH DAMAGES. THIS LIMITATION SHALL APPLY NOTWITHSTANDING ANY FAILURE OF ESSENTIAL PURPOSE OF ANY LIMITED REMEDY PROVIDED HEREIN.

- Should any provision of this Agreement be held by a court of competent jurisdiction to be illegal, invalid, or unenforceable, that provision shall be deemed amended to achieve as nearly as possible the same economic effect as the original provision, and the legality, validity and enforceability of the remaining provisions of this Agreement shall not be affected or impaired thereby.

- The failure of either party to enforce any term or condition of this Agreement shall not constitute a waiver of either party's right to enforce each and every term and condition of this Agreement. No breach under this agreement shall be deemed waived or excused by either party unless such waiver or consent is in writing signed by the party granting such waiver or consent. The waiver by or consent of a party to a breach of any provision of this Agreement shall not operate or be construed as a waiver of or consent to any other or subsequent breach by such other party.

- This Agreement may not be assigned (including by operation of law or otherwise) by you without WILEY's prior written consent.

- Any fee required for this permission shall be non-refundable after thirty (30) days from receipt by the CCC.

- These terms and conditions together with CCC's Billing and Payment terms and conditions (which are incorporated herein) form the entire agreement between you and WILEY concerning this licensing transaction and (in the absence of fraud) supersedes all prior agreements and representations of the parties, oral or written. This Agreement may not be amended except in writing signed by both parties. This Agreement shall be binding upon and inure to the benefit of the parties' successors, legal representatives, and authorized assigns.

- In the event of any conflict between your obligations established by these terms and conditions and those established by CCC's Billing and Payment terms and conditions, these terms and conditions shall prevail.

- WILEY expressly reserves all rights not specifically granted in the combination of (i) the license details provided by you and accepted in the course of this licensing transaction, (ii) these terms and conditions and (iii) CCC's Billing and Payment terms and conditions.

- This Agreement will be void if the Type of Use, Format, Circulation, or Requestor Type was misrepresented during the licensing process.

- This Agreement shall be governed by and construed in accordance with the laws of the State of New York, USA, without regards to such state's conflict of law rules. Any legal action, suit or proceeding arising out of or relating to these Terms and Conditions or the breach thereof shall be instituted in a court of competent jurisdiction in New York County in the State of New York in the United States of America and each party hereby consents and submits to the personal jurisdiction of such court, waives any objection to venue in such court and consents to service of process by registered or certified mail, return receipt requested, at the last known address of such party.

**WILEY OPEN ACCESS TERMS AND CONDITIONS**

Wiley Publishes Open Access Articles in fully Open Access Journals and in Subscription journals offering Online Open. Although most of the fully Open Access journals publish open access articles under the terms of the Creative Commons Attribution (CC BY) License only, the subscription journals and a few

of the Open Access Journals offer a choice of Creative Commons Licenses. The license type is clearly identified on the article.

**The Creative Commons Attribution License**

The Creative Commons Attribution License (CC-BY) allows users to copy, distribute and transmit an article, adapt the article and make commercial use of the article. The CC-BY license permits commercial and non-

**Creative Commons Attribution Non-Commercial License**

The Creative Commons Attribution Non-Commercial (CC-BY-NC)License permits use, distribution and reproduction in any medium, provided the original work is properly cited and is not used for commercial purposes.(see below)

**Creative Commons Attribution-Non-Commercial-NoDerivs License**

The Creative Commons Attribution Non-Commercial-NoDerivs License (CC-BY-NC-ND) permits use, distribution and reproduction in any medium, provided the original work is properly cited, is not used for commercial purposes and no modifications or adaptations are made. (see below)

**Use by commercial "for-profit" organizations**

Use of Wiley Open Access articles for commercial, promotional, or marketing purposes requires further explicit permission from Wiley and will be subject to a fee.

Further details can be found on Wiley Online Libraryhttp://olabout.wiley.com/WileyCDA/Section/id-410895.html

**Other Terms and Conditions:**

**v1.10 Last updated September 2015**

Table **Questions? customercare@copyright.com or +1-855-239-3415 (toll free in the US) or +1-978-646-2777.**

## A.3 ACS Publications License